



CHARACTERIZING EFFECTS AND BENEFITS OF BEAM DEFOCUS ON HIGH
ENERGY LASER PERFORMANCE UNDER THERMAL BLOOMING AND
TURBULENCE CONDITIONS FOR AIR-TO-GROUND ENGAGEMENTS

DISSERTATION

Scott N. Long, Lieutenant Colonel, USAF

AFIT / DS / ENS / 08-05

**DEPARTMENT OF THE AIR FORCE
AIR UNIVERSITY**

AIR FORCE INSTITUTE OF TECHNOLOGY

Wright-Patterson Air Force Base, Ohio

The views expressed in this dissertation are those of the author and do not reflect the official policy or position of the United States Air Force, Department of Defense or the United States Government.

AFIT / DS / ENS / 08-05

CHARACTERIZING EFFECTS AND BENEFITS OF BEAM DEFOCUS ON HIGH
ENERGY LASER PERFORMANCE UNDER THERMAL BLOOMING AND
TURBULENCE CONDITIONS FOR AIR-TO-GROUND ENGAGEMENTS

DISSERTATION

Presented to the Faculty

Graduate School of Engineering and Management

Air Force Institute of Technology

Air University

Air Education and Training Command

in Partial Fulfillment of the Requirements for the

Degree of Doctor of Philosophy

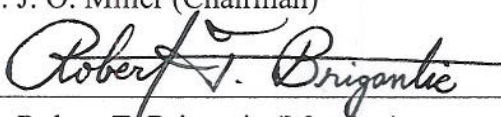

Scott N. Long, B.S., M.S.

Lieutenant Colonel, USAF


CHARACTERIZING EFFECTS AND BENEFITS OF BEAM DEFOCUS ON HIGH
ENERGY LASER PERFORMANCE UNDER THERMAL BLOOMING AND
TURBULENCE CONDITIONS FOR AIR-TO-GROUND ENGAGEMENTS

Scott N. Long, B.S., M.S.
Lieutenant Colonel, USAF

Approved:

	<u>29 Apr 08</u>
Dr. J. O. Miller (Chairman)	Date
	<u>21 May 08</u>
Dr. Robert T. Brigantic (Member)	Date
	<u>28 MAY 08</u>
Lt Col Matthew E. Goda (Member)	Date
	<u>6 Jun 08</u>
Dr. Mike Marciniak (Dean's Representative)	Date

Accepted:

	<u>17 June 08</u>
Dr. Marlin U. Thomas	Date
Dean, Graduate School of Engineering and Management	

Acknowledgments

I would like to thank my committee for their great patience with me and their tremendous guidance. I especially appreciate Dr Miller taking on this cross-departmental topic and never giving up on completing it. Beyond the committee, I thank AFIT staff members Dr Glenn Perram, Col Rick Bartell, Lt Col Steve Fiorino, and Mr Jim Gray, as well as AFIT interns Matt Krizo, Zack Manning, and Amanda Fellows for all their assistance and willingness to listen to my ideas.

I want to express my admiration for the late Dr Won B. Roh, my optics professor. He was a gifted instructor and truly kind soul who constantly expressed interest in my research, progress, and well being. He is sorely missed, and I dedicate this work to him.

I thank my friends in Dayton old and new: from church, the neighborhood, work, *etc.*, as well as San Antonio friends and colleagues. You made my life seem normal and fun in spite of the long research hours, and you gave me far more support than I was able to give in return. I hope to repay this great debt someday and to serve others in kind.

I thank my Mom, Dad, siblings, and in-laws for their prayers and physical and emotional support, both to me and to my family. I couldn't have done it without them.

My wife and children put up with far more than anyone ought to have through this experience. They loved me at my most unlovable and then some. I am amazed by them, deeply grateful to them, and I would be lost without them.

Finally, I thank God for strength to finish, for revealing my many faults, and for adopting me despite them yet with help to overcome them. Let us glorify and enjoy Him!

Table of Contents

	Page
Acknowledgements	iv
List of Figures	viii
List of Tables	xii
List of Symbols and Notation	xiii
Abstract	xv
1. Introduction	1-1
1.1 Research Significance	1-1
1.2 Research Scope	1-6
2. Literature Review	2-1
2.1 High Energy Lasers	2-1
2.1.1 Average Power	2-1
2.1.2 Laser Type	2-1
2.2 Atmospheric Turbulence	2-5
2.2.1 Introduction	2-5
2.2.2 Random Characterization of Turbulence	2-5
2.2.3 Relevant Descriptors	2-7
2.2.4 Other Important Literature	2-13
2.3 Thermal Blooming	2-15
2.3.1 Introduction	2-15
2.3.2 Descriptive Equations	2-16
2.3.3 Critical Power	2-18
2.3.4 Interaction with Turbulence and Jitter	2-20
2.4 Wave-Optics Modeling	2-23
2.4.1 Introduction	2-23
2.4.2 The Fresnel Approximation	2-23
2.4.3 Phase Screens	2-26

	Page
2.5 Scaling Law Modeling	2-28
2.5.1 History and Use	2-28
2.5.2 Other Important Literature	2-31
2.6 Systems Analysis & Modeling of HEL Systems	2-33
2.6.1 Major Assumptions	2-33
2.6.2 Scenario Parameters	2-34
2.6.2 Target Vulnerability Issues	2-37
3. Characterizing Defocus as Means to Improve No-Turbulence ATG COIL Performance	3-1
3.1 Introduction	3-1
3.2 Thermal Blooming Distortion Number	3-4
3.3 Baseline Scenario	3-7
3.4 Phase Screen Modeling Requirements	3-10
3.5 Phase Screen Selection	3-11
3.6 ATG HEL Scenario Performance Under Defocus	3-15
3.7 Velocity Vector Relative to Target	3-18
3.8 Target Range	3-21
3.9 Ground Wind	3-25
3.10 Absorption	3-32
3.11 Altitude	3-35
3.12 Aligning These Dimensions of Sensitivity Using N_D	3-38
3.13 Optimal Defocus Performance by Obscuration Size	3-39
3.14 Thermal Blooming Strehl	3-46
3.15 Conclusion	3-49
4. Interaction between Turbulence and Thermal Blooming in ATG Scenarios and Relation to Use of Defocus for Irradiance Improvement	4-1
4.1 Introduction	4-1
4.2 Defocus Versus Turbulence	4-

	Page
4.3 Interaction Strehl	4-4
4.4 ATG Scenarios Considered	4-8
4.5 Phase Screen Selection	4-9
4.6 Relationship of $S_{interact}$ with Defocus and Power	4-12
4.7 Velocity Vector Relative to Target	4-17
4.8 Target Range	4-21
4.9 Case Study	4-24
4.10 Conclusion	4-32
5. Summary and Recommendations	5-1
5.1 Introduction	5-1
5.2 Summary of Research Contributions	5-1
5.2.1 Improvement with Defocus	5-1
5.2.2 Defocus Stability for 10% Obscuration	5-2
5.2.3 Sensitivity to Obscuration Size	5-3
5.2.4 Thermal Blooming-Turbulence Interaction	5-3
5.2.5 Phase Screen Count	5-4
5.2.6 Defocus Improvement at Lower ATL Powers	5-5
5.2.7 Higher Altitude, Transverse Propagation Improve Performance	5-6
5.2.8 Improved HELEEOS Scaling Law Model	5-7
5.2.9 Scaling Law Consistency Analysis Technique	5-7
5.2.10 Defocus Scaling Law Structure	5-8
5.2.11 Wave Optics Processing Improvements	5-8
5.3 Recommendations & Suggestions for Future Research	5-9
5.3.1 Power-in-the-Bucket Scaling Law	5-9
5.3.2 Higher Order Approaches	5-10
5.3.3 Investigate Other Wave Optics Codes	5-11
5.4 Conclusion	5-11
6. Bibliography	BIB-1

List of Figures

Figure		Page
2.1	Comparison of wave-front error Strehl approximations	2-11
2.2	Relationship of peak intensity to critical power	2-20
3.1	This is a graphical illustration of some of the baseline scenario settings: range, altitude, velocity, wind, and platform orientation to target	3-8
3.2	Phase screen density as a function of altitude for 10, 20, 30, and 40 screen cases	3-12
3.3	Schematic of path phase screen density as it relates to altitude density	3-13
3.4	Effect of increasing phase screens on peak irradiance	3-14
3.5	Peak irradiance as a function of focal length for baseline scenario with 30% central obscuration	3-15
3.6	Peak irradiance as a function of focal length for baseline scenario with 10% central obscuration	3-16
3.7	Peak irradiance as a function of power for the baseline scenario, focused and optimally defocused cases, by aperture obscuration size (10% and 30%)	3-17
3.8	Irradiance functions of focal length for perpendicular propagation and 30% obscuration	3-18
3.9	Irradiance functions of focal length for perpendicular propagation and 10% obscuration	3-19
3.10	Peak irradiance as a function of power for the perpendicular propagation version of baseline scenario, focused and optimally defocused cases, by aperture obscuration size (10% & 30%)	3-20
3.11	Improvement factor for perpendicular propagation versus parallel propagation for otherwise baseline scenario, focused and optimally defocused cases, by aperture obscuration size (10% & 30%)	3-21
3.12	Improvement of target peak irradiance at optimal defocus over focused case as function of range to target of otherwise baseline scenario	3-22
3.13	Peak irradiance improvement factor of 10% obscuration relative to 30% obscuration by range for otherwise baseline scenario	3-24
3.14	Peak irradiance for given obscuration and focus assumptions as a function of range relative to the $1/r^2$ rule applied to peak irradiance at 3 km for otherwise baseline scenario	3-25

Figure		Page
3.15	The peak irradiance response to defocus for the 50 kW baseline scenario for windspeeds of 10, 5, and 2.5 m/s	3-27
3.16	The peak irradiance response to defocus for the 100 kW baseline scenario for windspeeds of 10, 5, and 2.5 m/s	3-28
3.17	The peak irradiance response to defocus for the 100 kW baseline scenario for wind speeds of 10, 5, and 2.5 m/s and 10% obscuration	3-29
3.18	Peak irradiance at optimal defocus as a function of ground wind speed, by power (kW) and obscuration size (%) in otherwise baseline scenario	3-30
3.19	Improvement factor in peak irradiance at optimal defocus over focused case as function of ground wind speed, by power (kW) and obscuration size (%) in otherwise baseline scenario	3-31
3.20	Optimal defocus multiple of target range as function of ground wind speed, by power (kW) and obscuration size (%) in otherwise baseline scenario	3-31
3.21	Peak irradiance as function of defocus for mid-latitude 80 percentile winter (50 and 100 kW) and 80 percentile summer (50 kW)	3-34
3.22	Peak irradiance as function of defocus for mid-latitude 80 percentile winter (100 and 200 kW) and 80 percentile summer (100 kW)	3-35
3.23	Peak irradiance response to defocus for baseline scenario by aircraft altitude. Range is held constant at 6 km	3-36
3.24	Phase screen density effect on defocus profile. Peak irradiance response to defocus for baseline scenario by aircraft altitude and phase screen setting. Range is held constant at 6 km	3-38
3.25	Optimal focal length multiple of slant range (defocus) for 100 kW baseline scenario (30% obscuration) and varied parameters, as function of focused-case N_D	3-41
3.26	Same as Figure 3.25 except for 10% obscuration	3-42
3.27	Peak irradiance improvement at optimal defocus for 100 kW baseline scenario (30% obscuration) and varied parameters, as function of focused-case N_D	3-43
3.28	Same as Figure 3.27 except for 10% obscuration	3-44

Figure		Page
3.29	Breaux N_D exhibits some inconsistency across the scenario variables in its correlation to S_{TB} for the air-to-ground case. Pivot point is baseline scenario at 100 kW	3-47
3.30	Use of Smith correction factor removes gross inconsistency in Breaux N_D with respect to defocus scaling	3-49
4.1	Peak irradiance at optimal defocus for baseline scenario by obscuration and turbulence assumption	4-6
4.2	Critical power graphs for baseline scenario under HV 5/7 turbulence, by obscuration size illustrate defocus is beneficial in the presence of turbulence	4-7
4.3	Peak irradiance improvement factor for perpendicular propagation over parallel propagation (at optimal defocus) as function of laser power by obscuration and turbulence assumption for otherwise baseline scenario	4-8
4.4	S_{turb} as function of target slant range for otherwise baseline scenario by HV 5/7 turbulence multiple	4-9
4.5	$S_{interact}$ at optimal defocus for otherwise baseline scenario as function of power, by phase screen setting in ACS. An insufficient number of phase screens exaggerates the interaction of TB and turbulence	4-11
4.6	$S_{interact}$ for the 10% obscuration case as function of focal length by laser power for otherwise baseline scenario	4-13
4.7	$S_{interact}$ for the 30% obscuration case as function of focal length by laser power for otherwise baseline scenario	4-14
4.8	Peak irradiance as function of defocus for 200 kW baseline scenario (30% obscuration) under two turbulence assumptions: no turb and 1x HV 5/7	4-15
4.9	Peak irradiance as function of defocus for 10% obscuration and 200 kW for otherwise baseline scenario under two turbulence assumptions: no turb and 1x HV 5/7	4-16
4.10	$S_{interact}$ at optimal defocus as a function of laser power by obscuration and turbulence assumption for otherwise baseline scenario	4-17
4.11	Peak irradiance as function of defocus for baseline scenario with 30% obscuration comparing perpendicular propagation performance to parallel case with turbulence and to perpendicular with no turbulence	4-19

Figure		Page
4.12	Peak irradiance as function of defocus for baseline scenario with 10% obscuration comparing perpendicular propagation performance to parallel case with turbulence and to perpendicular with no turbulence	4-20
4.13	$S_{interact}$ at 200 kW as function of focus setting by obscuration size and propagation vector for otherwise baseline scenario	4-21
4.14	$S_{interact}$ for baseline scenario (100 kW) by turbulence multiple and obscuration size as function of slant range	4-22
4.15	Improvement of target peak irradiance at optimal defocus over focused case as function of range to target of otherwise baseline scenario, for no turbulence and HV 5/7 turbulence cases	4-23
4.16	Peak irradiance improvement factor of 10% obsc. relative to 30% obscuration by range for otherwise baseline scenario by turbulence assumption	4-24
4.17	Irradiance improvement factor (vertical axis) due to 5% defocus at 2 km, 3km, and 4 km (top to bottom, respectively) by case study variable setting	4-26
4.18	Improvement factor of 5% defocus as function of platform altitude by wind and power setting	4-27
4.19	Irradiance in W/m^2 (vertical axis) with 5% defocus at 2 km, 3km, and 4 km (top to bottom, respectively) by case study variable setting	4-28
4.20	Peak irradiance at target for 50 kW output power as a function of platform altitude by target range and target azimuth averaged across all other settings in the case study	4-30
4.21	Peak irradiance at target for 100 kW output power as a function of platform altitude by target range and target azimuth averaged across all other settings in the case study	4-31

List of Tables

Table		Page
2.1	Parameters of interest for HEL systems analysis	2-35
2.2	Measures of performance for HEL systems analysis	2-37
3.1	Combined absorption and scattering coefficients due to molecular and aerosol effects in this study	3-9
3.2	Average across focus ranges 6000-7500 m of magnitude percentage change in peak irradiance for each increment increase in phase screen number	3-14
3.3	Target plane peak irradiance values (W/m^2) for given settings by range for otherwise baseline scenario (100 kW)	3-23
3.4	Scenario values and associated Breaux N_D for this study	3-39
4.1	Values of S_{turb} to check adequacy of phase screen count to model turbulence in ACS at otherwise baseline scenario	4-10
4.2	“High” and “Low” settings for variables in the case study for otherwise baseline scenario at 10% obscuration	4-25

List of Symbols and Notation

a_i	initial radius of the laser beam at the propagating aperture
a_f	final radius of the laser spot at the target for the given degree of focus as well as diffraction and other linear effects
a_{geom}	ray-optics radius of the beam at given point along optical path
c_P	specific heat of atmosphere
k	wave number (2π divided by wavelength)
n_0	unperturbed refractive index of air
$\partial n / \partial T$	rate of change refractive index with respect to local temperature
N_D	thermal blooming (phase) distortion number
N_{focus}	focus adjustment multiple for N_D
P	laser output power at aperture
R_{target}	distance from the aperture to the target plane.
s	spread of the beam at given point on optical path due to diffraction and beam quality effects as well as specialized estimate of the spread due to blooming
S_{TB}	Strehl ratio for thermal blooming effect in absence of turbulence
S_{turb}	Strehl ratio for turbulence effect in absence of thermal blooming
$S_{TB+turb}$	Strehl ratio for combined effect of turbulence and thermal blooming
$S_{interact}$	Strehl ratio for the interaction of turbulence and thermal blooming effects
T_0	atmospheric baseline temperature (300 K, for this research),
T	atmospheric temperature at given altitude
V_E	effective wind velocity perpendicular to optical path

α_{abs}	absorption coefficient
α_{scat}	scattering coefficient
ρ	air density
τ	transmission (fraction of power transmitted over a given optical path)

Abstract

This dissertation makes contributions towards knowledge of optimizing of laser weapon performance when operating in the air-to-ground (ATG) regime in thermal blooming conditions. Wave optics modeling techniques were used to represent laser weapon performance in a high fidelity sense to allow progress to be made toward improving lower-fidelity scaling laws that can be used in systems level analysis which has need for better representations of thermal blooming.

Chemical-oxygen iodine laser (COIL) based weapon systems that operate near the ground will experience thermal blooming due to atmospheric absorption if output power is sufficiently high. The thermal lens in the ATG case is predominantly in the far-field of the optical system which puts the problem outside the envelope for most classical phase correction techniques. Focusing the laser beyond the target (defocus) in the air-to-ground regime is shown to improve irradiance at the target and can be thought of as reducing the thermal blooming distortion number, N_D , rather than phase correction. Improvement is shown in a baseline scenario presented and all variations from it explored herein. The Breaux N_D is examined for potential use in a defocus scaling law, and a correction factor due to Smith (1977), developed for a different context, is proposed to address deficiencies. Optimal defocus settings and expected improvement are presented as a function of Breaux N_D . Also, the generally negative interaction between turbulence and thermal blooming is investigated and shown to further limit performance potential of ATG laser weapons. This negative interaction can impact the weapon design trade space and operational methods for minimizing the interaction and thermal blooming are explored in a case study.

CHARACTERIZING EFFECTS AND BENEFITS OF BEAM DEFOCUS ON HIGH ENERGY LASER PERFORMANCE UNDER THERMAL BLOOMING AND TURBULENCE CONDITIONS FOR AIR-TO-GROUND ENGAGEMENTS

1. Introduction

1.1. Research Significance

With the development of high energy laser (HEL) technology as well as the supporting technologies over the past four decades, it appears the United States is within a year or two of fielding actual HEL weapons, and there is little doubt that HEL weapons will find wider applicability beyond the originally planned missions. As an example, it would not be too controversial to say that the preeminent HEL weapon development in the USAF today, and perhaps even in the Department of Defense (DoD), is the Airborne Laser (ABL) program. The ABL prototype consists of a cargo version of the Boeing 747 aircraft which is being heavily modified to carry a megawatt class chemical oxygen-iodine laser (COIL), as well as the necessary equipment to propagate (“fire”) the laser with destroying effect against enemy launched ballistic missiles hundreds of kilometers away. Another US weapon under advanced development, conducted in cooperation between Israel and the US Army, is the Mobile Theater HEL (MTHel, pronounced “EM-thel”). The MTHel is designed to shoot down short range artillery rockets of the type sometimes used by anti-Israel terrorists, but has even had success at destroying incoming artillery shells! MTHel uses deuterium-fluoride laser technology described later. Another COIL weapon development is the Advanced Tactical Laser (ATL)

demonstrator, in which a Lockheed C-130 cargo aircraft will be fitted with a slightly different COIL technology than ABL that allows the laser to fire in denser air near the ground. Primary targets for ATL will be stationary or slow-moving ground targets, and much interest in ATL comes from the USAF Special Operations community.

HEL weapons are progressing quickly indeed, but none of the foregoing is meant to suggest that HEL weapons are a panacea for force protection or force application. First, despite the given progress, there is the issue of what the technology has promised versus what is delivered. Though this concern is by no means unique to HEL weapons, the fact remains HEL weapons have often taken much longer to develop than was expected when the programs were sold to DoD leadership. Second, even if HEL weapons work as advertised, they are not “all weather” weapons: Lasers cannot shoot through clouds or thick fog, and even though the ABL flies above the weather, its performance still suffers during some types of atmospheric phenomena. In the DoD’s capabilities-based acquisition perspective, this may not be much of a problem, since the deciding factor is, “If its value-to-cost ratio is high enough, buy it in spite of its shortcomings.” But being more realistic, money spent on HEL weapons (operational ATLs) would very likely—though not certainly—reduce the amount of money spent on different technology weapons that have greater weather capability (C-130 Gunships). As such, the decision to pursue of HEL technology is one of balancing, or trading, risks and benefits. In the notional example of ATLs procured instead of Gunships, the USAF and the supported combatant commanders inherently would have accepted a risk (*e.g.*, reduced all-weather engagement capability, reduced kinetic attack ability) in order to get the benefit of the HEL when it can be used (*e.g.*, farther stand off range, reduced

collateral damage), as well as accepted the risk that the ATL performance can be delivered.

To support HEL investment decisions at all levels, it is necessary to develop a robust capability to evaluate the risks of competing technologies (*e.g.*, HEL vs. conventional, or HEL #1 vs. HEL #2). In the notional ATL example above, the decision was at the major program level; however, decision support is needed at other levels as well, such as the selection of which HEL technologies to invest in given limited research and development budgets. The DoD and the services have vast experience in conducting technology and weapons trade studies. Very often, one of the major aspects of these studies is the use of computer modeling and simulation to determine potential military utility of the various competitors by judging how well they perform in a simulated battle environment.

An advantage to using computer simulation is that a large number of possible scenarios can be examined in a relatively short period of time in an attempt to determine the likely utility of a given technology at various performance/risk levels. It is the inclusion of technology performance at different risk levels in a study that gives decision makers the most insight into the decision problem. Here is typical risk/performance breakout: high performance (*i.e.*, the technology delivered most of what could be hoped for—riskiest), medium performance (*i.e.*, the technology delivered a moderate portion of what was hoped for—less risky), and low performance (*i.e.*, the technology delivered only some of what was hoped for—least risky). The effect of examining lots of scenarios for competing technologies for a number of risk levels is that many runs of a computer simulation are necessary.

Usually one of the internal scoring parameters, and sometimes a major output, of these simulations is the probability of kill, or P_k , when a technology/weapon under examination is engaged against an enemy target. The rules that determine P_k as a function of the engagement scenario variables are the heart of these simulations. For many weapons, the P_k relationship to the scenario can be derived from testing of the weapon itself, *e.g.*, the ratio of successful outcomes to the number of trials. However, such testing is itself expensive, its results subject to confidence limits due to the sample size, and allowances must be made in the simulation for aspects of the battlefield that were not addressed in testing (*e.g.*, expected future countermeasures, different weather, new upgrades). Some of these issues speak to confidence bounds in the simulation results in aggregate, which will be addressed later, but let us continue to examine issues with weapons representation in particular.

The very nature of technology and weapons decision making is future-oriented, since any product that arises from those decisions is typically years away from employment. As such, even weapons that have an extensive current database for building P_k relationships must have their performance extrapolated to some risk level of future performance. Regarding HEL weapons, their future performance must also be estimated, as is true with any new system. However, extensive databases do not currently exist to support that estimation as they do for more traditional kinetic weapons, so there is potential for additional uncertainty.

Another difference is that HEL performance is typically described in terms of output power (usually in kilowatts, kW, or megawatts, MW), magazine (usually in seconds of laser time), and/or duty cycle (*e.g.*, time between shots) rather than range and

speed. With a kinetic weapon, if it can get to the target (range) in the time required (speed), then a success/fail determination can be made based on the assessed vulnerability of that target to that weapon. However for an HEL weapon, the propagation of the laser energy from the weapon to the target must be modeled, which is a primary focus of this research. Also, range and P_k are more fluid for HEL weapons than for kinetic weapons, though they can certainly be characterized. For example, if an HEL can kill a target ($P_k=1$) at range x in time $t(x)$, then since the amount of power delivered typically falls off with range, it may also be able to kill the target at range $2x$, but it will usually require more laser time, or *dwell time*, to do so, $t(2x) > t(x)$. Also, for kinetic weapons, P_k for engagement ($P_k^{(e)}$) is a function of whether or not the weapon arrived:

$$P_k^{(e)} = \begin{cases} P_k, & \text{if weapon arrived} \\ 0, & \text{if weapon failed to arrive} \end{cases}$$

On the other hand, for an HEL engaging most targets, P_k will be an increasing function of dwell time, and it will also depend on other factors such as range and atmospheric conditions. This relationship of P_k to dwell time arises from an assumption about the primary success mode of HEL weapons: that targets are typically destroyed by heating them up in a vulnerable area around an aimpoint until they fail. When this is the case, and all other aspects of a scenario being equal, increased dwell time means additional energy delivered to the target (energy = power \times time), which translates into additional heating and increased P_k . The need for a functional relationship between P_k and energy delivered to (or more accurately absorbed by) the target places an increased burden on the DoD intelligence and vulnerability community relative to the already

difficult requirement for developing P_k relationships for kinetic weapons. This will be discussed in more detail later.

The issue of energy deposited in a given area on the target is an important one for the present research. Much attention has been focused in the literature on characterizing the peak intensity of the beam at the target, which in terms of units is usually represented as W/m^2 . (An equivalent term for *intensity* is *irradiance*, sometimes used herein.) However, since peak intensity only occurs at one point in the beam profile on target (often falling off quickly as a function of distance from the peak), it is usually not adequate for determining energy deposited in a given area at the target over some time. What is needed when peak intensity alone is inadequate to predict mission success is the *average intensity* impinging upon the area in question. The product of that average intensity and the specified area is the power incident upon that area, which is sometimes referred to as a “bucket”, giving rise to the term *power in the bucket* (PIB).

Returning to the issue of modeling the laser propagation from the weapon to the target, there are two primary effects that must be accounted for, especially for HEL's operating near earth surface: atmospheric turbulence and thermal blooming. The atmospheric turbulence effect is the distortion of a laser beam that is caused by random spatial variations in the refractive index of the atmosphere along the optical path of the laser. Turbulence, from a time-averaged perspective, causes the laser beam to spread out, resulting in reduced average power over a given area in the target plane.

The thermal blooming effect is a distortion due to the laser beam itself causing a change in the refractive index of the atmosphere in the optical path (due to heat absorption by atmospheric gases). In the absence of wind, thermal blooming typically

causes the beam to expand. This is because higher temperature usually means lower density and lower refractive index in the center of the beam path, and light bends away from lower refractive indices. In most situations, there will be some kind of wind (either actual wind or effective wind due to beam slewing, or platform or target motion). In these cases, the wind brings cooler, more dense air into the beam path, displacing the heated less dense air, and following the principle given above, experiments have long shown the beam will bend into the wind, spreading in the cross wind direction into a crescent shape bowing into the wind direction.

Additionally, besides the effects of turbulence and thermal blooming, there is the interaction of those two effects which can be important. To illustrate, consider a focused HEL beam propagating in a low turbulence environment; since the beam spread is low, intensity along the center of the beam path (the optical axis, or *on-axis*, intensity) can become quite high, resulting in rapid atmospheric heating and significant thermal blooming distortion at the target. On the other hand, this time consider the same beam in a high turbulence environment; turbulent spreading keeps the on-axis intensity low, reducing the effect of thermal blooming and resulting in *less* total beam distortion at the target than in the previous case.

Extensive theory and associated computer models, called wave-optics codes, do exist that allow for reasonably accurate calculation of such propagations, including interaction effects. However, wave-optics code evaluations are very time intensive and are not conducive to the rapid evaluations needed to conduct trade studies as described above. Scaling law models—defined as more closed-form representations of laser propagation derived either directly from theory, by curve fitting empirical or wave-optics

simulated data, or a combination—have been developed that address many aspects of the propagation problem and which are, by design, much faster than wave-optics codes. However, there was no research found that simultaneously addressed the issues of average power prediction and the thermal-blooming/turbulence interaction. Such a capability would significantly enhance the ability to conduct trade studies using modeling and simulation since an increased number of scenarios can be investigated over the number that could be investigated using wave-optics modeling. Additionally, representing the performance on target from a power in the bucket perspective (PIB), as well as accurately accounting for the interaction effect mentioned above, would improve the accuracy of these studies versus those conducted with the peak intensity perspective (when a thermal kill paradigm is more appropriate) or lesser specified scaling law models.

1.2. Research Scope

The presented research focuses upon two areas: (1) Accurate prediction of peak intensity performance across a wide range of air-to-ground HEL scenarios under thermal blooming and turbulence; and (2) development of PIB scaling law codes that allow prediction of power in a radial bucket that accounts for the non-radial nature of many thermally bloomed beams.

In addressing these areas, first the performance of existing peak intensity scaling laws will be examined in relation to wave-optics generated ATL-like data. This will give insight into where additional analysis should be focused. Additionally, some candidate PIB parametric approaches will be constructed and fit to the same data to assess their

promise for development into a scaling law. Next, the results of the peak intensity analysis will be tested using a broader wave-optics experimental design that includes additional parameters not in the ATL scenarios. To allow for a broader investigation in this step, a surrogate for turbulence (such as beam defocus) will likely be used as a time-saver. At a later stage, turbulence will be re-introduced and corrections will be applied, if necessary. Potential theoretical contributions lie in the extension of the peak intensity scaling laws to a continuum of aperture irradiance and obscuration profiles, accounting for apparently stronger focusing effects in air-to-ground propagation than exists in current analytic scaling law, and development of PIB parametric predictors. Culmination of research is expected to be fast-running, flexible, and accurate code for ATL-like application, as well as other scenarios, that can be used in representing HEL weapons in the present and future battlespace.

2. Literature Review

2.1. High Energy Lasers

2.1.1. Average Power

The definition of a High Energy Laser (HEL), or equivalently a high average power laser, is somewhat subjective since the average power threshold to be classified as “high” depends on the target. Often, an HEL is defined as a laser which could potentially cause a heat-induced effect (usually damage) to its target. More specifically, that damage would occur to a non-cooperative target such that the effect would have some practical value, often in a military sense—this is the perspective of the present research effort. A very rough scale of HEL classification according to average power would be: 1 kW, probably not; 10 kW, maybe; 100 kW, usually; and 1 MW, certainly. It is important to emphasize the phrase “potentially cause”; the reason is that many lasers have been denoted as HEL’s that have never been fashioned into a weapon that actually caused heat-induced effects to a non-cooperative target (especially those HEL’s that are still on the drawing board).

2.1.2. Laser Type

There are several categories of laser construction that have or are currently being scaled to use as HEL’s. The category to achieve HEL status the earliest is the gas dynamic laser. First, a discussion on the construction of a laser is useful: Lasers usually consist of an optically resonant cavity that can contain a gain medium. The gain medium is a substance whose atoms can be excited to a state such that a photon of light at a

certain wavelength passing near the excited atom will stimulate the emission of another photon (returning the atom to a less excited state) at the same wavelength traveling in the same direction with the same phase as the first photon—in other words, the power of the first photon has been amplified. LASER is actually an acronym for *light amplification by stimulated emission of radiation* (Smith, 1977), and from the forgoing, you can see why. When the excited gain medium is placed in an appropriate resonant cavity, all of the stimulated emission will quickly align itself with the cavity, and when a portion of the light energy is released from the cavity (often by a partially silvered mirror or an opening in one end of the resonator), the resulting beam of light propagates with very low divergence, or spreading—this is the laser beam.

In a gas dynamic laser, the gain medium is a gas that is forced (often perpendicularly) through the resonant cavity and which contains atoms that have been excited to the appropriate state by means of some prior chemical reaction—for this reason they are also called chemical lasers. The purpose of the forced flow is to continually re-supply the resonator with excited gain material. Examples of gas dynamic lasers include the chemical oxygen-iodine laser (COIL), invented at Kirtland AFB, NM. This is the basis for the USAF's AirBorne Laser (ABL) and Advanced Tactical Laser (ATL) programs, with average powers of approximately 1 MW and 25 kW at a wavelength (λ) of 1.315 μm , respectively. Another example is the deuterium-fluoride (DF) laser, extensively tested at White Sands Missile Range, NM, and the basis for the US Army's Mobile Theater High Energy Laser (MTHL) program. Finally, there is the hydrogen-fluoride (HF) laser, which operates at primary wavelengths that cannot be propagated efficiently in the atmosphere, but which is still an excellent candidate for a

space-based laser (SBL) for anti-missile defense (AMD). As one might guess from the programs just cited, gas dynamic lasers have reasonable power-to-system-weight ratios at HEL-like average power levels. However, they are still quite heavy and often their weight cannot be scaled efficiently to lower power levels. Another oft cited drawback to gas dynamic lasers is that they require a fuel supply (the gain medium chemicals), which means they have a limited magazine, or amount of “laser on” time, due to depletion of the chemicals. Also, there are the added logistical requirements of transporting and storing laser fuel, and in some cases the fuel and/or the by-products of the chemical reaction are hazardous.

The drawbacks of gas dynamic lasers have increased the research emphasis on solid-state lasers (SSLs), also called electric lasers. SSLs under consideration for HEL application are usually characterized by having a rare-earth doped crystal as the gain medium, the excitation of which is accomplished by flash lamps or diode lasers that direct energy into the gain crystal (often from a direction perpendicular to the resonant cavity optical axis). The resulting excited atoms then give up that energy to the resonant optical field. The only resource required to fire an SSL is electricity; hence as long as there is electric power, there is an “unlimited” magazine. Quotes are used because there is another limiting factor that applies to both gas-dynamic lasers and SSLs, and that is *reliability*. The fact that the finite magazine is thought to be the most limiting factor in gas dynamic lasers is a reason reliability was not mentioned earlier. However, reliability will likely be a limiting factor for SSLs. This potential drawback is underscored by the fact that the closer to design limits one operates SSLs to produce more power, the faster they experience component failures. Another drawback of SSLs is heat production: A

by-product of gain medium pumping is excess heat that must be removed from the laser. Heat management techniques include adding weight for cooling devices, reducing shot time lengths, increasing time between shots, or a combination of the three. Heat management is related to reliability because many component failures are heat related. Another drawback is that current power-to-weight ratios are relatively low, though improving this is an active area of research. There are no working examples of SSLs that are squarely in the HEL category, but technologies that are being pushed in that direction include Nd:YAG (neodymium-doped yttrium aluminum garnet crystal, $\lambda = 1.064 \mu\text{m}$) as the gain medium (Verdeyen, 1995, pp. 359-362).

Other laser types include the free-electron laser (FEL) which the US Navy is attempting to scale in power up to 1 MW, but these are so heavy that they can only realistically be deployed on ships. FELs do not have a gain medium; rather they use magnets to vibrate accelerated electrons in the resonant cavity to produce and amplify the resonant optical field (Verdeyen, pp. 417-423). Also, there are gas-discharge lasers where the gain medium is a gas contained in a cell inside the resonant cavity which is excited a similar manner to SSLs. Examples of the latter include the common red HeNe (helium neon) laser ($\lambda = 0.6328, 1.15 \mu\text{m}$) and the venerable CO₂ laser ($\lambda = 9.4$ to $10.6 \mu\text{m}$), versions of which can achieve significant average powers (Andrews *et al.* 1998, p. 16). Though they are not great candidates for use as HELs as understood in this research, CO₂ lasers are used extensively in laboratory experiments that simulate the expected effect of the atmosphere on HEL weapons (Smith, 1977).

This is not meant to be a complete discussion on HEL technology, but rather a primer from the perspective of HEL weapons. There are exceptions—*e.g.*, in the early

1980's, the Airborne Laser Lab used a gas dynamic CO₂ laser against non-cooperative targets—as well as other technologies and other novel concepts under development. For most of this research, we will focus on the air-to-ground mission of an ATL-like platform using a COIL device.

2.2. Atmospheric Turbulence

2.2.1. Introduction

The propagation of lasers through the atmosphere, not surprisingly, is affected by the optical characteristics of the beam path that arise from fluctuations in air mass velocity, pressure, and temperature. These fluctuations are random in nature, though they have been shown to follow definable statistical rules in many instances. These statistical rules can be very mathematically intensive, even though, according to Andrews and Phillips (1998), their derivation has largely been based upon physical insight and empiricism, and not from “first principles” (p. 44). Kolmogorov first developed the foundations of modern turbulence theory by describing the distribution of velocities at different scales in the atmosphere. It turns out that Kolmogorov's main results could also be applied to atmospheric temperature distributions, which are more directly related to optical turbulence because of the direct effect that temperature has on index of refraction (Andrew and Phillips, pp 48-50).

2.2.2. Random Characterization of Turbulence

The temperature of the atmosphere as a function of distance along a vector from a point can be thought of as a spatial stochastic process in each of the component vectors

with distance as the independent variable. When the atmosphere is *statistically homogenous* and *isotropic*, then the stochastic process is statistically identical along any vector regardless of starting point or direction (pp. 31-32).

Let $\langle \cdot \rangle$ denote ensemble average, or expected value, and $T(x)$ be the temperature function, then the *structure function* under the above assumptions is (p. 28)

$$D_T(r) = \langle [T(x+r) - T(x)]^2 \rangle,$$

where r is a radial distance from point x in the atmosphere. Also, the *covariance function* is given by (p. 24)

$$B_T(r) = \langle [T(x) - m][T(x+r) - m] \rangle,$$

where m is the mean value for the temperature process $T(x)$. It turns out that under the homogeneity assumption, these functions are related by (p. 28)

$$D_T(r) = 2[B_T(0) - B_T(r)],$$

which allows for measurement of the structure function with sensitive atmospheric instruments (p. 50). The *temperature structure constant*, C_T^2 , is determined from (p. 48)

$$D_T(r) = C_T^2 r^{2/3}, l_0 \ll r \ll L_0,$$

where l_0 and L_0 are the lower and upper limits of the *inertial subscale*, the distances for which the assumptions of homogeneity and isotropy of the stochastic process hold (p. 45). Finally, the index-of-refraction *structure parameter* for optical and near-infrared wavelengths can be found (Andrew and Phillips, pp. 49-50) by

$$C_n^2 = \left(79 \times 10^{-6} \frac{P}{T^2} \right)^2 C_T^2,$$

where P is pressure in millibars and T is temperature in Kelvin. C_n^2 has units of $\text{m}^{-2/3}$, and has a value of about 10^{-17} or less when turbulence is “weak” and 10^{-13} or more when turbulence is “strong” (p. 51). C_n^2 is a strongly inverse function of altitude since turbulence is typically worse near the ground, becoming more benign with increased altitude, and with knowledge of C_n^2 along an optical path, one can completely describe the turbulence behavior of that path. (See sections 4.2.2. and 4.2.3 below.)

2.2.3. Relevant Descriptors

There are several statistics that have been developed for describing the turbulence for a given optical path, and often C_n^2 figures prominently in them. One of the more common statistics is atmospheric coherence length, r_0 , which is given by Lukin and Fortes (1998) to be:

$$r_0 = \left(0.423 k^2 \int_0^L C_n^2(x) Q^{5/3} dx \right)^{-3/5},$$

where k is the wave number ($k = 2\pi/\lambda$), $C_n^2(x)$ is the strength of turbulence profile as a function of distance x from the aperture along the optical path of length L , and $Q = 1$ for a plane wave or $Q = 1 - x/L$ for an expanding spherical wave arriving at the aperture (or equivalently, a converging spherical wave departing the aperture). The measure r_0 has units of meters and represents the limiting performance of an optical system in imaging resolution or propagated beam diffraction. In free space propagation without turbulence, the divergence angle of the laser will be approximately λ/D (in radians), where D is the diameter of the aperture. On the other hand, in propagation through a turbulent medium, the divergence angle will be approximated by λ/r_0 , when $D > r_0$ (Andrews & Phillips, p. 141). As turbulence increases, r_0 decreases, and the propagated beam diverges (without adaptive atmospheric compensation), reducing the average power over a given area at the target. A similar measure, the isoplanatic angle, θ_0 , expresses the angular distance (in radians) for which the atmosphere is nearly uniform with the vertex at the target (p. 145). This is discussed in more detail in Section 4.2.2. and 4.2.3.

In addition to calculating the spreading due to turbulence when $D > r_0$, one can also estimate the peak intensity of a spot focused at distance L by (from the brightness equation in Golnick, 1993, p. 451):

$$I_p \cong P \frac{\pi r_0^2}{4\lambda^2 L^2}. \quad (2.1)$$

where I_p represents the peak irradiance point and P is the laser output power uniformly illuminating a circular aperture. As before, without turbulence (and whenever $D < r_0$), I_p can be found by substituting D for r_0 in Eq. 2.1.

A different metric for turbulence, often used in scaling laws predicting peak intensity of a beam, is wavefront error (WFE) and its associated Strehl ratio (denoted S with a subscript). Strehl ratio, for the purpose of laser propagation, is the fraction remaining of the undistorted peak intensity of a beam at its target after a given degrading effect is applied. Usually the effects are considered to be independent, thus total Strehl ratio is the product of individual contributing Strehl ratios. For example, there can be a Strehl ratio due to turbulence of 0.9, and a Strehl ratio due to absorption of 0.95. If only these two effects are applied to a laser, the final peak intensity of the beam will be $0.9 \times 0.95 = 0.855$ of its value without these effects. WFE gives rise to two different components of total Strehl, system and atmospheric. System WFE is the departure from the ideal wavefront at the output aperture that the beam experiences due to an imperfect optical system or laser resonator (Tyson and Ulrich, 1993, p. 173). Whereas, atmospheric WFE can be thought of as the imperfections in a wavefront arriving at an aperture from a point source at the target plane. The imperfections are typically measured with respect to a spherical wavefront. We consider spherical wavefronts because laser weapons are generally represented as focused on the target plane, which implies a spherical wavefront.

Let Φ_p be the difference between the actual wavefront and the ideal spherical wavefront, then the mean square WFE is (p. 173): $(\Delta\Phi_p)^2 = \langle \Phi_p^2 \rangle - (\langle \Phi_p \rangle)^2$. Under the restriction that a given type of wavefront imperfection is “small,” the Strehl ratio for that aberration is derived by Born and Wolf (1999, p. 522):

$$S_{WFE} = 1 - \left(\frac{2\pi}{\lambda} \right)^2 (\Delta\Phi_p)^2. \quad (2.2)$$

Though do they not specify what the limits in WFE are for the utility of this expression (*i.e.*, what “small” is), they use Marechal’s standard that a system is “well corrected” when the Strehl ratio is 0.8 or higher. From Eq. 2.2, then, one can find that this corresponds to a root mean square WFE constrained as follows: $|\Delta\Phi_p| \leq \lambda/14 \cong 0.07\lambda$ (p. 528), a very small WFE indeed.

Tyson and Ulrich (1993, p. 174) take advantage of the “small” wavefront error assumption, and the fact that equation Eq. 2.2 is the first two terms of a Maclaurin Series, to justify the approximation:

$$S_{WFE} = \exp\left(-\left(\frac{2\pi}{\lambda}\right)^2 (\Delta\Phi_p)^2\right). \quad (2.3)$$

These authors suggest that independent sources of WFE can be considered separately with this formula, with their Strehl ratios multiplied as above for cumulative Strehl.

Fig. 2.1 below compares equations 2.2 and 2.3 with respect to $|\Delta\Phi_p|$. Note that the graphs diverge at about $|\Delta\Phi_p| = 0.07\lambda$, and then the *source* equation 2.2 decreases parabolically to negative numbers, which is unphysical since intensity must be positive. The *approximation* equation 2.3 is better behaved and more intuitive (since it remains positive and decreasing with $|\Delta\Phi_p|$), suggesting perhaps that relaxing the small WFE assumption underlying the derivation of Eq. 2.2 would yield an expression that is even better approximated by Eq. 2.3. The point of this discussion is that Eq. 2.3 is often used

to represent WFE in scaling law approximations for peak intensity, but appears to be inaccurate for $|\Delta\Phi_p| > 0.07\lambda$.

In any case, taking advantage of what Hogge (1974, p. 190) calls the “reciprocity of the linear turbulence operator,” we could test the utility of Eq. 2.3 in modeling turbulence by using wave-optics to simulate a point source at the target plane propagating spherical waves through a turbulent atmosphere to a receiving aperture. Then WFE could be captured at the aperture and applied to an outgoing beam back to the target plane in a vacuum propagation. Repeating the experiment with multiple settings (with replications to achieve averaging) and calculating the ratios with their respective diffraction limited cases will produce points on the coordinate system in Fig. 2.1 that could be used to validate Eq. 2.3.

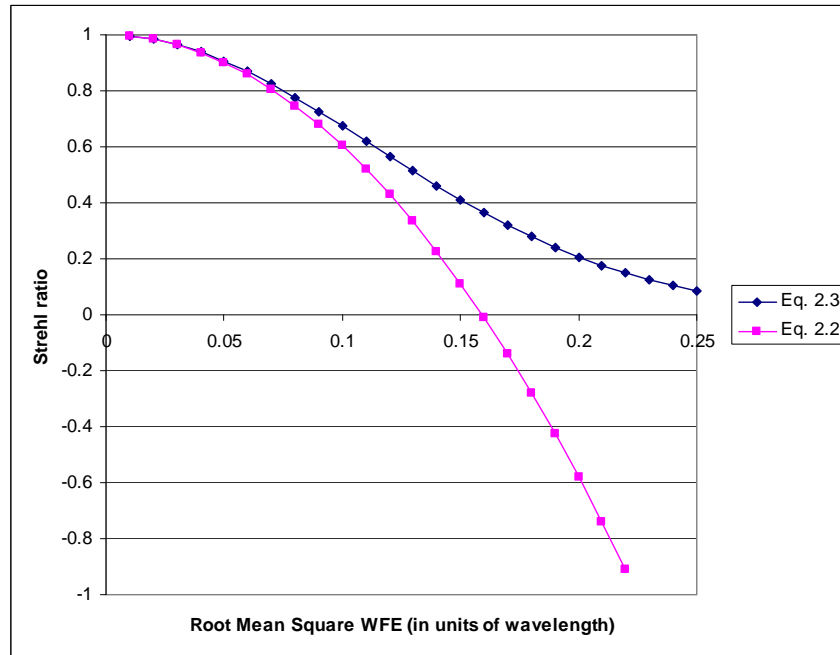


Figure 2.1. Comparison of wave-front error Strehl approximations.

Finally, much has been written on the turbulence spreading of Gaussian beams. The applicability to HEL systems is two-fold: First, when SSL HEL systems are deployed, they very likely will have a Gaussian intensity profile at the aperture. Second, even those systems with more uniform beams (such as some gas-dynamic systems with unstable resonators) usually focus the beam, which makes the beam similar to a Gaussian in the optical path. Additionally, considering an ATL scenario when shooting at ground targets, the focused beam propagates through the thicker atmosphere (which has the most turbulence) when it is in this state. As such, these results may be useful in applying turbulence effects. A nice feature of Gaussian beams is that beam spreading is directly related to Strehl ratio, thus if the beam remains Gaussian near its peak, then the irradiance profile near the peak is also specified. Let W be the Gaussian beam waist at the target plane without the effect of turbulence and W_b designate the larger beam waist after turbulent spreading. Tyson and Ulrich (p. 180) say that turbulence Strehl $S_{turb} = (W/W_b)^2$, which in plain words means that pushing down the peak of a Gaussian beam with constant power requires the beam to spread out.

Ishimaru (1981) showed that under the short range condition of $Z_i \gg L \gg Z_c$ (for ATL, typical values are $Z_i = 120$ km, $Z_c < 100$ m, and $L = 3 - 25$ km) the resultant beam waist due to turbulent spreading is given by:

$$W_b^2 = \frac{W^2}{2 \int_0^\infty \exp\left(-t^2 - 3.1 C_n^2 k^{1/3} L^{8/3} W^{-5/3} t^{5/3}\right) dt}$$

Tyson and Ulrich, as well as Andrews and Phillips (p. 147), have developed their own expressions for Gaussian beam spreading due to turbulence, and it was difficult to see similarities, except for two: (1) Both of those expressions assume constant C_n^2 , meaning integral expressions would be needed to accurately determine beam spreading in ATL's case, where C_n^2 will vary along the path; and (2) as with Ishimaru's method, the ATL missions appear to fall into the "short range" or "low turbulence" category in all methods except for the most extreme scenarios.

2.2.4. Other Important Literature

Fried (1966) conducted significant early work in imaging through turbulence regarding the potential utility of short exposures over long exposures with respect to image quality, since the time averaged effect of tilt due to turbulence would be eliminated. In particular, when $D/r_0 \sim 1$, his results show that image quality, measured in resolution, is primarily degraded by tilt turbulence and that by correcting for tilt alone, especially in the near field case, one can recover a large portion of the diffraction limited performance. However, as D/r_0 increases beyond 2, less than half of the lost diffraction limited performance is achievable with tilt correction alone, and worsening as the ratio increases further (*e.g.*, at $D/r_0 = 4$, less than 25% of the lost performance is recoverable with tilt correction alone). The remainder of the diffraction limited performance is only recoverable (to some degree) through higher-order adaptive optics correction. One may view laser system performance from the atmospheric standpoint first, that is use r_0 as a beam spreading parameter, per suggestion in Section 2.2 above. In this case, Fried provides a performance multiplier that adds the effect of aperture size. Treating r_0 as a

limiting aperture, Fried's short exposure near field Strehl for a physical aperture such that $D/r_0 \sim 1$ is actually greater than 1! This result has sometimes been referred to as "super resolution" (Goda, 2004), but in reality its performance is less than the diffraction limited performance of the physical aperture in a vacuum. Vernon and St John (2003) take this approach when modeling turbulence in SAIC's High Energy Laser CONsolidated Modeling & Engagement Simulation (HELCOMES). This technique is particularly insightful for application to ATL since ATL's aperture diameter (0.5 m) is on par with r_0 values associated with ATL scenarios in Long (2004a).

Many authors have addressed the issue of laser beam spreading due to turbulence. Lutomirski and Yura (1971) and Yura (1971) address uniform plane and spherical waves propagating from circular apertures, as well as Gaussian beams. Yura's approach is adopted by Smith (1977) for scaling law development; however, these papers do not address the issue of short exposure beam spreading. Ishimaru (1981), quoted earlier, revisited turbulent beam spreading and provides potentially useful relationships, but also did not to have address the short exposure issue. However, for very far propagations, he does address the issue of beam spread dependence upon the inner scale of the inertial subscale, l_0 (described in Section 2.2.2).

Valley (1979) showed that short-exposure Strehl is strongly dependent on the inner scale value, whereas long-exposure Strehl is not. The opposite is true for the outer scale, L_0 (again, see Section 2.2), especially for ATL specifications and scenarios. He also demonstrated some limitations of using wave-optics for evaluating the effect of the outer scale. Fante (1980) demonstrates a method for removing the beam spread due to atmospheric tilt alone, and shows that significant improvements in short exposure (or tilt-

corrected) intensity can be realized when $2 \leq D/r_0 \leq 5$. Fante (1983) addresses the issue of the inner scale on scintillation (which is related to the short exposure of an aberrated beam) and finds that the non-zero inner scale values significantly increase the variance of the irradiance probability density function (PDF). Unless the time constants for the effect of the inner scale are small, and their effect has a zero mean, the inner scale value may be a candidate for inclusion in a scaling law model.

2.3. Thermal Blooming

2.3.1. Introduction

Thermal blooming refers to the self-induced distortion of laser beams propagating through the atmosphere caused by the heating of the atmospheric components by the beam itself. Temperature gradients are then created in the atmosphere, from which arise refractive index gradients which, as discussed in the turbulence section above, distort the beam. This is a non-linear process since the beam starts undistorted, causes initial heating, which distorts the beam. But the distortion of the beam simultaneously changes the dynamics of the atmospheric heating (Smith, 1977), affecting the next stage of beam distortion. If the conditions are sufficiently constant, the beam will pass through this transient state and settle into a steady state. One of the more important conditions concerning HEL weapons is wind relative to the optical beam path. In the presence of a nearly constant wind profile (that is non-zero everywhere along the beam path), the steady state beam shape has been shown (*e.g.*, Smith, 1977; Gebhardt, 1993; Hogge, 1974) by both experiment and computer modeling to deform into a crescent shape that bends into the wind. For HEL weapon scenarios, this distorted shape almost always has

reduced peak intensity relative to the undistorted beam and it represents a loss of radial symmetry associated with un-bloomed beam spots.

2.3.2. Descriptive Equations

Since light is a wave phenomenon, the bending a of beam of light can be described as the result of a non-uniform retardation of the wavefront of the beam. For example, when a planar wavefront of light impinges on a focusing lens, after passing through the lens, its wavefront is no longer planar but has a converging spherical form that will focus the beam at the center of that sphere. What happened? The focusing lens, being thicker in the middle and thinner at its edges, applied a non-uniform retardation of the beam resulting in the center portions of the beam having the greatest retardation, while the edges of the beam had little retardation—the resulting spherical wavefront represents (or one could say “causes”) a focusing of the light.

Cooler, denser air is optically thicker than warmer, less dense air—we saw that random distribution of temperatures is the cause of optical turbulence. This temperature-density concept is also critical for understanding thermal blooming. Under the non-restrictive assumption (Gebhart, p. 293) that there is a prevailing wind across HEL beam path, the wind will bring cooler air into the beam path, and push warmer air out. In the steady state, then, there is a temperature gradient across the beam path in the wind axis, and we can think of this as a lens: The cooler air retards the wavefront of the laser more than the warmer air, so the overall wavefront bends in the direction of the cool side of the beam path. In the cross wind direction, since there is no wind motion in that axis, the

temperature profile is generally warmer in the middle than on the edges. This has the effect of a diverging lens, causing the beam to spread in crosswind axis.

To show these effects physically, Gebhart (p. 297) assumes geometric optics (neglecting the effects of diffraction caused by the aperture and atmospheric lenses) and finds that for a Gaussian beam with wind velocity, v , in the positive x direction, the blooming phase distortion in the plane transverse to the optical axis (positive z direction) is:

$$\begin{aligned}\varphi_{BG} &= -\frac{N_D}{4\sqrt{\pi}} \exp\left(-\left(\frac{y}{a}\right)^2\right) \left(1 + \operatorname{erf}\left(\frac{x}{a}\right)\right) \\ &\cong -\frac{N_D}{4\sqrt{\pi}} \left(1 + \frac{2}{\sqrt{\pi}} \left(\frac{x}{a}\right) - \left(\frac{y}{a}\right)^2 - \frac{2}{\sqrt{\pi}} \left(\frac{1}{3} \left(\frac{x}{a}\right)^3 + \left(\frac{x}{a}\right) \left(\frac{y}{a}\right)^2\right) + \frac{1}{2} \left(\frac{y}{a}\right)^4 \dots\right)\end{aligned}\quad (2.4)$$

where $\operatorname{erf}(x) = 2\sqrt{\pi} \int_0^x \exp(-t^2) dt$ is the error function (MatLab 7.0 user documentation, 2004), N_D is the thermal blooming distortion number (a function of z as defined below), and a is the distance from the center of the initial Gaussian beam in the transverse plane such that the intensity at that point is $1/e$ times the peak intensity. Note in the series expansion version of Eq. 2.4 (the second line), that the second term of the expansion represents advancement of the wavefront as an increasing function of x , that is the cause of the tilting of the beam into the wind. The third term represents astigmatism: The wavefront is retarded in the y -axis as a function of distance from $y = 0$. This accounts for beam spreading in the crosswind direction, as discussed above. The factor N_D (p. 299) is defined as a product of the collimated beam distortion parameter, N_C , and the Fresnel

number, N_F : $N_D = 2\pi N_C N_F$ (2.5), where $N_F = ka^2/z$, z being the propagation distance, and for a Gaussian beam:

$$N_C = \frac{-n_T \alpha P z^2}{\pi n_0 \rho C_p V a^3} \quad (2.6)$$

where n_0 , ρ , and C_p are the average refractive index prior to heating, density, and specific heat of the medium, respectively; $n_T = \partial n / \partial T$; α is the absorbance coefficient (in units of length^{-1}); P is output power; and V is wind velocity. This is a scaling parameter, about which more will be said later, but note that it combines the effects of many different aspects of the scenario into a single parameter.

Gebhardt (p. 296) derives a different blooming phase formula than Eq. 2.4 for a uniform circular beam and shows the blooming effect to be significantly lower than for a comparable Gaussian beam. Smith shows some experimental data that verifies this; however, in neither case is it clear that the beams were considered to have propagated to a far-field pattern. When such is the case, any blooming advantage of a uniform beam may be lost since the far-field pattern of a uniform circular beam is the Airy pattern, which is very Gaussian-like. Smith displays uniform and other beam results with respect to a parameter containing N_C , in spite of the latter's underlying Gaussian assumption. To do so, a reasonable substitution for a is assumed: the radius of the aperture.

2.3.3. Critical Power

One of the more interesting and, from a weapons perspective, important results of HEL thermal blooming is that computer experiments substantiated by laboratory results

(Smith; Hogge, p. 224) show that for a given scenario, the steady state peak intensity of the laser spot at the target will rise as a function of power level until a certain power value is reached called the critical power, P_c . At power levels greater than P_c , the peak intensity is a decreasing function power. The value of P_c varies with the scenario, but for a strongly focused Gaussian beam with low atmospheric absorbance, P_c can be estimated when the other parameters of the scenario are known and N_D from Eq. 2.5 above is set equal to 4π (Gebhardt, p. 301). Smith gives a normalized approximate relationship for this phenomenon:

$$I_p/I_{pc0} \cong \frac{P/P_c}{1 + (P/P_c)^2}$$

where I_p is the peak intensity of a bloomed beam at power P , and I_{pc0} is the peak intensity for an *unbloomed* beam with power P_c . This function is graphed (solid line) in Figure 2.2. The axes are relative intensity and relative power, of course.

When I_p is the measure of a weapon's performance, P_c is an important limiting factor, and actions are usually undertaken to increase P_c to improve weapon performance (*e.g.*, different wavelength, different engagement geometry). The proposal to use PIB as an alternative to I_p as the primary laser performance metric can be understood in this light. If a plot of I_p vs. P for a specific weapon in a specific scenario were included, and we overlaid a plot of PIB for a given bucket size, the power at which the PIB plot peaks will necessarily be greater than P_c .

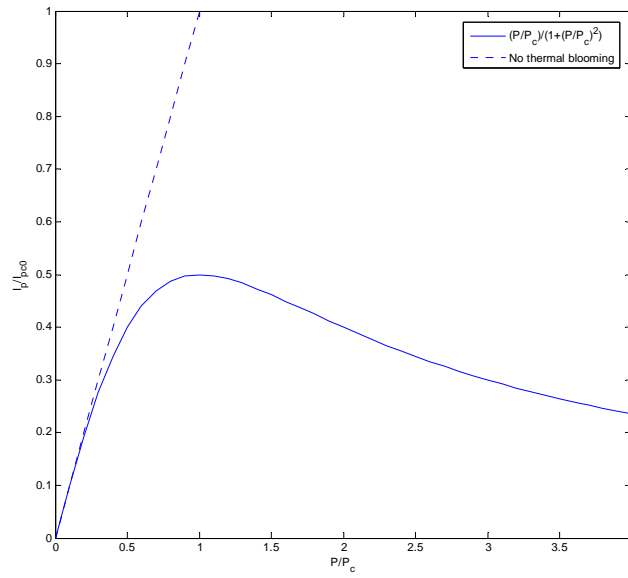


Figure 2.2. Relationship of peak intensity to critical power.

2.3.4. Interaction with Turbulence and Jitter

Not surprisingly, it turns out that focused beams suffer worse thermal blooming than collimated beams. This is because the intensity gradient can tend to get very large in the optical path as the target plane is approached, especially if atmospheric turbulence is relatively low, thus allowing the beam to achieve near-diffraction limited spot sizes in the absence of thermal blooming. As we will discuss with more detail in the scaling law section below, in a thermal blooming regime, near diffraction-limited beam sizes can experience severe blooming distortion due to the large laser induced temperature gradients, erasing any peak intensity gains that came from the “quiet” atmosphere. On the other hand, should some turbulence be present, the effective focusing of the beam is reduced, which results in a smaller thermal blooming effect than in the quiet atmosphere case. For high beam jitter, in some cases we can treat it similarly to turbulence in that in

a time average sense, it merely spreads the beam. In a recent simulation study of ATL scenarios using wave-optics code, we have seen that for a constant thermal blooming distortion number, increased turbulence actually increased the peak intensity (Long, 2004a). Similarly, MIT's thermal blooming lab showed that adding high-bandwidth transverse jitter and/or artificially spreading the beam by defocusing likewise can increase peak intensity (Edwards, 2004).

Smith (1977) and Tyson and Ulrich (1993, p. 198) noted this interactive effect and noted that the difficulty of the interaction problem is dependent upon the relative bandwidths of the effects. Sticking with turbulence alone for clarity, the bandwidth (BW) of turbulence is related to the minimum amount of time Δt it takes for the atmosphere along a ray in the beam path to be independent of the atmosphere along that same path at time Δt (either due to wind, beam slewing/motion, or both). At high BW, this time is “small” (thus placing a greater demand on the tracking system, *etc.*). The thermal blooming BW is related to the amount of time the propagated beam takes to achieve its steady state shape. Again for clarity, when the thermal blooming BW is high, this settling time is “small”. Smith points out that when $BW_{\text{turb}} \gg BW_{\text{bloom}}$, the effects can be handled separately: apply turbulence first to spread the beam, then apply thermal blooming treatment. In the opposite case, apply blooming first, then spread the resulting beam in accordance with turbulence. In the case where $BW_{\text{turb}} \cong BW_{\text{bloom}}$, Smith flatly states that “no analytical treatment is possible”.

The latter may present a worthy, perhaps insuperable, challenge and it is unclear how the circumstance applies to the present proposal. In the ATL scenario studies, we found that the thermal blooming transient takes on the order of 0.25 to 0.5 seconds to

settle, the longer times needed for the milder thermal blooming cases (lower power, shorter distances, *ect.*). Gebhardt quoted a study of horizontal (apparently ground level) propagation with a particularly challenging thermal blooming assumption: a stagnant air mass at some point along the beam path. In this case, the thermal blooming settling times were between 0.1 and 0.3 seconds. These times seem long, but it is not certain at this point that they are long compared to atmospheric turbulence refresh times. Gebhardt (1976) suggests that usually turbulence bandwidth, which under Taylor's frozen flow hypothesis (Roggemann and Welsh, 1996, p. 65) is primarily driven by effective wind (either due to real wind or beam motion), is sufficiently greater than blooming bandwidth to allow application of the $BW_{\text{turb}} \gg BW_{\text{bloom}}$ rule above. However, Hogge (p. 231-3) has shown that for focused beams, such as ATL is likely to use, most of the blooming effect occurs near the target plane. Since ATL targets are likely to include slow moving and stationary ground targets, beam motion at this critical range may be limited. When the wind velocity perpendicular to the optical path is also small (though not necessarily small enough to violate Taylor's hypothesis), Gebhardt's suggestion regarding relative bandwidth may not apply. On the other hand, Andrew, Phillips, and Hopen (2001, p. 116) say that as the "strength of turbulence increases, the power in the [temporal irradiance] spectrum shifts to higher frequencies," which suggests an increase in BW_{turb} . Since turbulence is highest near the ground, this offsets the above concern to an extent, but it doesn't resolve it.

2.4. Wave-Optics Modeling

2.4.1. Introduction

Given the high dimensionality of the HEL turbulence thermal blooming propagation problem, one successful approach to predicting performance has been to mathematically simulate the entire system in the time domain with as few assumptions as possible. The core of this approach is to treat light propagation, not geometrically, but with a technique that accurately represents diffraction due to its wave nature: the Fresnel approximation. The atmosphere is represented as a sequence of thin planar irregular lenses, called phase screens, that represent turbulence or an air mass with which the simulated laser beam can also interact to represent thermal blooming. This so called wave-optics modeling approach gives accurate results (Smith; Gebhardt, p. 302) but are difficult to set up for a scenario and are very computationally intensive.

2.4.2. The Fresnel Approximation

The Fresnel approximation refers to a simplification of the Huygens-Fresnel principle of light propagation. The latter, embodied in the theories of Kirchoff and later of Rayleigh-Sommerfeld (Goodman, 1996, p. 35), treats the amplitude of the light wave as a scalar value rather than a vector whose coordinates can interact with each other via the environment. Scalar theory can be used in vector representations of light when the two polarization coordinates are assumed not to interact by treating each coordinate with a separate scalar representation (Born and Wolf, 1999, p. 430). The Huygens-Fresnel principal says that light can be thought of as a wavefront along which there are infinitely many points that re-emit the wave as a sphere. The exterior locus of the wavefronts of

these secondary spherical wavelets after a period of time t describes the result of the original wave after propagating for time t . The conditions for the Huygens-Fresnel principle to be valid are that (1) an aperture is large compared to the optical wavelength and (2) observation of the radiation takes place “far” from the aperture (Goodman, p. 35), and both are easily met in HEL weapon scenarios.

The first Rayleigh-Sommerfeld theory of the Huygens-Fresnel principle is given as follows (Goodman, p. 66):

$$U(x, y) = \frac{z}{i\lambda} \iint_{\Sigma} U(\xi, \eta) \frac{\exp(ikr)}{r^2} d\xi d\eta \quad (2.7)$$

where $U(\xi, \eta)$ represents the complex electric field at the aperture Σ (an area in the starting plane), $U(x, y)$ represents the complex electric field at a parallel plane (the plane we’re propagating to) at distance z from Σ , and $i = \sqrt{-1}$. The double integral represents the adding up of the wavelets emanating from each point in the aperture as they intersect (and interfere) at a point (x, y) . The value r is a distance function between the points on the two planes:

$$r = \sqrt{z^2 + (x - \xi)^2 + (y - \eta)^2}.$$

To get the Fresnel approximation, the distance function r in the denominator of Eq. 2.7 can be approximated by $r \cong z$. However, that is inadequate for the argument of the exponential function in the numerator. For that, a few terms of the binomial expansion are necessary (p. 67):

$$r \cong z \left(1 + \frac{1}{2} \left(\frac{x - \xi}{z} \right)^2 + \frac{1}{2} \left(\frac{y - \eta}{z} \right)^2 \right). \quad (2.8)$$

Making these substitutions into Eq. 2.7, and executing the squares in the binomial expansion results in (p. 67):

$$U(x, y) = \frac{e^{ikz}}{i\lambda z} e^{i\frac{k}{2z}(x^2 + y^2)} \int_{-\infty}^{\infty} \int_{-\infty}^{\infty} \left\{ U(\xi, \eta) e^{i\frac{k}{2z}(\xi^2 + \eta^2)} \right\} e^{-i\frac{k}{2z}(x\xi + y\eta)} d\xi d\eta \quad (2.9)$$

Eq. 2.9, the Fresnel approximation, tells us that when the substitutions made above are valid, $U(x, y)$ is a function of the 2-dimensional Fourier transform of the expression in braces, $\{ \}$. The infinite integration limits are allowed when the aperture is defined within $U(\xi, \eta)$. The assumption needed for the Fresnel approximation, in addition to the Huygens-Fresnel principle assumptions, requires that the rays between points in adjacent propagation planes make small angles with respect to the optical axis (Goodman, p 72), which is also generally valid for HEL scenarios.

Fourier transforms, especially difficult ones, are often calculated using the fast Fourier transform (FFT) algorithm which is a numerical technique that requires sampling the complex field in the aperture plane at an appropriate spatial rate. If that rate is too low, anomalous results will occur; if too high, accuracy will not be hurt, but run time will be unnecessarily long.

2.4.3. Phase Screens

The propagation using the Fresnel approximation (or Fresnel propagation) represents a vacuum propagation between two planes. To utilize the power of Fresnel propagation for modeling turbulence and/or thermal blooming, the HEL propagation path is partitioned and the phase delay for each partition is represented by a thin irregular lens that applies all the phase delay for that partition at a single distance within that partition's length. This thin lens is called a phase screen. For modeling turbulence, the construction of a phase screen is a random process that is in keeping with the spatial correlation statistics for the atmosphere in that partition as discussed in Section 2.2.3. One method for building phase screens for turbulence is discussed in Roggemann and Welch (pp. 104-119). Taylor's frozen flow hypothesis (p. 65) states that for a given beam path the change in phase attributable to a partition of the beam path as a function of time is almost always dominated by wind for atmospheric propagations, and not by local changes in a turbulence pattern—that is, the turbulence moves across the beam faster than it changes within the beam. This assumption allows the use of large phase screens that are scanned across the beam path at a velocity representing local wind. There are at least two important things to remember regarding phase screens: (1) They are the result of a random process, so the laser spot determined by single run of a wave-optics code that models turbulence in this way is only a single sample of a statistical beam. Many runs will be needed to achieve a good estimate the statistical beam; and (2) since atmospheric turbulence will be correlated in the optical (z -) axis, having the screens too close to each other will require additional care in constructing them to take that correlation into account. To avoid computational problems associated with issue 2 above, one can

merely ensure the phase screens are far enough apart that they are effectively uncorrelated, assuming the impact on accuracy is not too negative.

To model turbulence and thermal blooming simultaneously, it is fairly straightforward to add additional thermal blooming phase screens along with the turbulence phase screens. This is the method employed by Link (2003a) in SAIC's Atmospheric Compensation Simulation (ACS), a prominent wave-optics code used in some DoD studies, and Smith (1977) also refers to several studies using this approach. In general, to reduce the number of Fourier transforms to compute in ACS, Link co-locates turbulence and thermal blooming phase screens in the simulation, computes their effects on the beam independently, adds them for their total phase delay, and propagates to the next screen location (2003b). The difference between thermal blooming and turbulence phase screens is that the thermal blooming screens change as a function of heat absorption from the beam that impinges upon it. The turbulence phase screens only change as a result of wind and the random turbulent process, and act upon but do not interact with the laser beam.

As mentioned, most HEL scenarios will have wind-dominated thermal blooming effects, so the thermal blooming phase screen will move in time with respect to the beam. According to Smith, and also Hogge (p. 215), atmospheric heating of the molecules translates to density changes that propagate acoustically (that is, at the local speed of sound) to the neighboring atmosphere. At the beginning of the simulation, the thermal blooming phase screen is uniform but still moving with the wind. Then as heating begins, the expansion of density waves is modeled as radial with respect to the heated point, but that expansion itself is moved away from the beam path because of the wind.

If the wind velocity is high enough, the phase screen lens will approach a steady state after some amount of simulated time for that portion of the beam path.

2.5. Scaling Law Modeling

2.5.1. History and Use

Scaling laws attempt to relate the variability in the aberration process to as few parameters as possible, often only one, which is itself a function of the scenario settings. Given such a parameter, the concept is that whatever scenario settings cause that parameter to be a certain value, the outcome of that scenario will be the same (or in the case of a stochastic system, drawn from the same distribution). In this section, we detail the method expounded by Smith (1977). Another common method due to Breaux will be important to this research as well.

Smith detailed the development of the most commonly used scaling law parameter for thermal blooming: the thermal blooming distortion number, usually denoted N . Different methods for calculating N have been developed over the last three decades, but Smith's derivation remains foundational. His approach uses the eikonal, the geometric optics equation of light rays in media with variable index of refractions (Born and Wolf, p119), and conservation of energy to describe the steady state result of light propagating through an absorbing medium. Of Smith's perturbation analyses, the most relevant to this study were those assuming convection, *i.e.*, wind. In this case, and under the assumption that the beginning irradiance profile is a collimated infinite Gaussian, the relationship between final and initial irradiance patterns is given by

$$\frac{I(x, y, z)}{I(x, y, 0) \exp(-\alpha z)} = \exp \left(-N_c \left(\frac{x}{a} e^{-(x^2+y^2)/a^2} + \frac{\sqrt{\pi}}{2} e^{-y^2/a^2} \left(1 - \frac{2y^2}{a^2} \left(1 + \operatorname{erf} \left(\frac{x}{a} \right) \right) \right) \right) \right) \quad (2.10)$$

when $\alpha z \ll 1$ and where N_c is defined in Eq. 2.6 above. Note that as described in Section 2.3, all of the scenario settings have been rolled into N_c with the single exception of a , which is the $1/e$ radius of the initial beam, that is the distance from the peak irradiance to the circular contour with irradiance of $1/e \times$ peak irradiance. These are a rather limiting set of assumptions; therefore, Smith derives additional multipliers to calculate the overall thermal blooming distortion number N for several cases.

Smith's correction factor for focusing (and apparently for diffraction) is given by

$$N_f = \frac{2(a_i / a_f)^2}{(a_i / a_f - 1)} \left(1 - \frac{\ln a_i / a_f}{a_i / a_f - 1} \right) \quad (2.11)$$

where a_i is the initial beam waist radius and a_f is the final beam waist radius (under no thermal blooming conditions). Gebhardt (1993, p. 301) provides a different form for this factor that uses the Fresnel number, but appears to assume the geometric focus is at the target. Smith's method is more general (though it requires a little more work for the calculation of a_f). This is essentially a strength of focusing term and was found to be useful in predicting performance under defocus in Chapter 3 with a different N formulation..

Smith provides a correction factor for slewing, though it appears that the paper's perspective on slewing was the ground-to-air mission. For ATL, aircraft velocity

dominates the wind for a significant portion of the beam path near the aperture, damping thermal blooming. Near the target, ground wind and target velocity (which is related to slew) will likely be the driving factors. Though its applicability to ATL is uncertain, the N multiplier for slew is

$$N_v = \frac{2}{(v_f / v_i - 1)^2} (v_f / v_i \ln v_f / v_i - (v_f / v_i - 1))$$

where v_i is the beam slew velocity at the aperture and v_f is the beam slew velocity at the target. Finally, Smith provides the multiplier for larger αz values:

$$N_s = \frac{2}{\alpha z} \left(1 - \frac{1 - e^{-\alpha z}}{\alpha z} \right)$$

Then, the composite thermal blooming distortion number is given by $N = N_c N_f N_v N_s$.

While Eq. 2.10 and its precursors give a description of the final irradiance field when given an initial Gaussian irradiance field, the thermal blooming distortion number as described above has often been used as a regression variable for curve fitting. Gebhardt (1976) and Smith both show N to be an explanatory variable for thermal blooming Strehl, S_{TB} , applied to collimated Gaussians by the relationship:

$$S_{TB} = \frac{1}{1 + 0.0625 N^2} \quad (2.12)$$

This model projects that critical power, P_C , occurs when $N = 4$. However, the relationship is not adequate for a collimated beam with a uniform irradiance profile (a tophat beam), which is better explained by the relationship (Gebhardt, 1993):

$$S_{TB} = \frac{1}{1 + 0.09N^{1.22}}, \quad (2.13)$$

which projects P_C occurs at $N = 25$. This means comparing a uniform tophat beam with a Gaussian beam having the same power and radius (as defined for each beam type), the uniform beam as will experience less thermal blooming distortion than the Gaussian, at least under collimated propagation to the near field.

There are minor discrepancies in the literature that have not been ironed out. (Smith reports a different tophat beam Strehl relationship to N than Gebhardt.) Also, it seems Smith's purpose for the factor modifications to N_C are to rescale any given Gaussian scenario such that Eq.2.12 could be applied. However, the development above appears inadequate in the air-to-ground case. Further, equations 2.12 and 2.13 could be considered extreme points on a continuum with respect to a Gaussian being clipped by an aperture. The infinite Gaussian representing no clipping and the tophat, which can be considered the limit of the Gaussian as the aperture radius approaches zero. This continuum might provide a better rescaling reference than 2.12 alone.

2.5.2. Other Important Literature

Smith (1977), referenced extensively above, and Gebhardt (1993, 1976), also referenced above, provide much of the body of knowledge for thermal blooming scaling

law utility as an alternative to wave-optics simulation. The underlying approach is to treat the optical propagation geometrically, then develop perturbation equations for optical interaction with the medium using fluid dynamics. The resulting perturbation equations are dependent on the irradiance field at the aperture and are particularly tractable when the initial irradiance profile is an infinite Gaussian. Under that assumption, a single constant emerges from this process that is a function of all the input variables and is called the thermal blooming distortion number, N . N , along with a functional form specific to the Gaussian assumption, predict the resulting thermal blooming effect. Diffraction effects, focus and slewing effects, and turbulence and jitter effects are applied after the fact. However, in order to develop scaling laws for peak intensity as well as application to other initial irradiance profiles, curve fitting techniques are used based on laboratory or wave-optics experiments.

Breaux (1979) and Breaux, Evers, Sepuche, and Whitney (1979) have developed what they call an algebraic predictive approach to thermal blooming for the purpose of systems analysis. Leveraging what they call the phase integral, and also employing some categorical variables for different initial beam shapes (derived apparently with some curve fitting techniques), their formula is prioritized for giving the peak intensity at the target. No mention was found of turbulence, but presumably turbulence effects could be added prior to their approach, since it is a linear effect. The HELCOMES scaling law model produced by SAIC uses the Breaux method (Vernon, 2003)

Recently, efforts have progressed in developing probability density functions for turbulence distorted irradiance patterns. Al-Habash, Andrews, and Phillips (2001) have developed what they have termed the Gamma-Gamma distribution for predicting the

moments of the irradiance profile. An attractive feature of this distribution, besides the fact that it performs well when compared to published data, is that it lends itself to parameter estimation, whereas the previous state of the art method did not. The purpose of irradiance PDF's appears to be in support of optical communications to enable robust system specification and predict signal fade statistics. However, this work should be translatable to predicting HEL irradiance statistics under turbulence (if existing theory isn't adequate).

2.6. Systems Analysis and Modeling of HEL Systems

2.6.1. Major Assumptions

There are many problems with designing, utilizing, and analyzing complex optical systems. Typically, in order to analyze one aspect of an overall system, assumptions about other aspects of the system must be made that will either be validated later or, if invalid, can be adjusted for without having to completely re-accomplish the analysis. For instance, under thermal blooming conditions, we saw that the peak of the beam is diverted from the optical axis. At this time, it is not clear how the peak of such a beam will be pointed at the aimpoint at the target. This is because the thermal blooming works both ways: distorting the outgoing beam as evidenced by the irradiance pattern at the target, and also distorting the image of the target (and any image of the laser spot) as seen by an aperture-sharing tracking/pointing sensor.

While there are some engineering challenges to overcome regarding beam pointing under such conditions, the community assumes that the challenges can and will be met. As such, we will allow the assumption that the beam in a future HEL weapon

operating under thermal blooming conditions can be pointed (at least at low bandwidth) at any desired aimpoint on a target under track (within the limits of the tracking bandwidth). With this assumption, we are alleviated from the need to predict the displacement of the beam peak at the target plane resulting from thermal blooming, and can concentrate on the shape or other distributional properties that are relevant.

Another major assumption has to do with tracking, or high bandwidth tilt correction. Even though we assume that only the time-averaged beam can be pointed, we assume that the time-averaged irradiance builds up under conditions that some amount of overall tilt caused by atmospheric turbulence is removed by a fast steering mirror, or something similar, inside a closed-loop system that is tracking the target. Residual tilt, that which the tracking system did not compensate for, between the aimpoint and the laser beam will be considered jitter that is high in bandwidth relative to the thermal blooming phenomenon that, therefore, effectively spreads the beam prior to blooming onset.

2.6.2. Scenario Parameters

Several mentions are made in this dissertation of the scenario settings. Our desire is to build relationships between these settings and HEL performance that allow the latter to be evaluated in a time period that is fast compared to using wave-optics. In particular, the performance we want to predict is the peak intensity and the circular PIB as a function of bucket radius. Table 2.1 provides a partial list of parameters that will be important for modeling HEL systems in the context of trade studies and other decision analyses. Note: “n.d.” stands for non-dimensional.

Table 2.1. Parameters of interest for HEL systems analysis

	Parameter	Symbol	Units	Description and Importance
1.	Output Power	P	W	Energy deposited on target scales linearly with P until thermal blooming onset.
2.	Aperture size, obscuration	a , %	m, n.d.	Aperture diameter is a crucial parameter determining limiting performance and thermal blooming. Central obscuration is single axis percent of diameter.
3.	Turbulence	C_n^2 , r_0 , θ_0	$m^{-2/3}$, m, rad	Turbulence spreads the beam, reducing peak intensity. Should look at multiple strengths. Second and third measures are derivative of C_n^2 .
4.	Absorption	α	m^{-1}	Reduces energy reaching target plan and results in atmospheric heating that underlies thermal blooming.
5.	Wavelength	λ	m	Affects diffraction, but also is a determinant of absorption strength.
6.	Range	z	m	Peak intensity falls of at as the square of the range in the diffraction limit.
7.	Focusing	F	m	Distance at which geometric focus is set—often but not always at target plane
8.	Residual jitter	θ_j	μm	High bandwidth angular motion of the due to undamped/uncompensated platform vibration effects and the remaining portion of the atmospheric tilt jitter beyond that removed by the tracking loop

Table 2.1 (cont). Parameters of interest for HEL systems analysis

	Parameter	Symbol	Units	Description and Importance
9.	Initial irradiance profile, truncation	type, A	n.d., n.d.	Top hat, Gaussian, apodized Gaussian; the truncation ratio is the radius of the aperture in units of 1/e radii of the underlying Gaussian irradiance surface
10.	Available dwell time	t_{fire}	sec	Includes magazine and duty cycle (if cooling between shots is required)
11.	Target vulnerability parameters	T_f, T_E, a_{bucket}	J/m ² , J, m	Fluence threshold (for fluence kill), Energy threshold (for energy kill), aimpoint geometry (plan for circle of some radius). Cooling/ heat dissipation effects (energy threshold as function of dwell time)
12.	System WFE	ω	rad	The minimum root mean square difference between the wavefront at the aperture and a perfect sphere with radius F
13.	Strehl	S	n.d.	Fraction of peak intensity remaining after applying an aberrating effect to a beam.
14.	Thermal blooming	N	n.d.	A roll-up of many of the above parameters--used as a scaling variable.
15.	Power-to-weight ratio	P/w	W/kg	Required knowledge for trade & architecture studies
14.	Volume-to-weight ratio	V/w	m ³ /kg	Required knowledge for trade & architecture studies

While the table above describes many of the parameters that are needed to describe a scenario, Table 2.2 gives some potential results needed to score the performance of a proposed system in that scenario. The first two entries are useful for comparing two different systems with each other in pure performance at the target plane. The last three bring target vulnerability into the problem. Valid target vulnerability

assessments are extremely important in system selection and design because it allows the examination of competing systems in simulated combat environments. We look at vulnerability issues next.

Table 2.2. Measures of performance for HEL systems analysis

	Measure	Symbol	Unit	Description and Importance
1.	Peak intensity	I_p	W/m^2	The time averaged maximum of an irradiance profile
2.	PIB	$P(a_{bucket})$	W	The time averaged power circumscribed by a circle of radius a_{bucket} at the target plane.
3.	Probability of kill	P_k	%	Chance of single engagement success. Increasing function of dwell time as irradiance/energy application cumulates toward the kill threshold. Possibility of distributional representation.
4.	Dwell time to get desired P_k	$t_{dwell}(P_k)$	sec	Inverse of above description. Also requires vulnerability thresholds from the JMEMS community.
5.	Stand off range	z	m	A function of system description, dwell time available, and target vulnerability. The farther the target, the slower irradiance/energy cumulates toward the kill threshold. However, long standoff ranges improve the possibility of covert operations.

2.6.3. Target Vulnerability Issues

The U.S. military uses Joint Munitions Effectiveness Manuals (JMEMs) as a guide for weapons employment in wartime operations. Effectiveness is often couched in

terms of P_k for a given engagement between a specific munition and a specific target type, and these assessments are developed (in part) upon munitions testing and years of experience. The drive to develop similar vulnerability assessments is gathering steam; for example, Williams (2004) discussed desired “DE weapon data in JMEM” at the Aug 04 Directed Energy Test and Evaluation Conference. Operational testers need operational criteria, and developing those for directed energy weapons is an important challenge.

It is common to limit the discussion of DE effectiveness to performance in terms of laser spot peak intensity at the target plane. While this is certainly an important performance metric—in that it is relatively easy to calculate and is correlated with other metrics such as PIB—it is important that the vulnerability community not become unnecessarily constrained to using peak intensity alone. As detailed elsewhere in this dissertation, the notion of a peak fluence kill criteria (peak intensity integrated over dwell time) has some counter intuitive implications for a target whose failure mode is based upon heating a component until structural failure occurs. In the latter case, total energy absorbed in a defined area bucket is likely to have more correlation to P_k , than peak fluence. One could call the former “energy in the bucket,” or EIB, which is PIB integrated over dwell time.

On the other hand, if the perception exists that EIB performance is not available by fast running models, the motivation of the JMEMs community to develop those vulnerability data (in spite of potentially better P_k correlation) could be thwarted. One of the goals of this research is to develop just such models with supporting theory so the

vulnerability community will not be constrained by standard performance comparison practices, if not actual modeling challenges in the DE community.

Of course an EIB threshold concept presents additional challenges to the vulnerability modelers, as well. The size of the bucket is a free parameter that either must be fixed to maximize P_k correlation to dwell time, or allowed to float resulting in a multivariate P_k function. It may be difficult to imagine the latter as a JMEM product, and determining the best bucket size for each target (not to mention the multiple aimpoints of each target) may increase the amount of vulnerability information needed, which can be expensive to gather. As such, detailed modeling and simulation of laser-spot/target interactions could be leveraged to supplement empirical vulnerability data.

Another issue affecting JMEMs analysis is heat dissipation. Given that heating energy absorbed by the target at the beginning of an engagement will dissipate through dispersion or cooling (at least to some extent) throughout the rest of the engagement, there may be an additional time component to P_k determination besides the time factor in fluence or energy accumulation. For example in engagement 1, if a given energy threshold T_E is reached in x seconds, let the outcome be $P_k^{(1)}(x)$, where the superscript 1 is the engagement number. However, in engagement 2 where it takes $2x$ seconds to reach T_E , if dissipation has been significant during the engagement, then it is likely that $P_k^{(2)}(2x) < P_k^{(1)}(x)$, even though they reached the same threshold T_E . This kind of target characterization would be useful, especially for the dense target environment where it is desirable to minimize the total dwell time across all targets.

Finally, some of these $P_k(x)$ issues are moot when the concept of operations depends on observation of secondary effects (*e.g.*, secondary explosion, halt of operation)

for determining when/whether the kill occurred. However, even in this paradigm, it is nonetheless desirable to know ahead of time approximately how long it will take to achieve the secondary effect. This is true for both mission planning models and for systems analysis and wargaming models.

3. Characterizing Defocus as Means to Improve No-Turbulence ATG COIL Performance

3.1. Introduction

The Department of Defense is developing a concept demonstrator of a high energy laser (HEL) air-to-ground weapon called the Airborne Tactical Laser (ATL). The ATL is being constructed with a chemical oxygen iodine laser (COIL), which operates at wavelength of $1.315\ \mu\text{m}$. Unfortunately, although COIL devices can generate high laser powers for propagation, $1.315\ \mu\text{m}$ light is readily absorbed by any water vapor in the atmospheric path. This absorption reduces the laser power that reaches the target, and if the atmospheric heating that accompanies the absorption is severe enough, the beam will also become distorted by resulting air density fluctuations in the optical path in a process called thermal blooming. Thermal blooming distortion usually reduces the peak irradiance of the laser spot at the target. One possibility for mitigating this effect of thermal blooming for a given engagement scenario is to focus the beam at a point beyond the target during propagation rather than directly at the target. When thermal blooming is a significant effect, the marginal reduction in the thermal blooming distortion is often a stronger function of relative defocus than is the defocusing effect itself on peak irradiance in the absence of absorption. When this is the case, peak irradiance of the laser spot at the target will rise, then crest, and then fall as a function of relative defocus. Thus, in many thermal blooming conditions, an appropriate amount of defocus should improve the overall peak irradiance at the target over the focused case.

Defocus has been known for some time to be a primary contributor to correction for thermal blooming in the presence of convection [Bradley and Herrmann, 1974; Kanev

et al, 1998]. Typically defocus is discussed as a portion of the optical wavefront correction. Wavefront correction implies that wavefront aberrations near the transmitting aperture are the subject interest in those articles, since phase correction is less effective as the aberrations occur at increasing distance from the aperture. In the air-to-ground case, however, most of the thermal blooming aberration occurs far from the aperture since the weapon platform is moving at aircraft velocities (high effective wind velocities reduce thermal blooming near the aperture) in less absorptive air at altitude, and the target on the ground is stationary in our case, though subject to wind, and in a more absorptive atmosphere. In view of this, we find it valid to think of defocus not as a wavefront correction, but as a method to reduce the thermal blooming distortion number, N_D , as compared to the focused case, with the resulting improvement in the Strehl ratio due to thermal blooming.

Further, it would be useful to know the conditions under which defocusing the beam will be beneficial to increasing peak irradiance of the laser spot on target, and when these conditions are met, knowledge of the optimal defocus distance, as well as the expected peak irradiance itself will be important. Not surprisingly, these results are highly multivariate functions of the engagement scenario, depending on, for example, atmospheric absorbance and scatter, optical path wind profile, laser power and beam profile, aperture specifications, range to target, and strength of turbulence. Wave optics simulations that account for these variables have been available for many years to study thermal blooming and other atmospheric effects. For this study, we are using Science Applications International Corporation's (SAIC's) Atmospheric Compensation Simulation (ACS). ACS is a Fortran-based code written and maintained by Donald Link

[2005] that can run on UNIX, LINUX, or WINDOWS platforms. The scenario and the weapon systems parameters are read by ACS from a text file, and in addition to these settings, many parameters have to be established including numbers and resolution of phase screens, number of replications to average, simulation time step, dwell time, and delay before gathering statistics. Output files include the irradiance profiles at the target with and without atmospheric distortions, and summary statistics for the engagement.

The important finding for this chapter is that all operating conditions studied herein benefited in terms of peak irradiance from having some amount of defocus. Since operating with a focused beam is an arbitrary decision (at least in the presence of thermal blooming), it should be relatively inexpensive to add defocusing capability to existing designs or operating procedures. Also, since there are other effects that may cause beam spreading in ATL scenarios, such as diffraction due to aerosols [Sadot *et al.* 1994] or aero-optic effects at the beam turret, we may find that weapons operated at thermal blooming wavelengths are not negatively impacted by these phenomena if the spreading effects are no larger than the spreading associated with optimal defocus. On the other hand, we note that time-averaged spreading due to turbulence does not always mitigate the thermal blooming effect, and often worsens it.

To illustrate these findings, the Breaux thermal blooming distortion number (N_D) is reviewed and a baseline scenario is defined. We then examine the sensitivity of system performance in many dimensions of the scenario which shows how much defocus is advisable and how much improvement might be gained. Finally, we present a modification to the Breaux N_D that makes defocus accessible as an added feature in scaling laws that use Breaux N_D .

3.2. Thermal Blooming Distortion Number

Historically, the effect of thermal blooming has been discussed with respect to the thermal blooming distortion number, N_D . N_D is designed to be a scaling variable that is correlated to blooming effect and which relates the effect of engagement scenario parameters to each other. For example, according to the N_D formula [see (3.1) below], the effect of doubling the wind (which reduces N_D), is the same as halving the power. There have been prominent scaling laws relating N_D to peak irradiance at the target plane that have been given by Smith [1977], Gebhardt [1990], and Breaux [1979]. These relate N_D to thermal blooming Strehl ratio, S_{TB} —the ratio of peak irradiance with thermal blooming to peak irradiance with no thermal blooming (but including power loss due to absorption)—which is a decreasing function of N_D .

Origination of N_D is often attributed to Bradley and Herrmann [1974], though Smith and Gebhardt [1971] had a similar construct. It was cast into integral form by Breaux [1979] among others (*e.g.*, Magee *et al.* [2005]), and Breaux's was modified by St. John *et al.* [2003] to explicitly include effective wind velocity (V_E) in the integrand rather than merely a scaling factor to account for slewing. St. John *et al.* also moved absorption coefficient (α_{abs}) and temperature (T) under the integral since those will vary with altitude, an important dimension in the ATL case. Starting with Bradley and Herrmann and leveraging the others' developments, formulation for N_D used in our research, then, is as follows:

$$N_D = \frac{kPT_0(-\partial n/\partial T)}{\rho c_P n_0} \int_0^{R_{target}} dr \frac{1 - (r/R_{target})}{\sqrt{a_{geom}^2(r) + s^2(r)}} \cdot \frac{\alpha_{abs}(r)\tau(r)}{V_E(r)T(r)} \quad (3.1)$$

where k is the wave number, P is laser power, T_0 is a temperature baseline (300 K, for this research), $\partial n/\partial T$ is the rate of change refractive index with respect to local temperature, ρ is air density, c_P is the specific heat of air, n_0 is the unperturbed refractive index of air, and R_{target} is the distance from the aperture to the target plane. The integration proceeds from the aperture to the target and, in addition to those functions mentioned earlier, the integrand consists of these functions of position along the optical path: a_{geom} is the ray-optics radius of the beam, s is a specialized function developed by Breaux [1979] that contains the spread of the beam due to diffraction and beam quality effects as well as an estimate of the spread due to blooming (the latter added to improve correlation of his scaling law), and τ is the transmission. St. John *et al.* added turbulence and other linear effects to s in their modeling. Note in Eq. 3.1 that the contribution of each portion of the beam to N_D is inversely related to the beam size at that point. However, Breaux also recommends weighting each beam position by the proportion of the path remaining to the target (*i.e.*, path leverage), hence the $1 - (r/R_{target})$ in the numerator. Because of this as well as the inclusion of s , we will refer to Eq. 3.1 as the Breaux N_D formulation. We note that Bradley and Hermann rejected path weighting by leverage and beam size since those tend to cancel each other out in the focused case; this reasoning is superseded by inclusion of Breaux's spreading term.

We follow St. John *et al.* as well as Magee *et al.* in modeling the transmission function in Eq. 3.1 as follows:

$$\tau(r) = \exp\left(-\int_0^r dr' [\alpha_{abs}(r') + \alpha_{scat}(r')]\right) \quad (3.2)$$

where α_{scat} is the scattering coefficient.

The construction of Eq. 3.1 suggests that it could be applied to defocused beams by modifying the beam size function, a_{geom} , to something other than the target-focused case. As we will show, however, it is not so simple. The difficulty lies in the special spreading function s , the estimated blooming portion of which appears to have been developed for the focused case. As a result, s dominates a_{geom} in the root-sum-squared (RSS) under the integral near the target for the defocused cases; this results in little change in calculated N_D as a function of defocus. Since wave-optics shows that defocus can result in significant improvement of peak laser intensity at the target in the air-to-ground case, the Breaux N_D cannot be applied without modification in a scaling law that seeks to model the effect of beam defocus.

To overcome this limitation of the Breaux formulation, we leverage Smith [1977] who developed correction factors for various aspects of the collimated thermal blooming case under constant wind and low absorption assumptions. In particular, the correction factor derived for converting a collimated distortion number to that for a focused case is:

$$N_{focus}(a_i/a_f) = \frac{2(a_i/a_f)^2}{(a_i/a_f - 1)} \left[1 - \frac{\ln(a_i/a_f)}{(a_i/a_f - 1)} \right] \quad (3.3)$$

where a_i is the radius of the propagating aperture and a_f is the radius of the spot at the target for the given degree of focus as well as diffraction and other linear effects (such as turbulence and jitter). Fitting our purpose, note that the focus distance, from which a_f is determined, need not be the same as the target distance, but can be beyond it. However, since the Breaux formulation already assumes the beam is focused at the target, determining N_D for a defocused (non-collimated) case requires first dividing Eq. 3.1 by Eq. 3.3 evaluated for the target-focused case, and then multiplying by Eq. 3.3 re-evaluated for the defocused case. N_D 's for defocused settings calculated in this way will be referred to as Breaux and Smith results. Results of this approach are discussed in a later section. Next, we describe a baseline air-to-ground HEL engagement scenario that is useful for evaluating our N_D formulation.

3.3. Baseline Scenario

In order to understand how a notional ATL will respond to defocus in view of the many factors that determine performance, we first establish a baseline air-to-ground scenario with two laser power values. We will then later examine sensitivities and expand our scope. Here are the particulars of the *baseline scenario*:

- Weapon platform: 2 km altitude, 100 m/s due east velocity vector
- Target point: located east of platform, on ground at sea level, and stationary;
6000 m slant range from platform
- Laser aperture: 0.5 m diameter, 30% single-axis central obscuration
- Atmosphere: 1976 US Standard for temperature [St. John, *et al*]; the Mani atmosphere for absorption and scattering (molecular and aerosol) [2004], Bufton

wind model with 10 m/s wind at ground from the north [St. John, *et al*]. No turbulence is assumed for most of the analysis. When turbulence is included, the HV 5/7 atmosphere is assumed [St. John, *et al*].

- Laser powers at aperture: 50 and 100 kW continuous wave, beam quality 1.0, uniform beam profile
- Beam control: closed-loop tracker for tilt correction only, no higher order correction

Figure 3.1 provides an illustration for many of these baseline scenario settings.

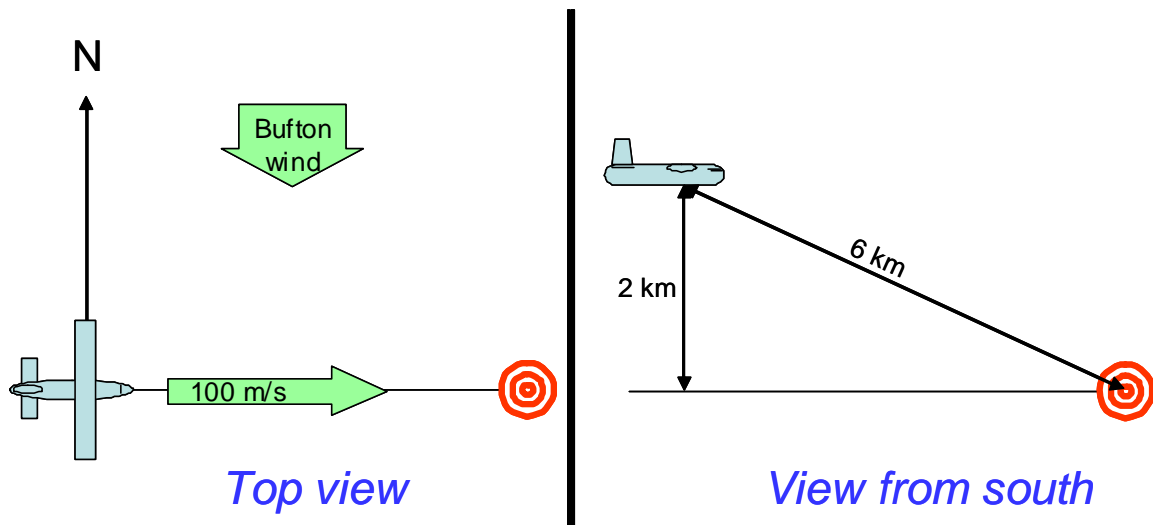


Figure 3.1. This is a graphical illustration of some of the baseline scenario settings: range, altitude, velocity, wind, and platform orientation to target.

In addition, for each of the variables described above, a range of settings is explored including the following.

- Weapon altitude: two, three, and four km
- Velocity vector: 100 m/s east and 100 m/s north
- Slant range: 3000, 4500, 6000, and 9000 m

- Laser power: 50, 75, 100, 125, 150, 175, and 200 kW
- Wind: 0.25x, 0.5x, and 1x Bufton from north
- Aperture central obscuration: 10% and 30% one-dimensional
- Turbulence: no turbulence (0x), 0.5x, 1x, and 2x Hufnagel-Valley 5/7 (HV5/7)
- Absorption and scatter: 80 percentile winter and 80 percentile summer mid-latitude

The absorption dimension is not single-valued, since it is a function of altitude, and we also include with it extinction due to scatter. Table 3.1 contains the combined molecular and aerosol absorption and scattering coefficients for the baseline (Mani) assumption, and the 80-percentile summer case. The Mani atmosphere constitutes an approximately an 80-percentile winter case. Note that the scattering (which is primarily due to aerosols) is left approximately unchanged between the cases.

Table 3.1. Combined absorption and scattering coefficients due to molecular and aerosol effects in this study.

Atmosphere	Altitude (km)	α_{abs}	α_{scat}
Mani (80-percentile winter)	0	0.03755	0.05376
	1	0.01905	0.02377
	2	0.00827	0.00702
	3	0.00401	0.00305
	4	0.00199	0.00169
80-percentile summer	0	0.06681	0.05376
	1	0.06226	0.02377
	2	0.02103	0.00701
	3	0.01187	0.00304
	4	0.00656	0.00168

The scope of this research did not allow for all combinations of these settings to be investigated, but the baseline scenario is used as a pivot point to investigate these variables one at a time. However, in several instances we changed more than one parameter to investigate interactions between scenario variables.

3.4 Phase Screen Modeling Requirements

Modeling ATG COIL engagements of interest to this research in ACS began with an initial model set up that included ten phase screen positions in the optical path to represent turbulence and blooming. This appeared to be a standard approach based on discussions with several in the HEL modeling community [Link, Vernon, Magee], though Link did document that while ten phase screens was understood to be adequate to represent turbulence, it had not been shown at that time to be adequate for representing thermal blooming. Further, the emphasis of many studies in the past two decades was ground to space, following the prevailing ballistic missile defense (BMD) interest. From a thermal blooming standpoint, BMD scenarios are fundamentally different than ATG scenarios since for BMD, the beam remains collimated while in the atmosphere, and most thermal blooming will occur near the aperture; whereas, the opposite of these is true for the ATG scenario as discussed above.

Nonetheless, significant data was gathered from ACS runs for ATG scenarios using ten phase screens, in part to build a comparison to previous studies that used similar phase screen count [Vernon and St. John] and also to avoid concern about having phase screens too close to each other [Link]. The latter is important since ACS generates the screens independently of each other, and having independent phase screens too close to one another can result in an overall turbulence effect that is more severe than intended

since turbulence in the atmosphere is spatially correlated. It was not until we began defocus investigations that inaccuracies arose caused by too few phase screens for properly modeling thermal blooming, though it was not clear at the time what the culprit was. Not surprisingly, the number of phase screens has an additional dynamic when turbulence is included in the model. This will be addressed in Chapter 4.

3.5 Phase Screen Selection

When using wave-optics to simulate thermal blooming, one typically divides the atmosphere into slabs, the refractive effects of which are each represented by thin phase screens. The refractive effects modeled here are turbulence, when assumed, and the interaction of the beam with the atmosphere through thermal blooming. Experience has shown [Link, 2003] that for the baseline scenario, ten phase screens are adequate to model the turbulence. However, we discovered ten screens are not adequate for accurately capturing thermal blooming effects.

In order to find an adequate number of phase screens to capture thermal blooming, we started with the baseline scenario at 150 kW for added conservatism with respect to thermal blooming, since the appropriate number of phase screens for the 150 kW power level should be adequate for power levels near or below that value. Then, using ten phase screen placements as a first case, phase screens were added on the target side of each existing phase screen to come up with 20, 30, and 40 phase screen distributions. Figure 3.2 shows the phase screen density as a function of altitude for each of these cases.

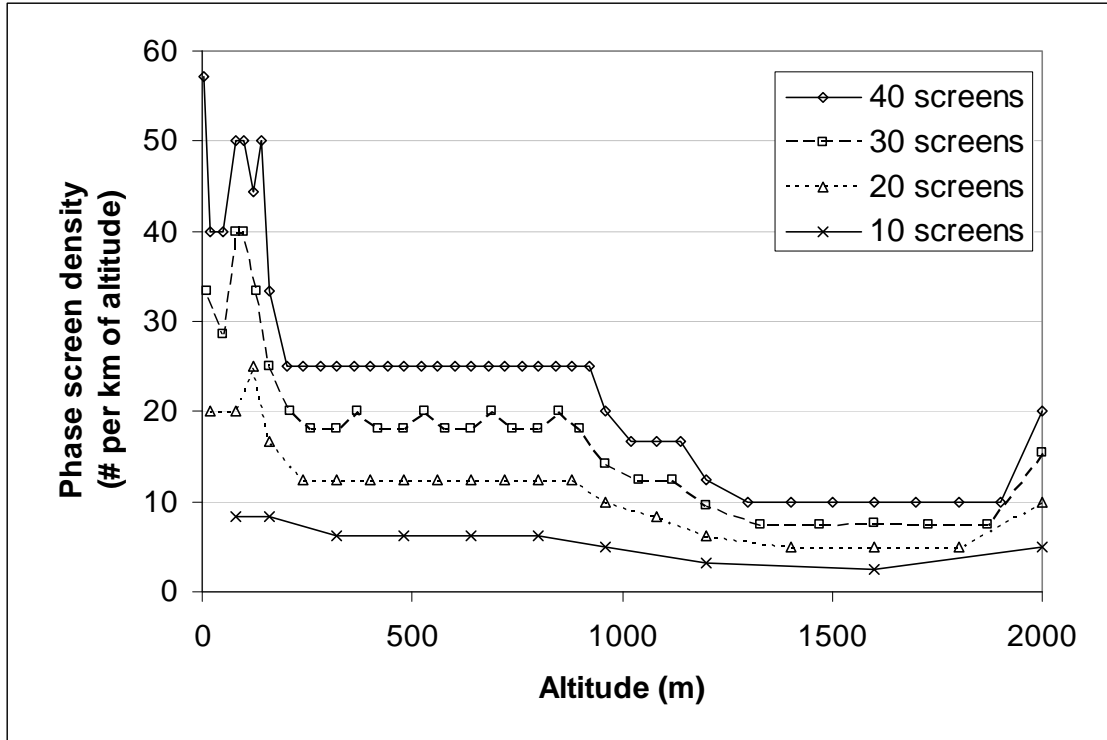


Figure 3.2. Phase screen density as a function of altitude for 10, 20, 30, and 40 screen cases.

Note that the phase screens are not uniformly distributed. There are three reasons for this. From the perspective of turbulence, the strength of turbulence is higher near the ground, calling for increased turbulence screen density near the ground. From the perspective of thermal blooming, there are two issues: Absorption is worse near the ground and the beam is coming to a near-focus near the ground, meaning the strength of thermal blooming is significantly biased toward the target for our analysis. The location of the most powerful thermal lensing effect near the target is illustrated by the fact that in the 20 phase screen case, we deleted the five new phase screens nearest to the laser aperture to come up with a 15 screen case, and the results were nearly identical to the 20 screen case. This suggests the additional screens near the aperture are much less important than the additional screens near the target. To get the phase screen density for

an optical path for a given platform altitude, one would multiply the altitude density by $\cos(\theta)$ where θ is the zenith angle of the platform from the target. Figure 3.3 illustrates how the altitude density relates to various path densities for slant ranges of 3000, 6000, and 9000 at the 2 km platform altitude.

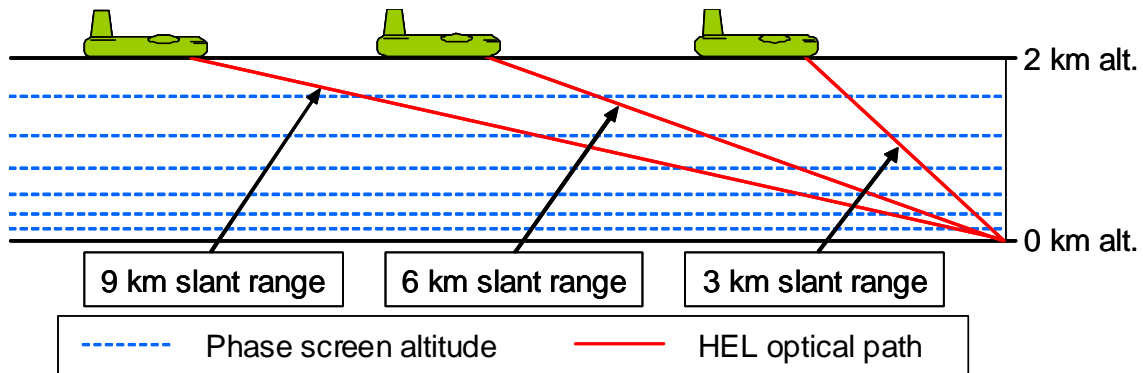


Figure 3.3. Schematic of path phase screen density as it relates to altitude density. Phase screens are placed perpendicular to the optical path at the intersection of the optical path and the altitude position. The dashed blue lines are representative phase screen altitudes with increasing density near the ground.

Next, we run the 150 kW scenario with each phase screen density in ACS for the focused beam (6000 m) and a range of defocused cases (6100 m to 7500 m) to determine the peak irradiance function of focal range for each phase screen density case. By observing the change in the function with each increment in phase screens (10 to 20, 20 to 30, and 30 to 40), it was determined that by the time 30 phase screens are used, the peak irradiance function had adequately stabilized. Figure 3.4 shows the magnitude percentage change in the peak irradiance values for each increment, plotted as a function focal length. As seen there, increasing the number of phase screens from 30 to 40 results in changes that are only 1% or smaller in magnitude. Table 3.2, shows the average irradiance change across the focal lengths of 6000-7500 m for each increment. The reason 30 screens is used instead of 40 is that additional phase screens significantly

increase the simulation run time, so the minimum number of screens that adequately represents the effect is desirable.

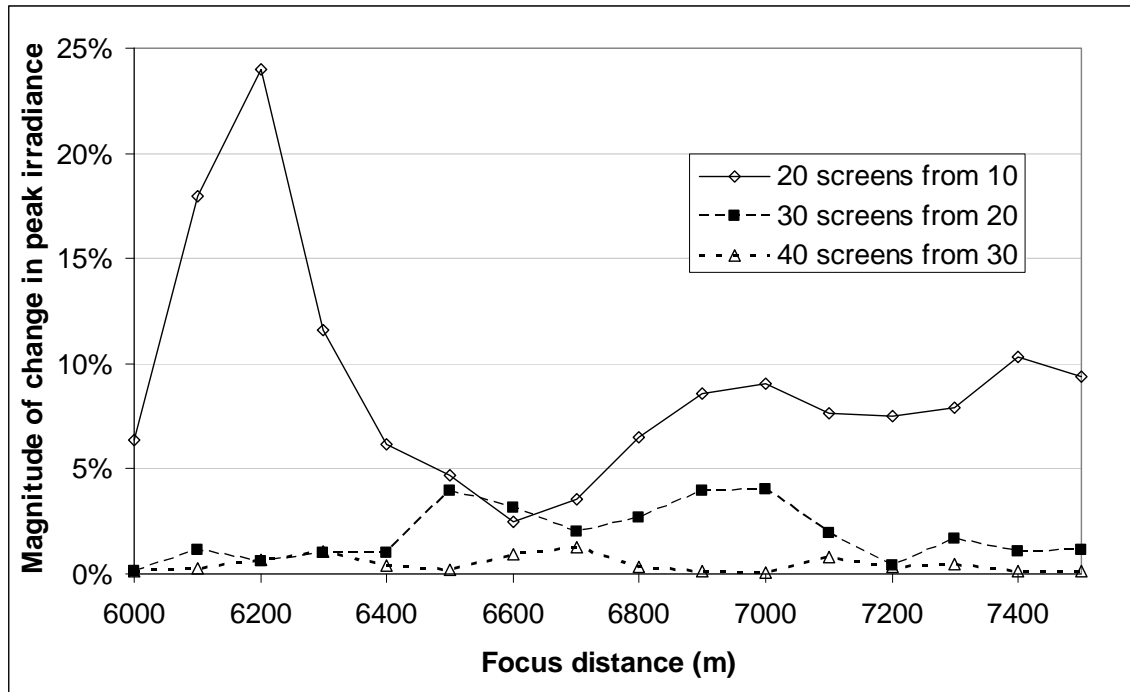


Figure 3.4. Effect of increasing phase screens on peak irradiance.

Table 3.2. Average across focus ranges 6000-7500 m of magnitude percentage change in peak irradiance for each increment increase in phase screen number

Phase screen change	20 screens from 10	30 screens from 20	40 screens from 30
Average change in peak irradiance	9.0%	1.5%	0.5%

While there is no penalty, besides simulation run time, for using more screens with respect to thermal blooming, there is a potential difficulty with high screen densities and modeling turbulence under certain assumptions we make, such as statistical independence of the turbulence phase screens. However, there were only negligible differences between baseline scenario peak irradiance values with thermal blooming off and turbulence turned on across phase screen density space described above. This is

possibly due to the fact that the atmospheric coherence length is on the order of the diameter of the aperture for these scenarios and is discussed in more detail in Chapter 4.

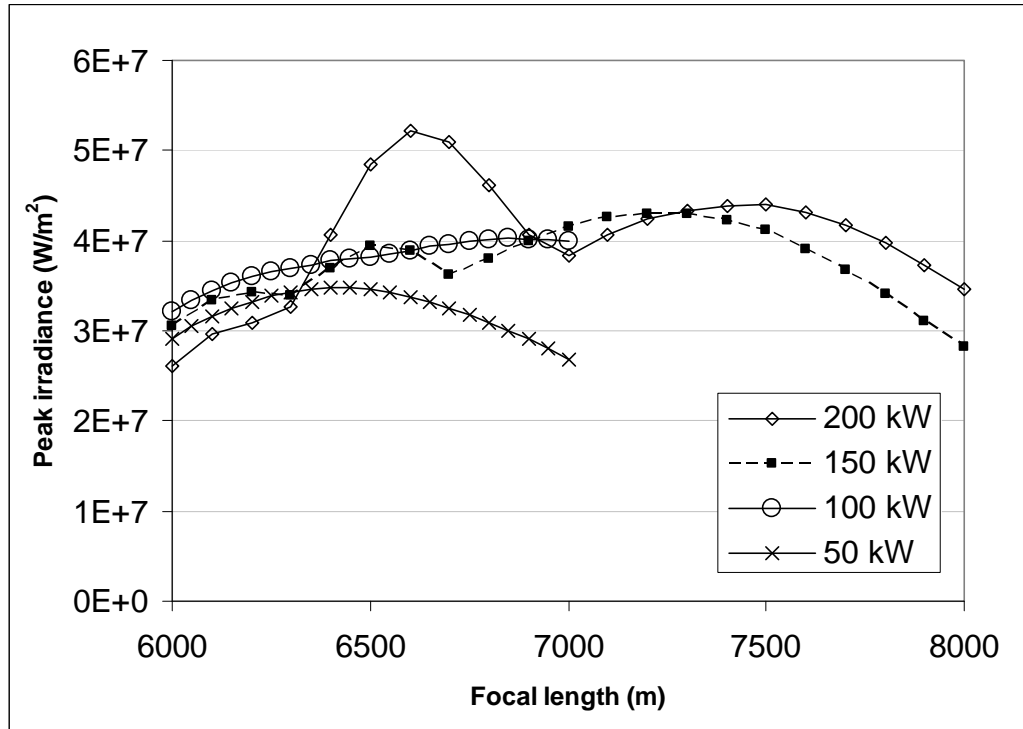


Figure 3.5. Peak irradiance as a function of focal length for baseline scenario with 30% central obscuration.

3.6. ATG HEL Scenario Performance Under Defocus

Using the baseline scenario, let us first illustrate the effect of using defocus to improve peak irradiance at different power levels under the assumption of each central obscuration size. Figure 3.5 shows the peak irradiance curves as a function of focal length for the 30% obscuration, while Figure 3-6 show the same curves for the 10% obscuration.

Note in Figure 3.5 that as power exceeds 100 kW, a higher order local optimum in the peak irradiance function emerges just as focal distance passes 6500 m. As shown in Chapter 4, HV 5/7 turbulence washes that optimum out, while leaving the second

optimum intact. For the purpose of investigating defocus distance relationships to peak irradiance, those local optima which are not washed out by turbulence will be used.

Figure 3.6 shows that the peak irradiance functions for the 10% obscuration case are unimodal across the power range of interest here. Also, it is apparent that the optimal defocus distance is not as strong a function of power as it is for the 30% obscuration case. However, turbulence interacts with the 10% obscuration optima more severely than it does the 30% obscuration optima so that when the obscuration is 10%, the optimum focal length will be impacted by turbulence more than the 30% obscuration case. Again, this will be explored further in Chapter 4.

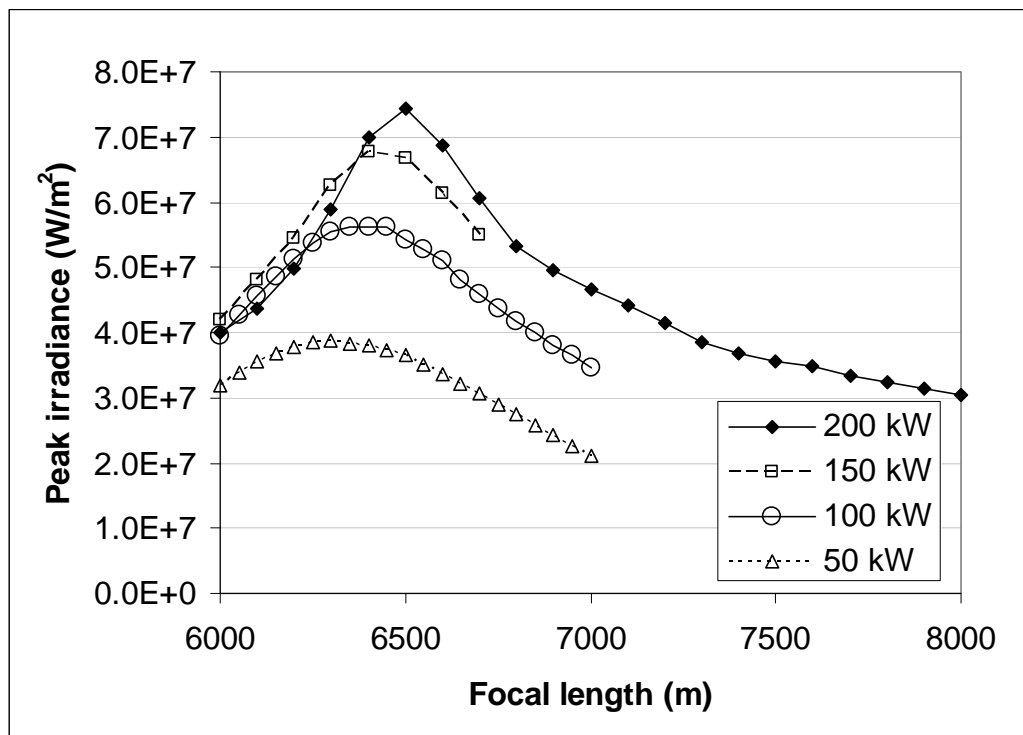


Figure 3.6. Peak irradiance as a function of focal length for baseline scenario with 10% central obscuration.

Using these results, we plot peak irradiance as a function of output laser power for the baseline scenario at focused and optimally defocused settings for both obscuration

assumptions (Figure 3.7). The power for which this function begins to decline rather than rise is known as the *critical power*. Figure 3.7 shows the peak irradiance functions for these cases. In each case, under the no turbulence assumption, optimal defocusing pushes the critical power to 200 kW or higher from approximately 150 kW (10% obscuration) and 100 kW (30% obscuration) for the focused cases. Also, the 10% obscuration case appears to have a distinct peak irradiance advantage over the 30% obscuration case, particularly under optimal defocus. This peak irradiance advantage will not be as pronounced under turbulence but it is still noteworthy. Turbulence likewise balances the disproportional defocusing improvement factor enjoyed by the 10% obscuration case (1.42 at 100 kW versus 1.25 for 30% obscuration case) under no turbulence.

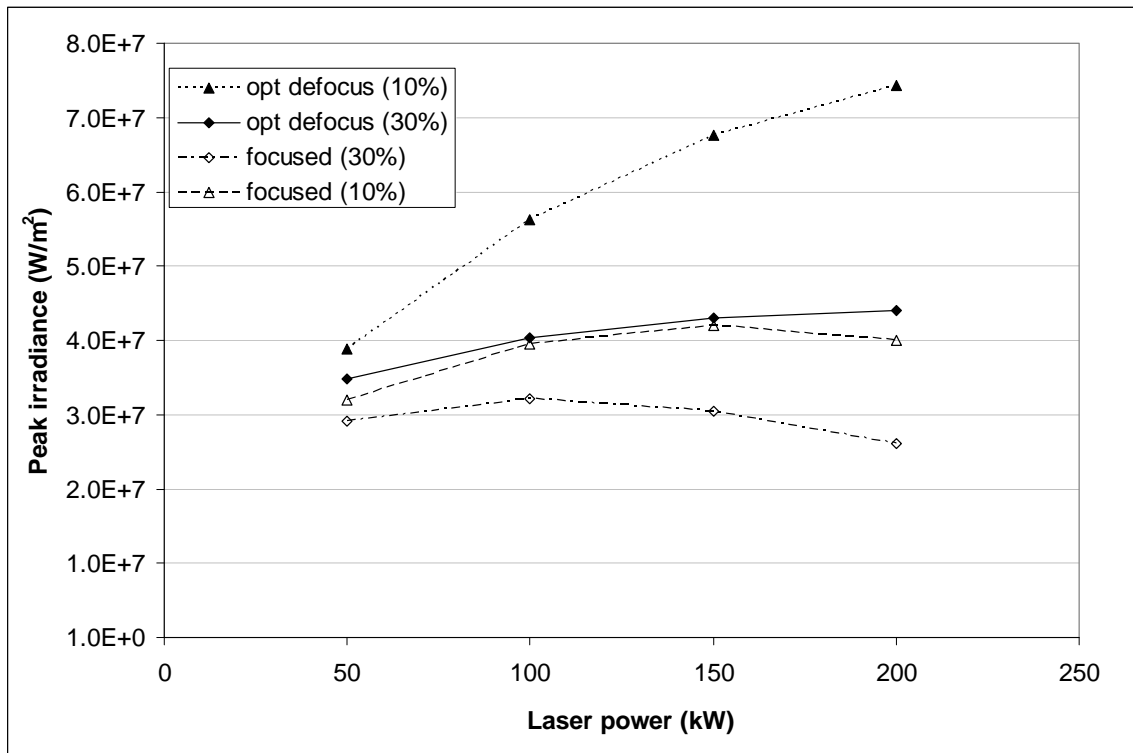


Figure 3.7. Peak irradiance as a function of power for the baseline scenario, focused and optimally defocused cases, by aperture obscuration size (10% and 30%).

3.7. Velocity Vector Relative to Target

The difference in behavior of the two obscuration sizes is present in all aspects of variation from the baseline scenario that were investigated. In particular, one scenario variable setting that represents a globally better operating variation from the baseline is that of having the velocity vector perpendicular to the target vector as depicted in Figure 3.8 (*e.g.*, north), rather than having the platform moving east toward the target. These will be referred to as “perpendicular” and “parallel” propagation, respectively. This time for perpendicular propagation, we repeat graphs of the irradiance functions of focal length with velocity vector north for the 30% obscuration case (Figure 3.8) and the 10% obscuration case (Figure 3.9).

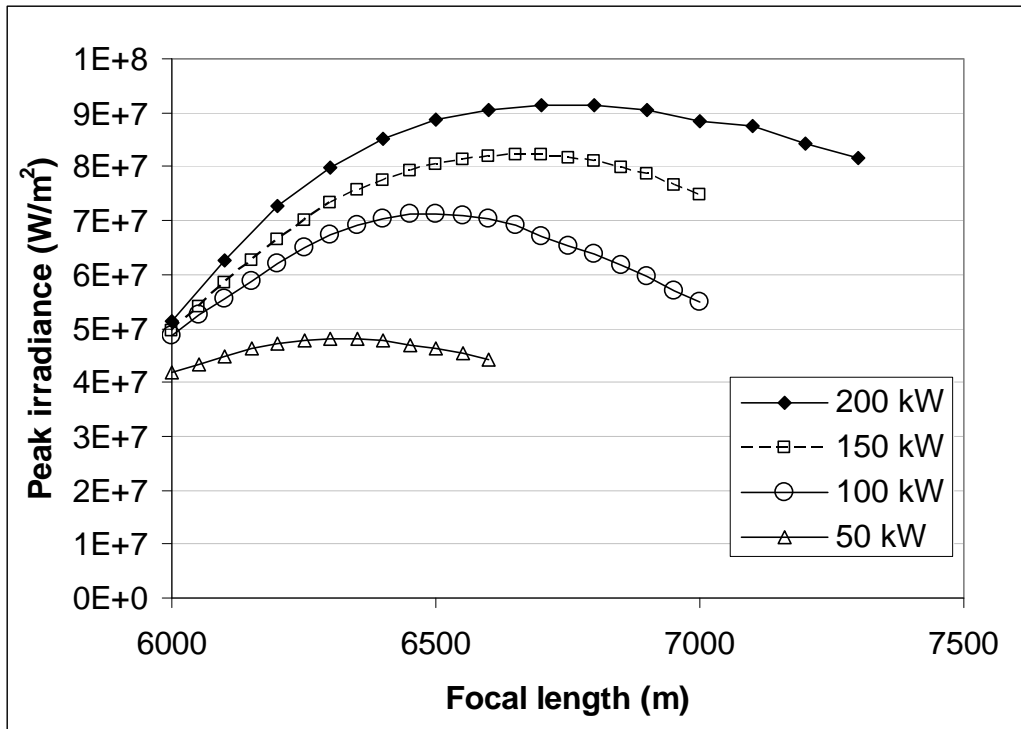


Figure 3.8. Irradiance functions of focal length for perpendicular propagation and 30% obscuration.

As in the case of parallel propagation, the 10% obscuration optima are generally sharper, higher, and occur at shorter focal lengths than the 30% obscuration cases. From these data, we build the critical power graph shown in Figure 3.10, and we see that again, critical power is increased to 200 kW or more from about 100 kW by using defocusing, and that the 10% obscuration case benefits more from defocus than does the 30% obscuration case.

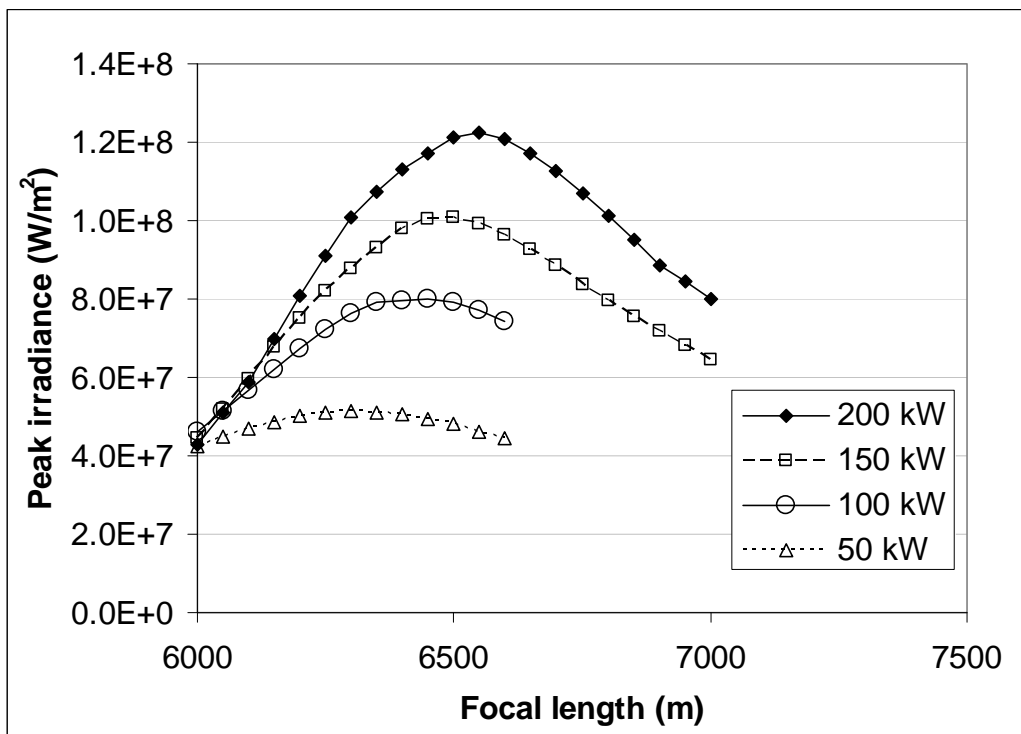


Figure 3.9. Irradiance functions of focal length for perpendicular propagation and 10% obscuration.

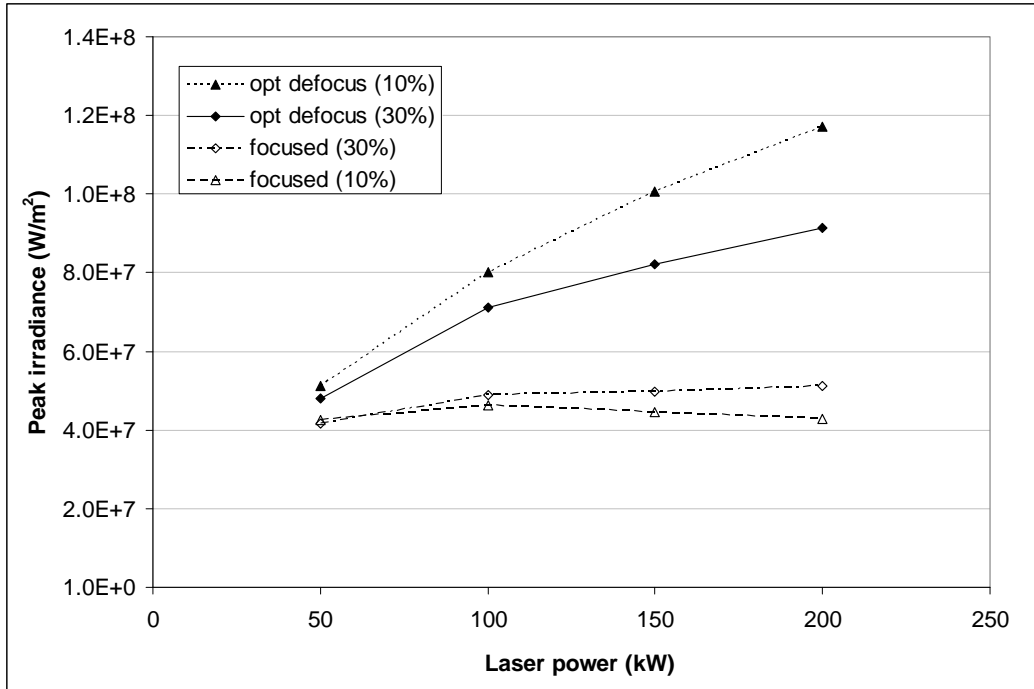


Figure 3.10. Peak irradiance as a function of power for the perpendicular propagation version of baseline scenario, focused and optimally defocused cases, by aperture obscuration size (10% and 30%).

As mentioned, perpendicular propagation is a globally better operating condition than in parallel propagation for the otherwise baseline scenario. The reason for this is that the effective wind velocity through the atmospheric beam tube is significantly higher when the platform is shooting to the side rather than forwards at a slightly depressed angle. This reduces N_D according to Eq. 3.1., and improves thermal blooming Strehl. Figure 3.11 shows the improvement factor achieved with no turbulence by using perpendicular propagation.

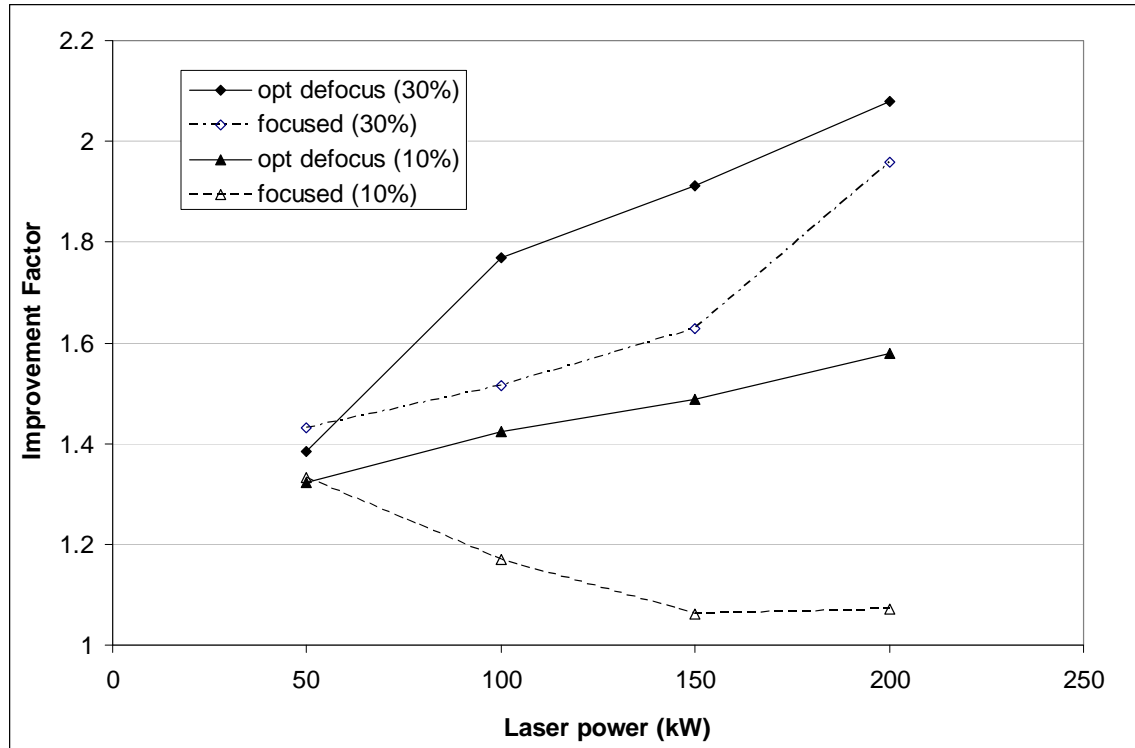


Figure 3.11. Improvement factor for perpendicular propagation versus parallel propagation for otherwise baseline scenario, focused and optimally defocused cases, by aperture obscuration size (10% and 30%).

3.8. Target Range

Peak irradiance at the target plane in a vacuum propagation is well known to be inversely proportional to the square of the range. In an absorbing atmosphere, increasing range also increases the absorption and usually increases the severity of the thermal blooming, which only strengthens the inverse relationship between peak irradiance and range.

The payoff due to optimal defocus is also a function of range as well as obscuration size. Figure 3.12 shows the improvement factor for defocus rises from 1.15 to over 1.3 for the 30% obscuration as range increases from 3 km to 9 km for an otherwise baseline scenario. For the 10% obscuration, the improvement factors are higher, rising from 1.28 to 1.54 over the same range. (These improvement factors appear

to be biased a bit low since they are calculated using wave optics data gathered using only 20 phase screens. A 30 phase screen anchoring point is plotted to illustrate that bias.)

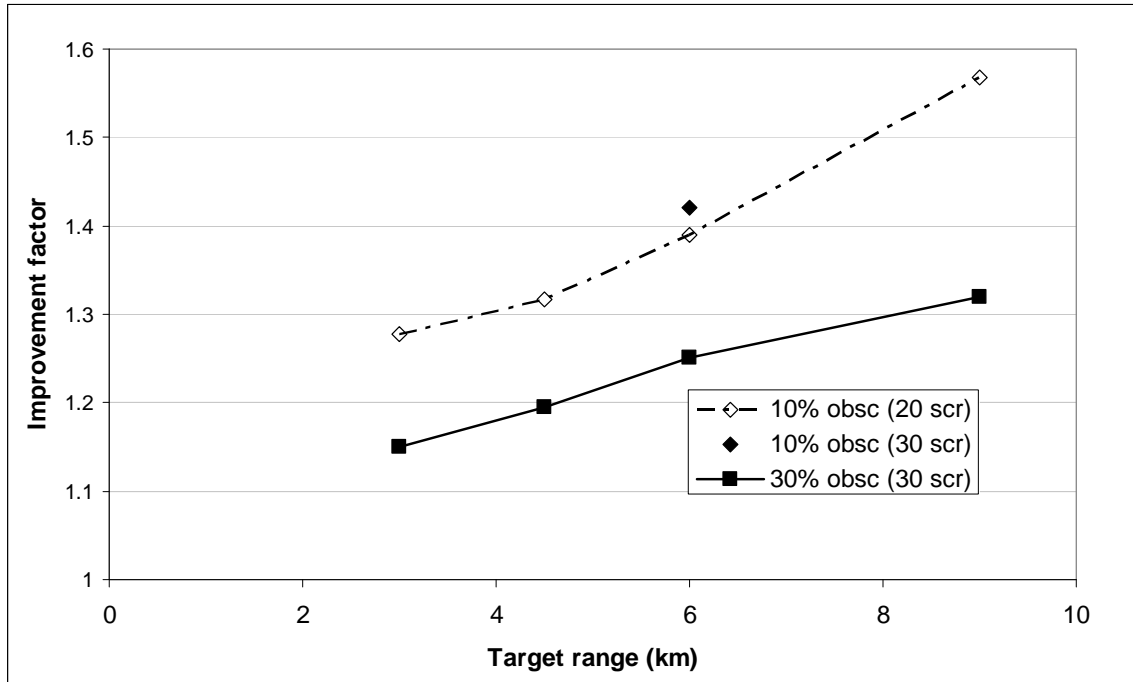


Figure 3.12. Improvement of target peak irradiance at optimal defocus over focused case as function of range to target of otherwise baseline scenario. Note: 10% obscuration dash-dot line is comprised of 20 phase screen results; 10% obscuration & 30 phase screen result at range = 6 km (solid diamond) added as reference to suggest 20 screen line may be biased a bit low.

The peak irradiance values for the baseline scenario (100 kW) for both obscurations and focused and optimally defocused settings are contained in Table 3.3. While the 10% obscuration has a definite advantage over the 30% obscuration under the no turbulence assumption, this advantage is reduced considerably under turbulence as will be shown in Chapter 4. Figure 3.13 graphs the peak irradiance improvement factor of 10% obscuration over the 30% obscuration under focused and optimally defocused

conditions. Recall from above that the optimal defocus distances are different for the two obscurations.

It is also instructive to think of the effect of defocus in the context of the $1/r^2$ rule. As range increases in the baseline scenario from 3 km to 9 km, additional extinction (due to absorption and scatter) occurs, so the $1/r^2$ rule is an upper bound on performance as a function of range. Also, due to the geometry chosen for the baseline scenario, a longer range to target results in a decrease in the angle between the laser propagation vector and the aircraft velocity vector, which in turn reduces the effective wind through the beam path. This increases the thermal blooming distortion number resulting in a reduction in thermal blooming Strehl.

Table 3.3. Target plane peak irradiance values (W/m^2) for given settings by range for otherwise baseline scenario (100 kW).

Range	10 % obscuration (20 phase screens)		30 % obscuration (30 phase screens)	
	Focused	Optimally defocused	Focused	Optimally defocused
3 km	2.73E+8	3.50E+8	2.47E+8	2.93E+8
4.5 km	9.11E+7	1.20E+8	7.46E+7	9.25E+7
6 km	4.03E+7	5.59E+7	3.22E+7	4.03E+7
9 km	1.23E+7	1.92E+7	9.75E+6	1.27E+7

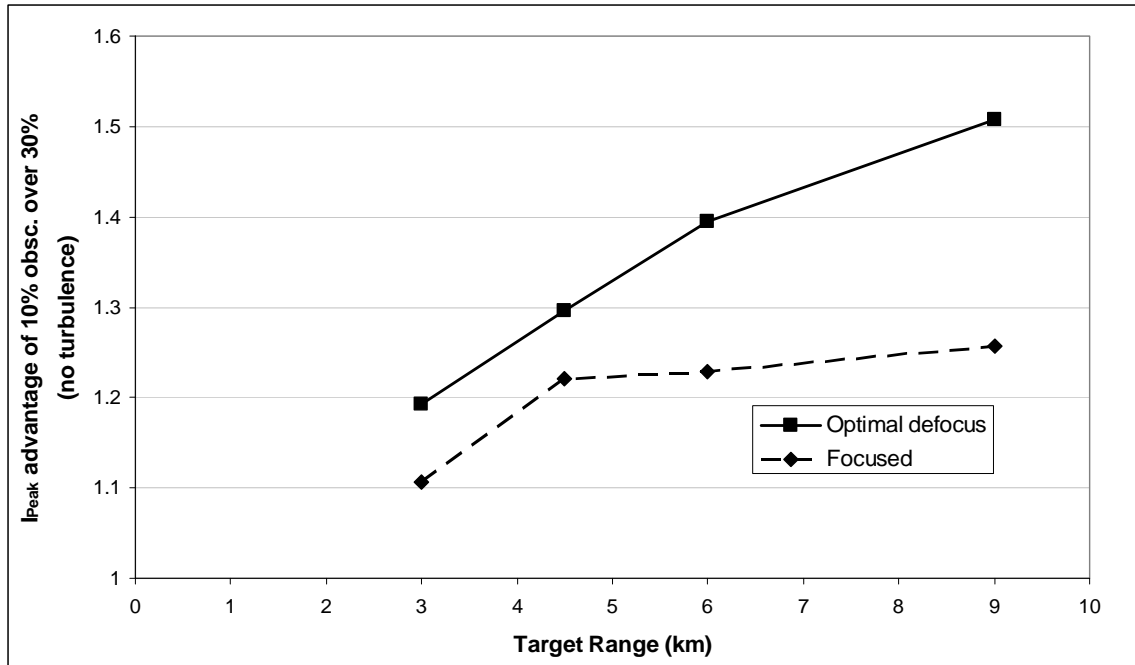


Figure 3.13. Peak irradiance improvement factor of 10% obscuration relative to 30% obscuration by range for otherwise baseline scenario.

Figure 3.14 shows the fraction of peak irradiance relative to the $1/r^2$ rule that is achieved as range increases from 3 km in the baseline scenario. Here we see that the 10% obscuration stays closer to one for both focus assumptions than does the 30% obscuration. Also, the benefit of defocus with respect to recovering $1/r^2$ performance is better for the 10% obscuration. The bottom line from this section is that the smaller obscuration is clearly advantageous over the larger one. However, this analysis has yet to include turbulence, the interaction of which with thermal blooming will impact the advantage we see here.

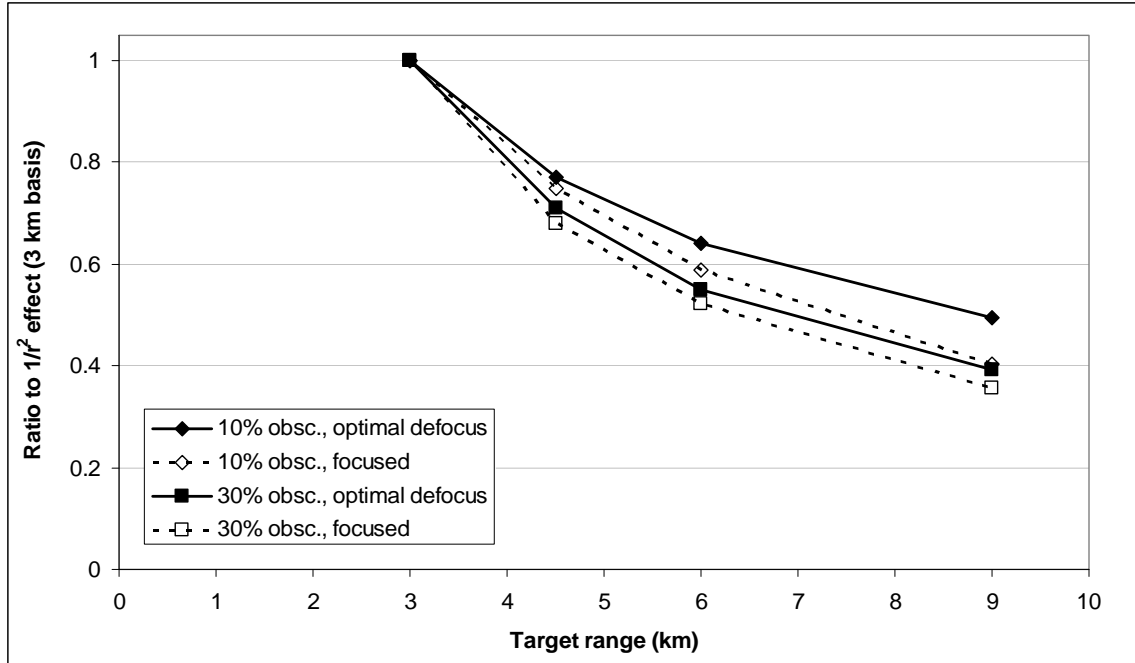


Figure 3.14. Peak irradiance for given obscuration and focus assumptions as a function of range relative to the $1/r^2$ rule applied to peak irradiance at 3 km for otherwise baseline scenario.

3.9. Ground Wind

According to the theory behind the use of scaling laws to predict TB effects in the presence of wind, the thermal blooming distortion number, N_D , should scale inversely with effective wind, especially when the scenario is simple—*e.g.* a collimated beam in a uniform wind for which the N_D contribution is approximately constant along the path. Our baseline scenario is more complex, having a focused beam and effective wind through the beam path at the aperture dominated by the aircraft velocity component perpendicular to the propagation vector; whereas at the target, the ground wind dominates (given our stationary target assumption). However, since the aircraft velocity is high and the beam is most expanded near the aperture, and oppositely, the effective velocity is lowest and beam is most tightly focused near the target, most of the N_D contribution is near the target, so N_D can be expected to vary almost inversely with ground wind. When

this is the case, laser output power and the inverse of the ground wind are aliased in the N_D equation so that halving of the wind is like doubling the power with respect to determining the thermal blooming effect.

The baseline scenario has the ground wind at 10 m/s (approximately 22.4 mph) at the target. Since the wind is from the north, and the target is to the east of the ATL platform, the effective wind at our stationary target equals the ground wind. From the perspective of wind alone, this is probably a best case that can be expected since increased wind increases S_{TB} (*i.e.*, counting on even higher ground wind velocities would be risky). Further, selecting an engagement geometry that has the beam path perpendicular to wind field at the target is also optimal. (The wind field at the target is the resultant of the ground wind and target velocity vectors.) Therefore, we examine the effects of reducing the ground wind in the baseline scenario (and variations) to 5 m/s and 2.5 m/s upon the peak irradiance-defocus relationship.

Figures 3.15, 3.16, and 3.17 illustrate these effects for three scenarios: the baseline scenario with 50 and 100 kW and the 100 kW baseline scenario with 10% obscuration, respectively. Notice that as wind drops, the peak irradiance potential also drops due to increased thermal blooming. Also, notice that the optimal focal range increases as wind speed drops; however, the relationship between these two factors is not as strong in the 10% obscuration case (see also Figure 3.20). In Figure 3.16, the graphs are not unimodal. This phenomenon is most likely related to the multi-modal behavior seen in Figure 3.5 for the baseline scenario with 150 and 200 kW, since wind and power are nearly aliased. These early modes in the 5 and 2.5 m/s lines will probably likewise be lost due to interaction with turbulence as mentioned in the case of the 150 and 200 kW

lines in Figure 3.5. As a result, we record the maximum of the second mode as the peak irradiance point, pointed out by arrows in Figure 3.16. An important caveat to keep in mind is that the data for Figures 3.15 and 3.16 were gathered using 20 phase screens due to time constraints. Based on 20 phase screen results for the 100 and 150 kW baseline scenario cases and for the 10 phase screen results for the 200 kW baseline scenario, the results for this section can still be considered a reasonable approximation to the relationships explored here. The most uncertainty lies in the 2.5 m/s, 30% obscuration, 100 kW baseline scenario: If power and wind are aliased, then this is the near-equivalent to a 400 kW baseline scenario. However, the results for this setting are not discontinuous with the other settings, and further, the largest impact of using too few phase screens is when turbulence is also modeled, which results in the overestimation of the turbulence-thermal blooming interaction. In this chapter, turbulence is not considered.

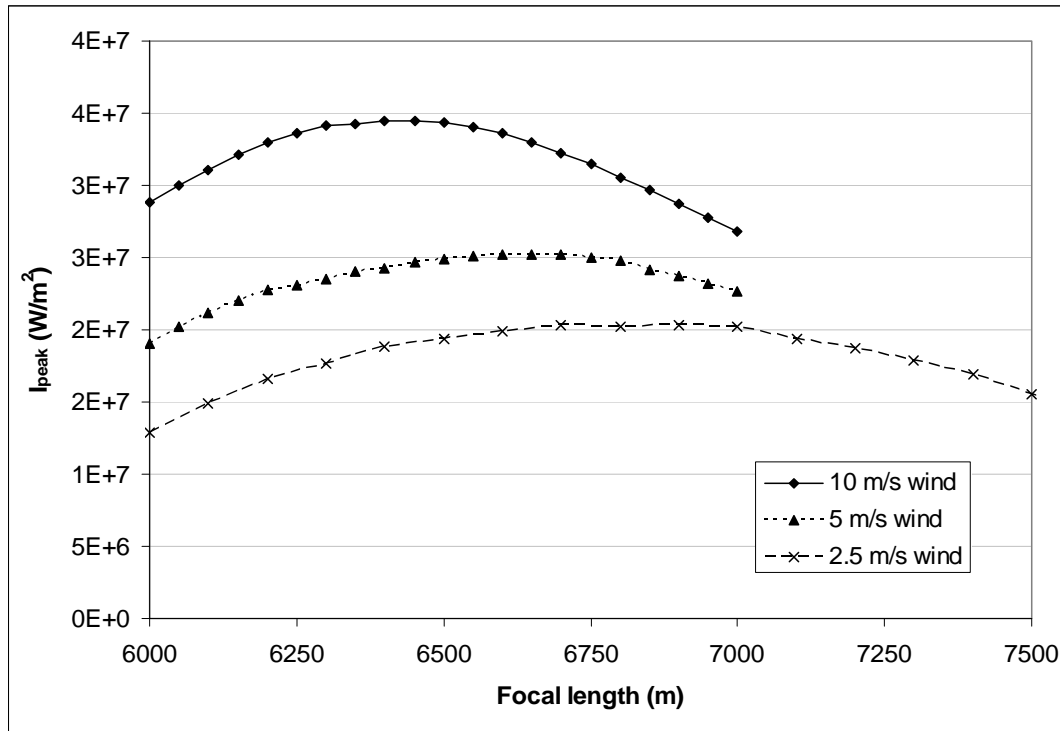


Figure 3.15. The peak irradiance response to defocus for the 50 kW baseline scenario for windspeeds of 10, 5, and 2.5 m/s.

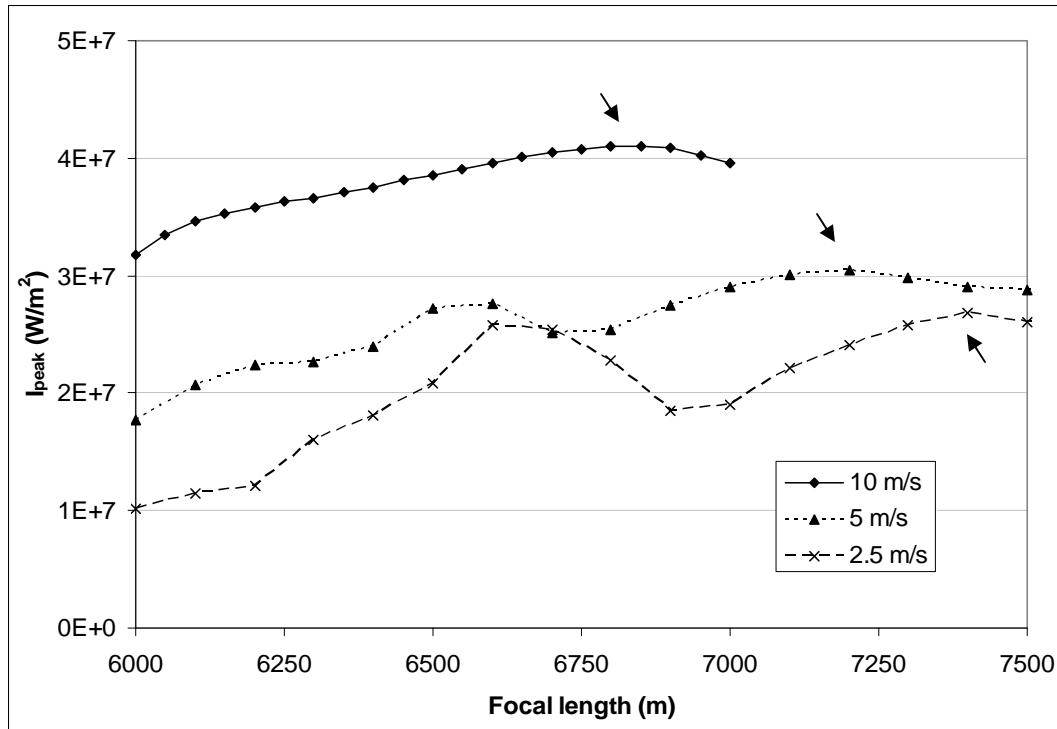


Figure 3.16. The peak irradiance response to defocus for the 100 kW baseline scenario for windspeeds of 10, 5, and 2.5 m/s. Arrows identify optimal performance.

Figure 3.17 shows that the optimal defocus response of the 10% obscuration case to changes in thermal blooming is not as strong as in the other two cases. Also, the peak irradiance is generally higher than the other 100 kW case in Figure 3.16. These data were gathered with 30 phase screens, with the exception of the 2.5 m/s wind case which required 40 phase screens before the graph settled down—and this was with no turbulence. This is likely related to the fact that for scenarios where the optimal defocus multiple is smaller, the more sensitive the peak irradiance function at optimum is to phase screen numbers. This held true for the shorter optimal defocus multiples that occurred for close range engagements on an otherwise baseline scenario. The defocus multiples for all scenario variations can be seen in the composite graph shown in Figures 3.24 and 3.25.

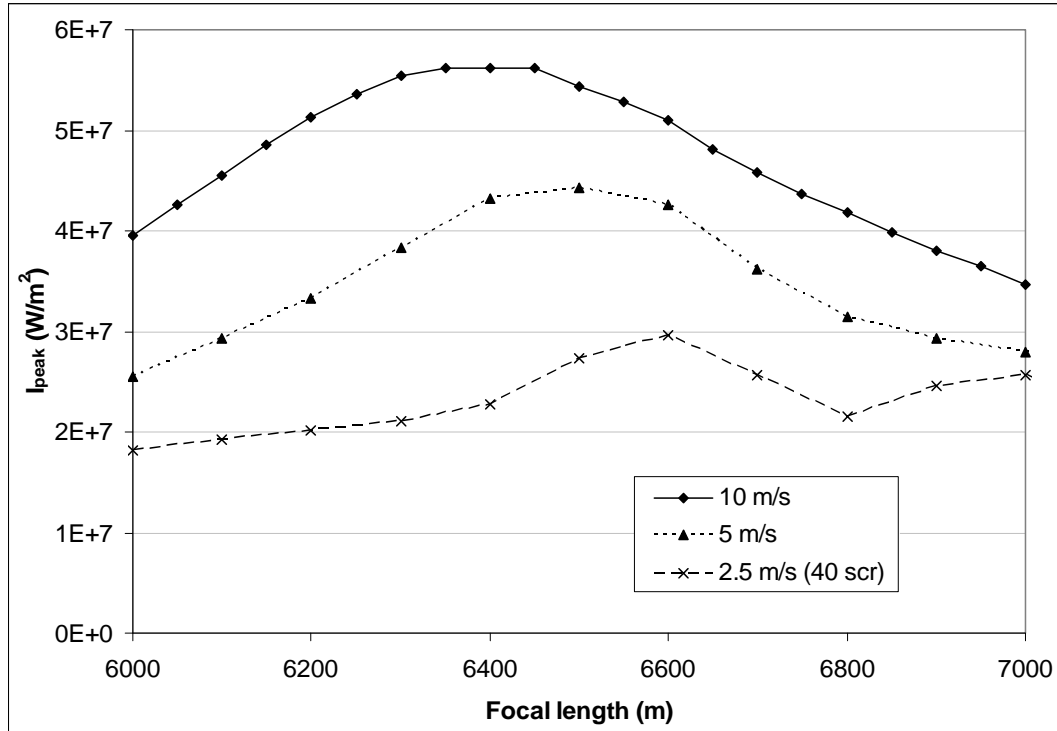


Figure 3.17. The peak irradiance response to defocus for the 100 kW baseline scenario for wind speeds of 10, 5, and 2.5 m/s and 10% obscuration.

Figure 3.18 plots optimal peak irradiance as a function of wind speed for the three scenarios. The most notable feature of this comparison is that the advantage the 10% obscuration has over 30% obscuration at 100 kW appears to fade as wind speed slows to 2.5 m/s (5.6 mi/h) though it remains distinct at 5 m/s (11.2 mi/h). Figure 3.19 highlights the benefit of using defocus for COIL ATG systems. At a wind speed of 10 m/s, our three scenarios show 20% to 40% improvement with defocus. However, the improvement potential increases markedly as wind speed drops.

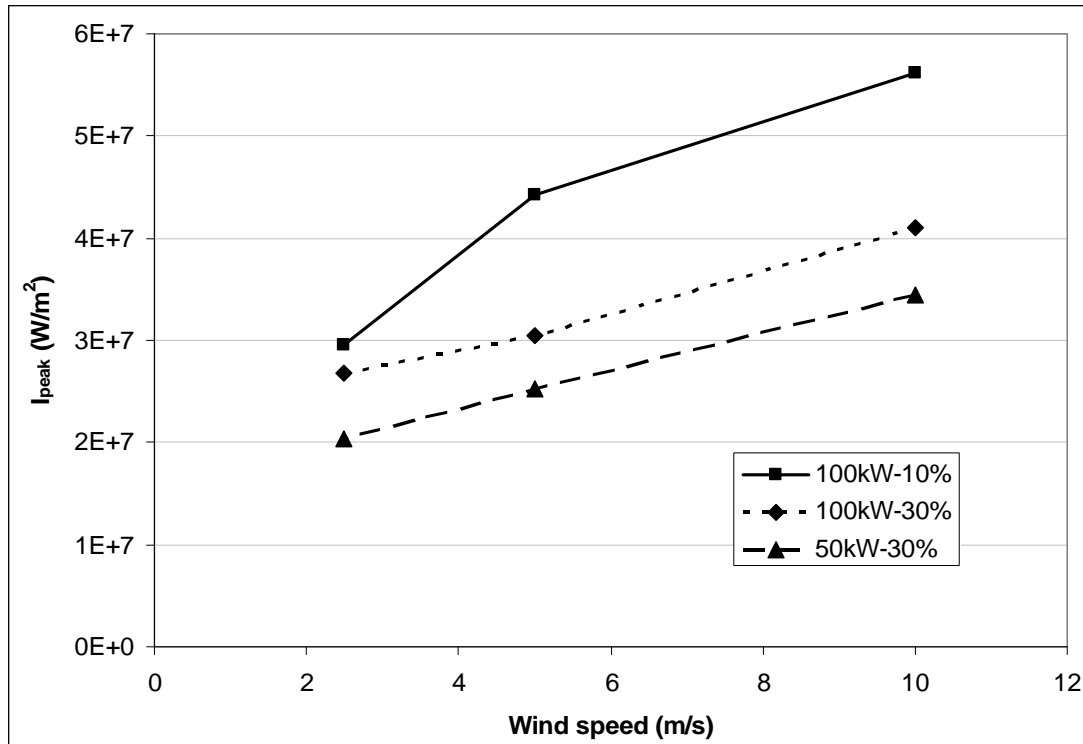


Figure 3.18. Peak irradiance at optimal defocus as a function of ground wind speed, by power (kW) and obscuration size (%) in otherwise baseline scenario.

COIL ATG systems will depend upon some amount of wind to allay thermal blooming, but the precise wind at the time of the engagement may be difficult to know. Figure 3.20 shows another advantage of the 10% obscuration in this regard: It has the flatter optimal focal length response to wind speed. While use of an active feedback system to optimally control defocus and pointing will probably be necessary in light of all the variables that can affect thermal blooming, the burden on such a system is reduced when the design is as insensitive as possible to scenario variables. As we will summarize later, the 10% obscuration is less sensitive than 30% obscuration across all scenarios; further, with a few exceptions, it also appears to benefit more from defocus.

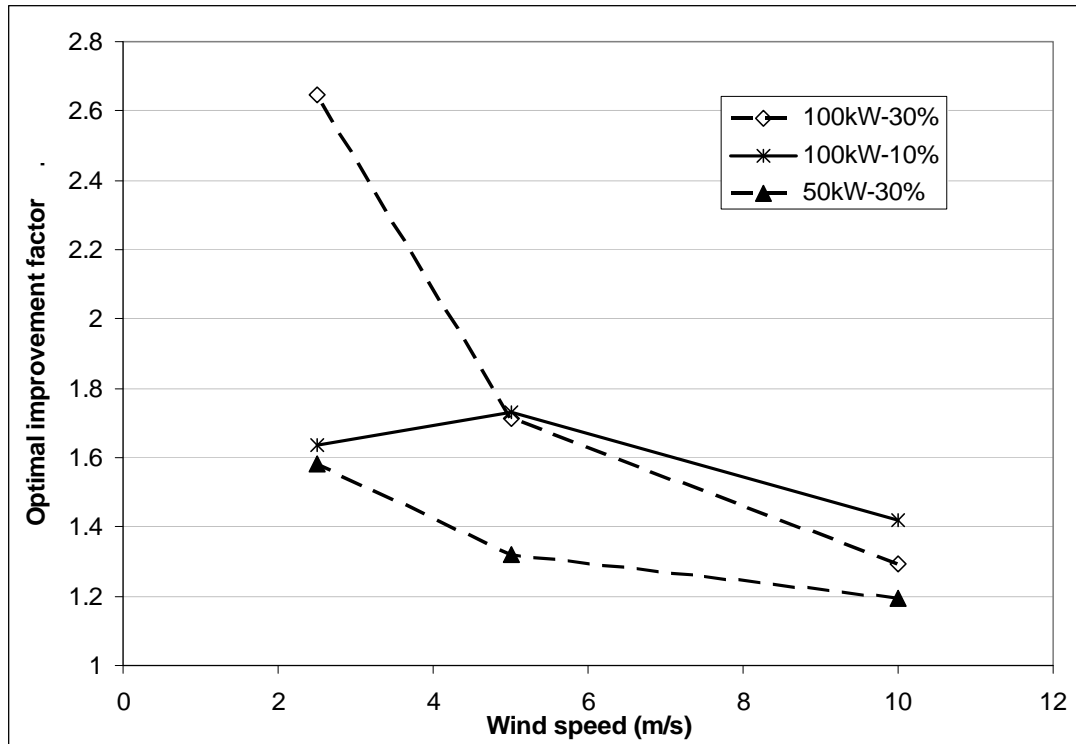


Figure 3.19. Improvement factor in peak irradiance at optimal defocus over focused case as function of ground wind speed, by power (kW) and obscuration size (%) in otherwise baseline scenario.

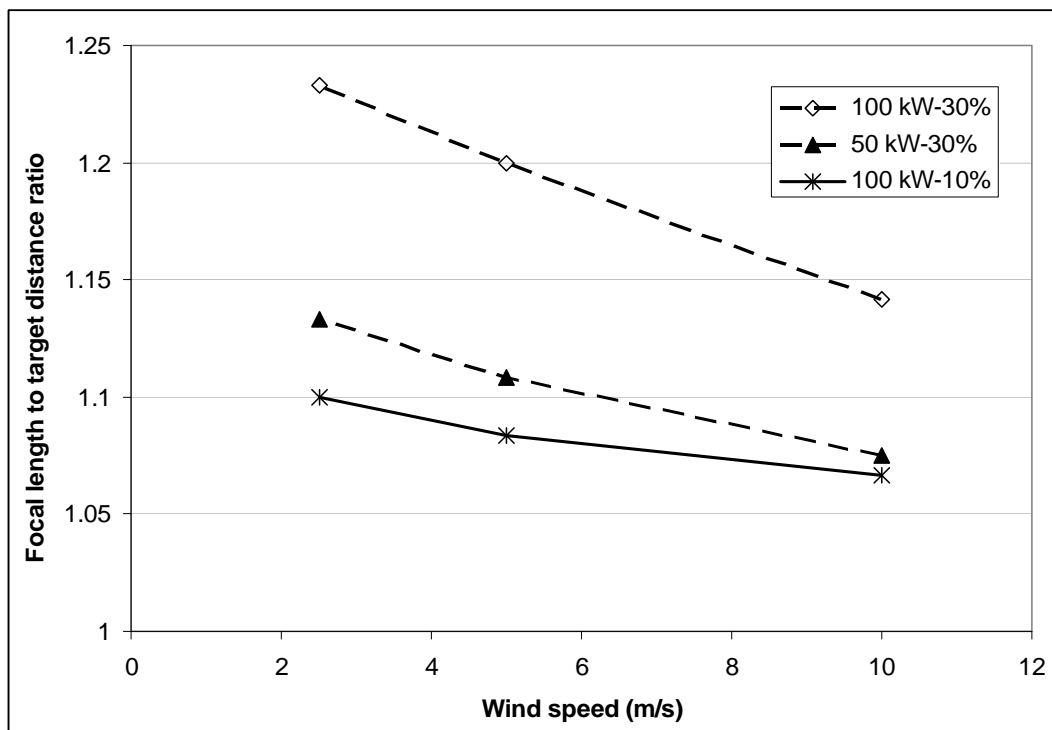


Figure 3.20. Optimal defocus multiple of target range as function of ground wind speed, by power (kW) and obscuration size (%) in otherwise baseline scenario.

3.10. Absorption

The Mani atmosphere used in our baseline scenario represents about an 80 percentile winter absorption and scatter profile for mid-latitude regions, meaning propagating conditions are better than Mani about 80% of the time in the winter. However, summer provides a more stressing atmosphere primarily due to increased humidity, which results in increased molecular absorption due to water vapor. Therefore, as a variation from the baseline scenario at 50 and 100 kW, we gathered peak irradiance and defocus results for an 80 percentile mid-latitude summer atmosphere. The combined molecular and aerosol absorption and scatter coefficients for these two atmospheres were given above in Table 3.1. It happens that this summer atmosphere is slightly less than twice as stressing than the Mani atmosphere in terms of distortion theory. The Breaux N_D values, described below, for the two cases are 53.5 and 27.3, respectively. As such, to the extent that the distortion theory is valid, the defocus profile under the summer atmosphere for a given scenario should take on a similar shape as the defocus profile for the same scenario but with a winter profile and twice the power.

Figures 3.21 and 3.22 show that this expectation is realized. Figure 3.21 plots the 50 kW baseline scenario with both the winter and summer atmospheres along with the 100 kW baseline (winter) scenario. The optimum of the 50 kW, summer line is the same as for the 100 kW, winter line. We expect the amplitude of the former to be no larger than half that of the latter since half the power is being subject to a similar amount of thermal blooming. In fact, it should be less than half because the cumulative extinction in the latter case will be approximately double that of the former case. Likewise in

Figure 3.22, we see that the 100 kW summer defocus profile is similar in shape to the 200 kW winter profile, both of which feature two modes. If the analogy is complete, the first mode will be washed out by turbulence as found for the 200 kW winter case and discussed in the next chapter—therefore we consider the second mode in Figure 3.22 graphs to be the optimum.

One important finding from this scenario variation is the validation of aliasing of power and absorption on thermal blooming Strehl. This validation is supported by defocus profile similarity for both comparisons, which includes similarity in the focal range for optimum performance. An important difference is also found, and that is the improvement at optimal defocus is not as good for the summer case as it is for the double power winter case. This may be due to the fact that increased absorption means that the thermal distortion contribution of the optical path near the target is reduced relative to the rest of the optical path. Defocus is primarily effective at countering thermal blooming near the target, rather than thermal blooming near the aperture or even the middle portion of the optical path. Figures 3.23 and 3.24 plot the peak irradiance improvement factor as a function of focal length for a closer comparison of our two sets of cases.

Absorption (as well as scatter) is similar to wind in that it is difficult to know in advance the actual atmospheric makeup at the time of an engagement. And like wind, the optimal focal length is sensitive to the atmospheric absorption conditions—though presumably this sensitivity would be reduced for 10% obscuration cases since that occurred with power and power and absorption are strongly aliased. (This sensitivity supports the notion that some sort of active defocus control with feedback from the irradiance pattern on the target would be ideal; on the other hand, if the optimum is fairly

flat in regimes where defocus does the most good, open loop control using knowledge gained about absorption and wind by some other means has possibilities.) However, unlike wind, there is little in terms of propagation vector that can be done to mitigate the effect of absorption—but an engagement geometry change in terms of altitude can offset the effects of absorption, which usually decreases with altitude, keeping the range constant.

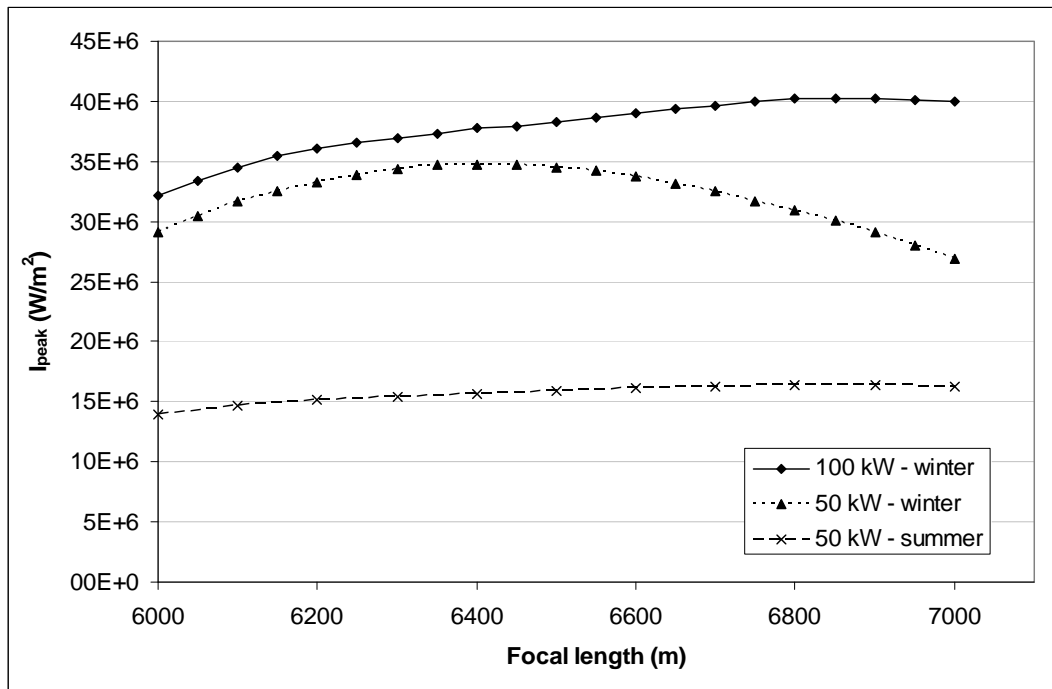


Figure 3.21. Peak irradiance as function of defocus for mid-latitude 80 percentile winter (50 and 100 kW) and 80 percentile summer (50 kW).

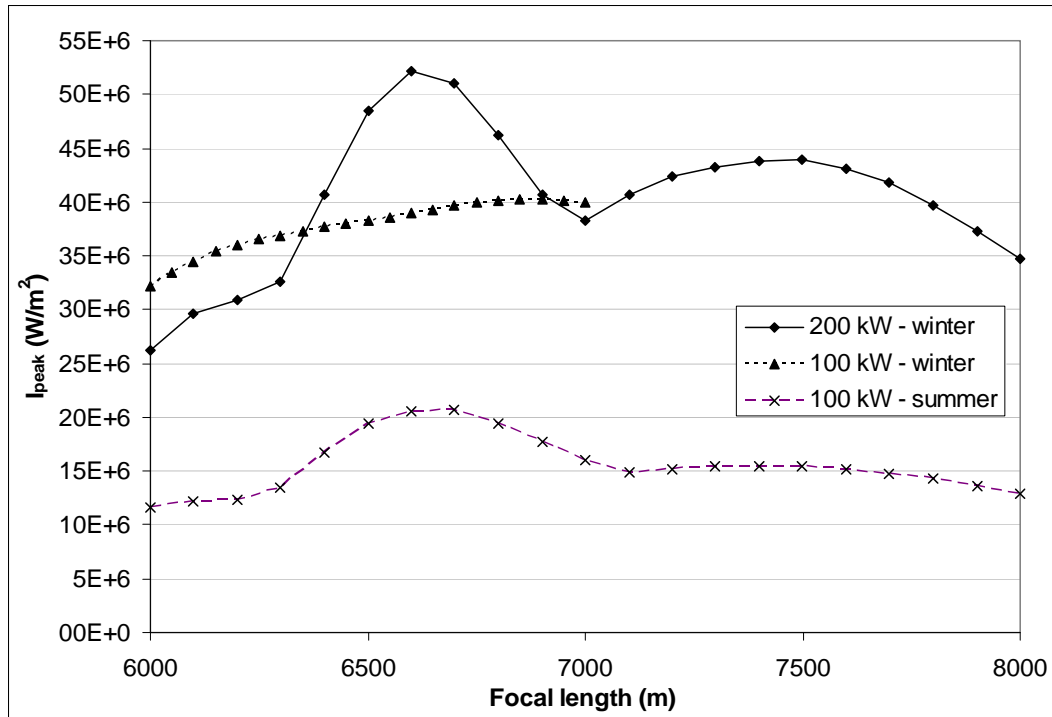


Figure 3.22. Peak irradiance as function of defocus for mid-latitude 80 percentile winter (100 and 200 kW) and 80 percentile summer (100 kW).

3.11. Altitude

Aircraft altitude will affect two important factors that determine the amount of thermal blooming experienced in propagation. First, since the absorption and scatter coefficients are inversely correlated with altitude, a constant-range altitude increase will reduce the amount of absorption that occurs, decreasing the thermal blooming distortion number. Second, when the propagation vector is not perpendicular to the aircraft velocity vector or the ground wind vector, increasing altitude will increase the acute angle between the propagation and local airmass vector—this increases the effective wind velocity through the beam tube and reduces the thermal blooming distortion number. In this section, we explore the baseline scenario increasing the altitude from 2 km to 3 and 4 km, but to improve comparison, we keep the aircraft range to target equal to 6 km. So the higher the aircraft is, the closer in terms of ground distance it is to the target. The

improvement in wind effect near the aperture is emphasized by the baseline scenario and these excursions: Since in these scenarios, the aircraft is flying level in the direction of the target, a constant-range (6 km), higher-altitude scenario will have an increased angle between the propagation and aircraft velocity vectors (*i.e.*, the laser aperture has to look down more relative to the horizon). Figure 3.23 shows the peak irradiance response to defocus at the altitudes studied. Note that not only did the focused and optimally defocused peak irradiance increase as altitude increased, but clearly the optimal focal length shortens as altitude moves from 2 to 4 km.

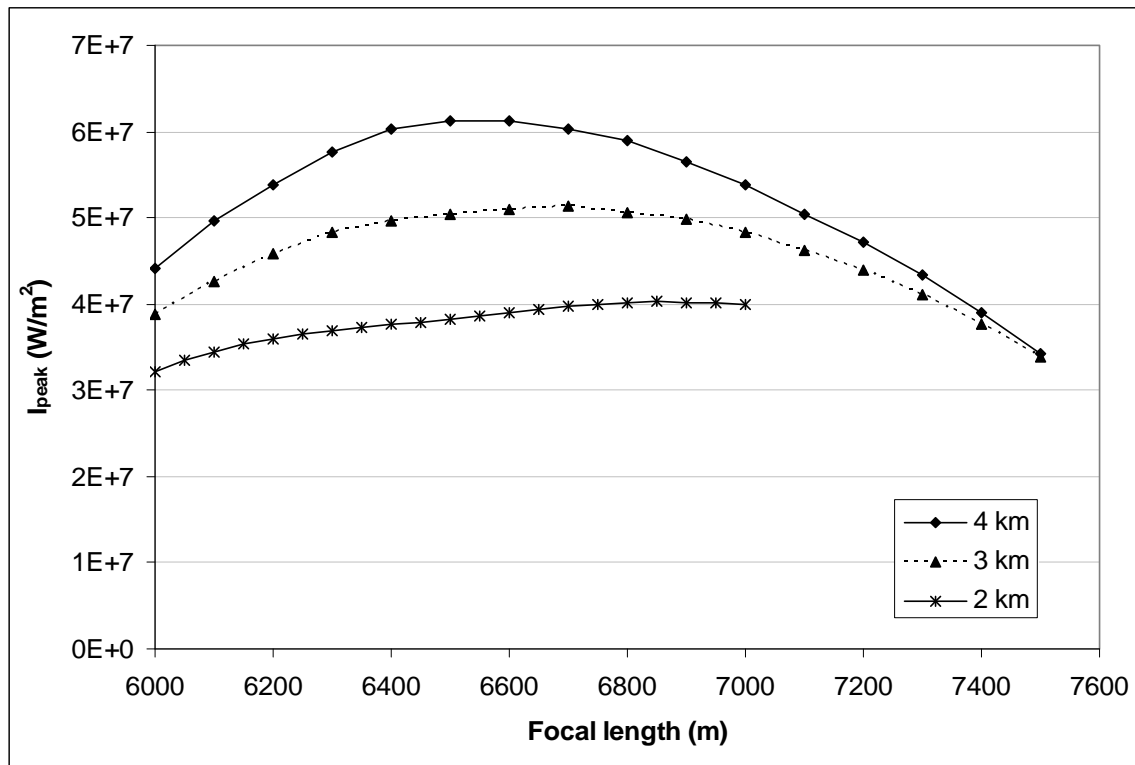


Figure 3.23. Peak irradiance response to defocus for baseline scenario by aircraft altitude. Range is held constant at 6 km.

Figure 3.23 suggests that the higher the altitude the better; of course, keeping the range constant at 6 km limits the altitude in such a strategy. However, as mentioned, ground distance to target decreases when the target range is constrained. If it is more

appropriate to constrain ground distance (perhaps due to defensive constraints), then a different optimization that seeks the best altitude for a given ground range should be undertaken—in which case, the third variable of range to target enters the factors that affect thermal blooming. The bottom line is that for a given range, the highest altitude possible to conduct the engagement is probably preferable, unless there are constraints on how large the angle between the velocity vector and the propagation vector can be—*i.e.*, if there are prohibitive aero-optic effects. Also, the higher altitude engagements may have a flatter optimal defocus response to other scenario variables which makes the defocus process easier to control.

Finally, the altitude excursion scenario provides a good illustration of the pitfall we experienced using only ten phase screens to represent thermal blooming. Figure 3.24 has the same top two lines as Figure 3.23, which are the 4 km and 3 km peak irradiance defocus profiles, respectively, calculated using 30 phase screens. Below them are plotted the profiles calculated when using ten phase screens. Clearly, use of ten phase screens underestimates the performance, but it also gives an irregular defocus profile that overestimates the optimal defocus distance. In fact, with an appropriate definition of “irregular,” one could conceivably detect whether the phase screen density profile is inadequate.

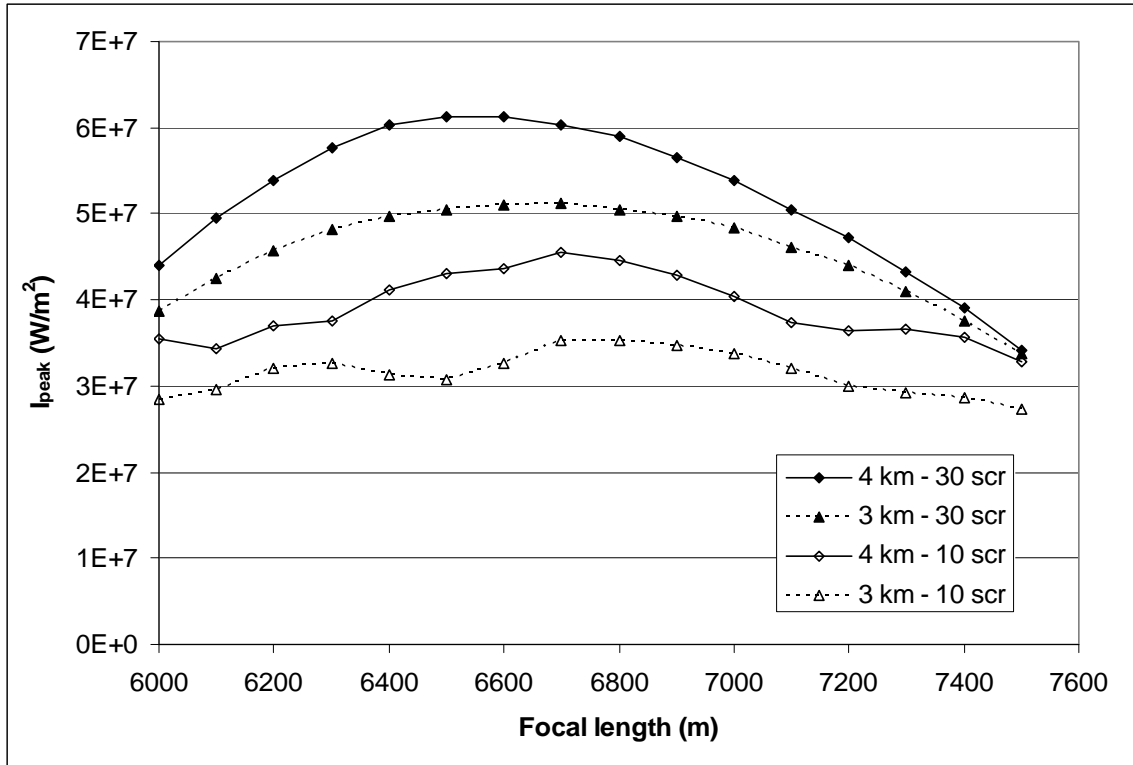


Figure 3.24. Phase screen density effect on defocus profile. Peak irradiance response to defocus for baseline scenario by aircraft altitude and phase screen setting. Range is held constant at 6 km.

3.12. Aligning These Dimensions of Sensitivity Using N_D

Our scaling variable, the Breux distortion number N_D calculated for the focused case, is a well-defined and empirically useful function of the scenario variables. Using N_D , a comparison of the above dimensions of ATG laser weapon sensitivity to defocus can be made. Leveraging the data from the forgoing sections, the 100 kW baseline scenario becomes a pivot point about which the performance space will be explored. The 100 kW baseline scenario values are fixed for all dimensions except one and values for each dimension of variation we evaluate are listed in Table 3.4 along with the Breux N_D value for that scenario--*i.e.*, we evaluate the sensitivity of performance in only one dimension of variation at a time. Then the optimal defocus multiples and irradiance

improvement factors are plotted in Figures 3.25-3.28 against Breaux N_D for all dimensions explored in this study. This approach also illustrates the utility of focused-case Breaux N_D as a predictor of optimal defocus and expected improvement.

Table 3.4. Scenario values and associated Breaux N_D for this study.

Scenario description		Variation value	N_D
Dimension to vary	Power (kW)	50	11.8
		100*	23.7*
		150	35.5
		200	47.3
	Slant range (km)	3	9.6
		4.5	16.6
		6*	23.7*
		9	37.2
	Absorption (Table 3)	80% winter*	23.7*
		80% summer	53.5
	Ground wind (m/s)	2.5	41
		5	32.7
		10*	23.7*
	Propagation vector	perpendicular	9.8
		parallel*	23.7*
	Altitude (km)	2*	23.7*
		3	16.6
		4	12.5

* 100 kW baseline scenario (pivot point)

3.13. Optimal Defocus Performance by Obscuration Size

Using Breaux N_D as the independent variable, we plot the optimal defocus multiple (optimal focal range divided by R_{target}) and performance improvement factor (optimal peak irradiance divided by focused-case peak irradiance) for the baseline

scenarios as well as their variations and we see that a relationship is apparent. Further, as suggested earlier, a clear distinction in that relationship appears between the 30% and 10% obscuration cases. Figures 3.25 and 3.26 show the respective optimal defocus multiples as a function of Breaux N_D for each dimension of variation (some of the dimensions were not explored for the 10% case since it was not the baseline scenario). For the 30% obscuration, the optimal defocus appears to rise about 6% per $\Delta N_D = 10$, until about $N_D = 30$, when the defocus multiple rolls flat at about 1.25. In contrast to that, the optimal defocus multiple for the 10% obscuration jumps about 5% immediately and stays between 1.05 and 1.10. (Note that Figures 3.25 and 3.26 have the same vertical scale for comparison purposes.) For the 10% obscuration case, given its susceptibility to turbulence interaction, it appears one could safely operate at about 5% defocus at all times to get most of the defocus benefit and stay to the left of the optimal point.

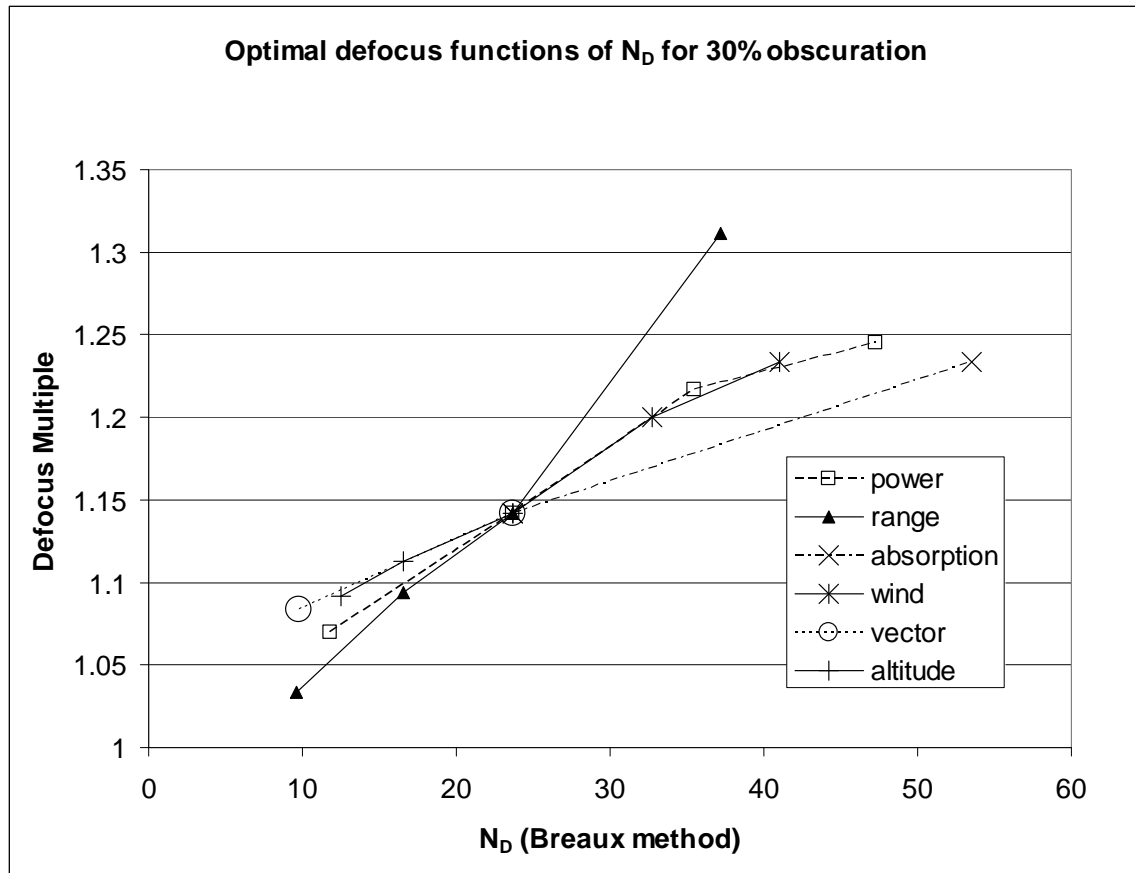


Figure 3.25. Optimal focal length multiple of slant range (defocus) for 100 kW baseline scenario (30% obscuration) and varied parameters, as function of focused-case N_D .

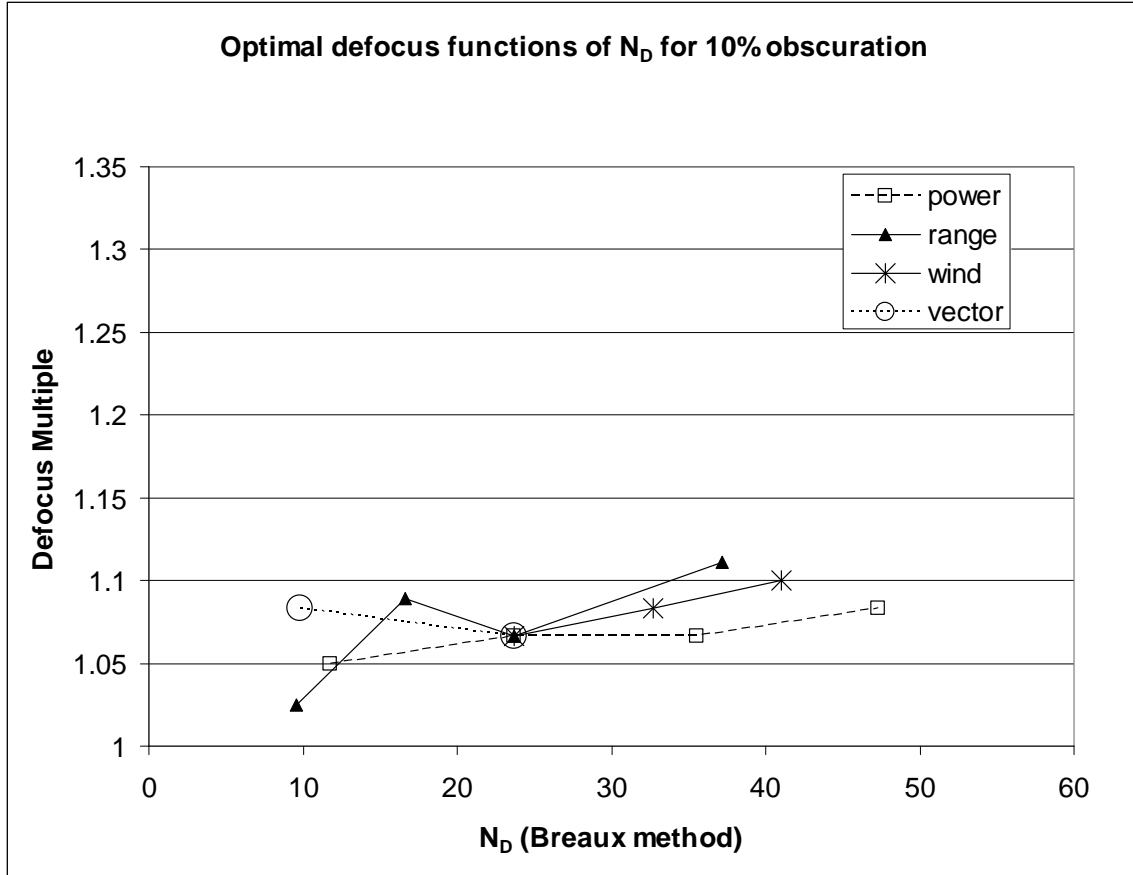


Figure 3.26. Same as Figure 3.25 except for 10% obscuration.

Next, we look at the peak irradiance improvement relative to the focused case as a function of N_D when operating at the optimal defocus shown above for each scenario. Figures 3.27 and 3.28 plot these results for the 30% and 10% obscuration cases, respectively, and as before, they have the same vertical axes to facilitate comparison. Figure 3.27 shows the improvement in peak irradiance for the 30% obscuration case is a factor of 1.2 for many settings that span the N_D range. Exceptions are wind and power, the former of which shows large improvements, but that is primarily due to the fact that the slow winds significantly knock down S_{TB} (as shown in Figure 3.29). This highlights the importance of wind as a major factor in determining a COIL-equipped ATL's performance, and when wind is low, defocusing the beam can offer significant assistance.

(The improvement factor value that exceeded the vertical axis range on the wind line is 2.7 for $N_D = 41$.) Similarly, 200 kW power pushes down S_{TB} , making the recovery due to defocus look remarkable, when in fact defocus is merely moving the critical power from a smaller value from 125 kW to 200 kW, as was shown in Figure 3.7. The altitude and propagation vector lines illustrate better operating scenarios than the baseline scenario. Not only does propagating perpendicular to the velocity vector improve S_{TB} , as shown in Figure 3.29, but that geometry also responds to defocus more readily. The same is true for increased altitude (keeping slant range the same). Combining the two geometries should yield additional benefit.

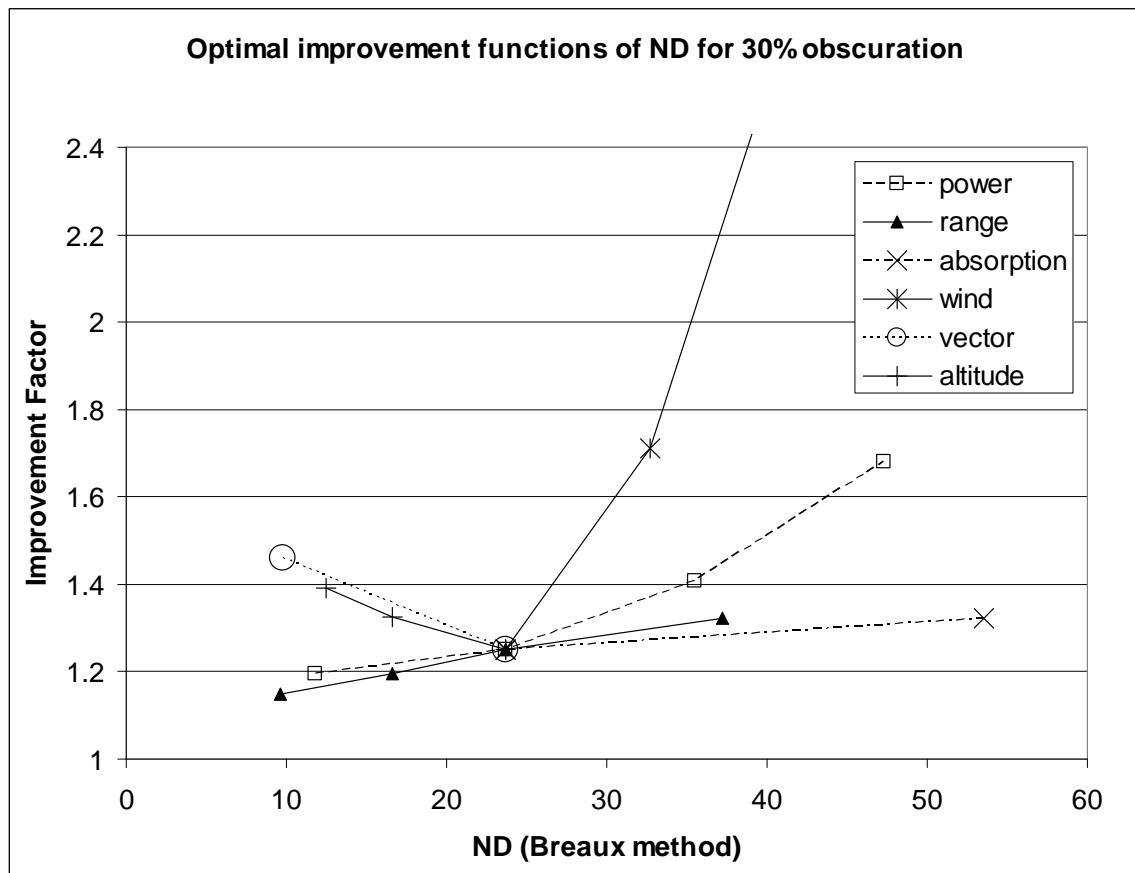


Figure 3.27. Peak irradiance improvement at optimal defocus for 100 kW baseline scenario (30% obscuration) and varied parameters, as function of focused-case N_D .

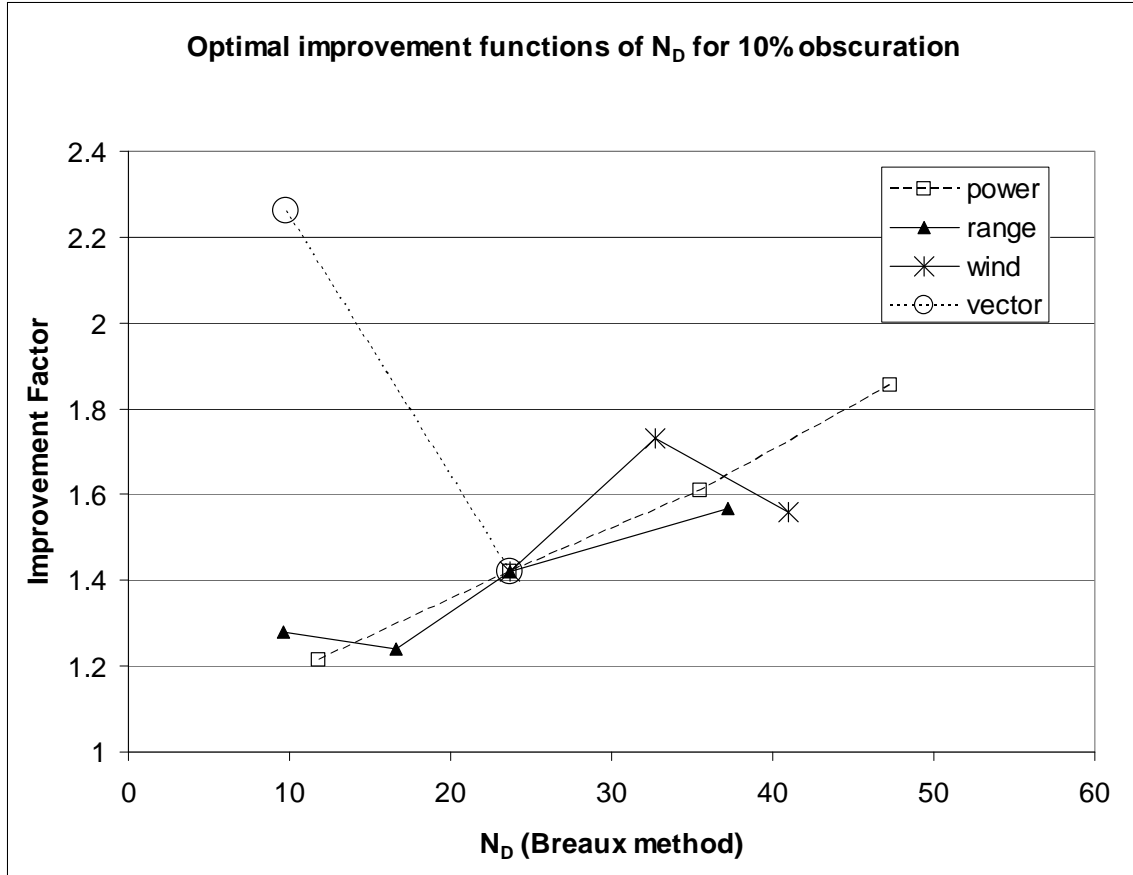


Figure 3.28. Same as Figure 3.27 except for 10% obscuration.

Figure 3.28 shows that in spite of the fact that the optimal defocus multiple is fairly flat for the 10% obscuration case (Figure 7), the improvement over the focused case increases as Breux N_D increases by about 18% per $\Delta N_D = 10$. It must be remembered that for the 10% obscuration, the larger improvements at high N_D will be offset by the thermal blooming-turbulence interaction that affects this case to a greater degree, as we will show for the case of laser power below. The perpendicular propagation geometry again represents a better operating point than the baseline scenario, and shows tremendous potential benefit from defocus; however, the interaction with turbulence will affect it also.

Wallace *et al.* [1977] have found that in the case of the thermal lens being strongest close to the target plane that the amount of potential correction by adjusting the phase at the aperture is limited to about a factor of two. As discussed above, the air-to-ground case results in such a thermal lens placement. We have found that defocusing the beam, in every air-to-ground geometry explored here, results in some irradiance benefit. In many of the cases, a significant portion of Wallace's recovery limit is realized with defocus alone. The improvements found herein are also consistent in magnitude with findings by Pearson [1978] for thermal lenses near the target plane.

Defocus appears to work, not because it constitutes a phase correction (most of the distortion being corrected with the small amount of focus we suggest is in the far field portion of the focused beam), but rather because it reduces the beam spreading transverse to the wind that occurs near the target plane. An intense focused beam with a wind perpendicular to it will set up steep temperature gradients in the beam path that constitutes a negative lens and spreads the beam transverse to the wind. A small amount of defocus only affects the beam near the target, but this slightly wider beam with the same wind will have shallower temperature gradients resulting in less spreading. To be sure, in the non-thermal blooming case, defocusing the beam results in a decrease in peak irradiance, to which the improved S_{TB} is in effect applied. However, the strength of the negative thermal lens, even close as it is to the target plane, is reduced at a faster rate than is the unbloomed irradiance for some amount of defocus. This view of the effect is supported by an experiment performed by Edwards [2004] in which he showed jitter transverse to the wind was equivalent to defocus in improving irradiance of focused thermally bloomed beams. Yeh *et al.* [1976] show that attempts to soften the transverse

wind temperature gradient with “guide beams” improves irradiance. Finally, when observing the laser spot produced by our wave optics runs, the classic thermal blooming crescent thickens as a function of defocus, and eventually a round core will emerge in the center of the crescent as the flattened temperature gradient allows the center of the beam to pass without spreading. This final effect usually occurs beyond the optimal defocus value, but its progression as a function of defocus supports the causal theory offered above.

3.14. Thermal blooming Strehl

Thermal blooming Strehl, S_{TB} , is defined as the ratio between peak intensity of a beam with blooming distortion operative and the same beam with blooming distortion inoperative, but including extinction effects due to absorption and scatter. Smith [1977] and Gebhardt [1990] report good correlation of S_{TB} to N_D and Gebhardt provides the following scaling law for uniform beams:

$$S_{TB} = 1 / (1 + 0.9 N_D^{1.2}) \quad (3.4)$$

Figure 3.29 shows the resulting S_{TB} from the variations described in the previous section. Each line represents a different dimension of variation, and the pivot point at $N_D = 23.7$ is the baseline scenario. All points on Figure 3.29 are focused cases. The open triangles are a plot of Equation 3.4, and it appears that the variation of S_{TB} as a function of N_D due to power variation is the closest to it’s shape, although there are reasons to expect the Gebhardt law would not match our wave optics results: he uses a different formula for N_D that has no lever arm in the numerator nor spreading function s . Ideally, a scaling variable would be constructed such that the slope of all the S_{TB} functions is the same near

a common starting point; this would imply the scaling relationship between the scenario dimensions had been captured. Where the line plots in Figure 3.29 do not exhibit a common slope at the pivot point suggests where improvements in the Breaux N_D could be made for application in an ATL scaling law. The higher slope of the power S_{TB} line and still higher slope of the wind S_{TB} line relative to the other lines point to an inconsistency in the scaling variable and suggests power and wind are not receiving enough weight relative to the other factors in the N_D calculation (or similarly that the other factors are receiving too much weight). The flatness of the non-wind and non-power lines led Vernon *et al.* to develop a transform for N_D for the other factors, as determined by

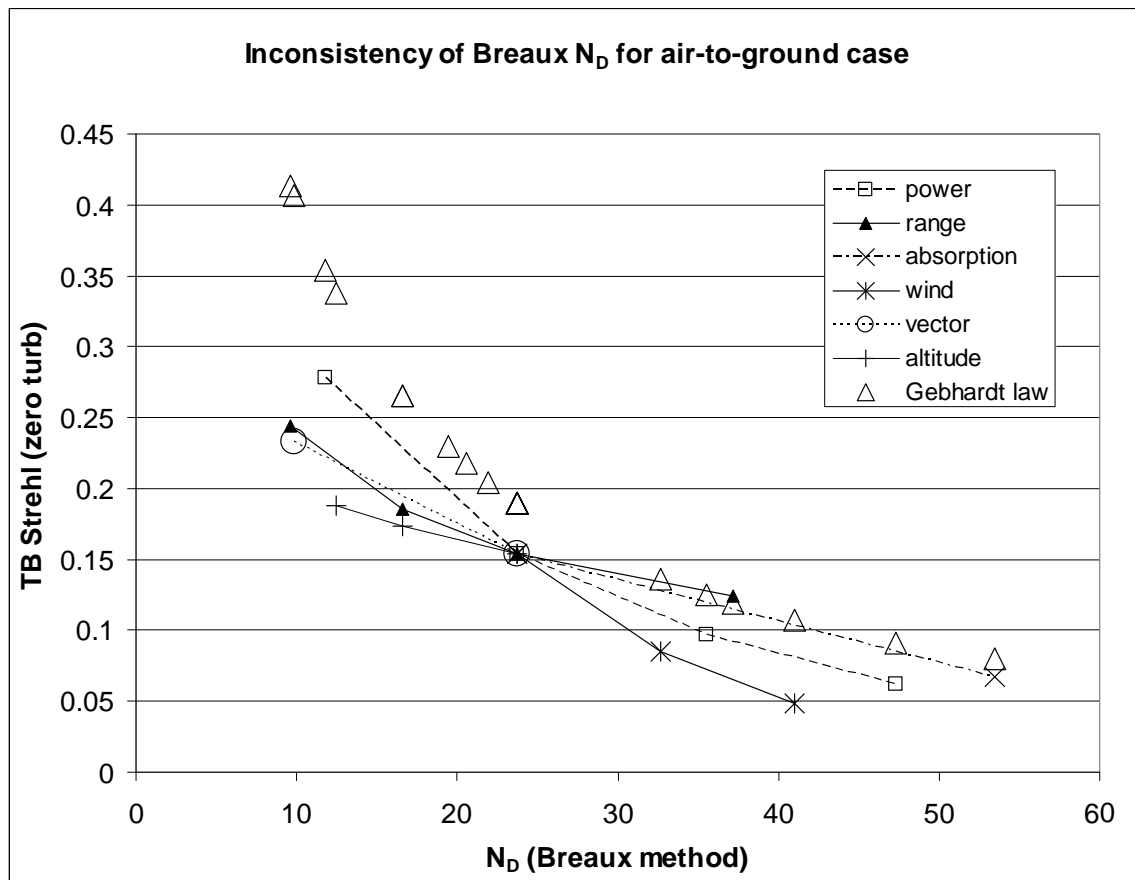


Figure 3.29. Breaux N_D exhibits some inconsistency across the scenario variables in its correlation to S_{TB} for the air-to-ground case. Pivot point is baseline scenario at 100 kW.

Equation 3.1, that remaps them more closely to the N_D response due to power (for the air-to-ground case).

Figure 3.30 contains all the same data as Figure 3.29 but with the lines removed and the Gebhardt law highlighted with a dashed line. Added in are the S_{TB} lines for defocus as a function of N_D , the latter calculated two different ways. One added plot (solid line, filled diamonds) is Breaux N_D calculated for defocus using Equation 3.1 where a_{geom} is modified to represent increasing the focus distance beyond the target by 5, 10, and 15 percent—longer focus distances for the given target range increases S_{TB} . The large difference in slope between this plot and the rest of the S_{TB} functions indicates the Breaux formulation in equation 3.1 alone is not constructed in a way that allows N_D to be calculated for the defocused case. As mentioned earlier, the reason for this lies in Breaux's special spreading function s that is RSS'ed with a_{geom} . The second added plot (dash-dot line, filled boxes) in Figure 3.30 is the S_{TB} function for the same defocus values with N_D calculated by applying the Smith correction factor Equation 3.3 to the Breaux N_D for the focused case. Interestingly, this approach yields an S_{TB} function that is not only more consistent with that of the other factors than is the solid, filled-diamond line, but is in fact very consistent with the non-power, non-wind factors to the left of the pivot point. This result suggests that those thermal blooming scaling law models that depend upon the Breaux technique for calculating N_D can capture the defocus effect in the scaling relationship by use of the Smith correction factor.

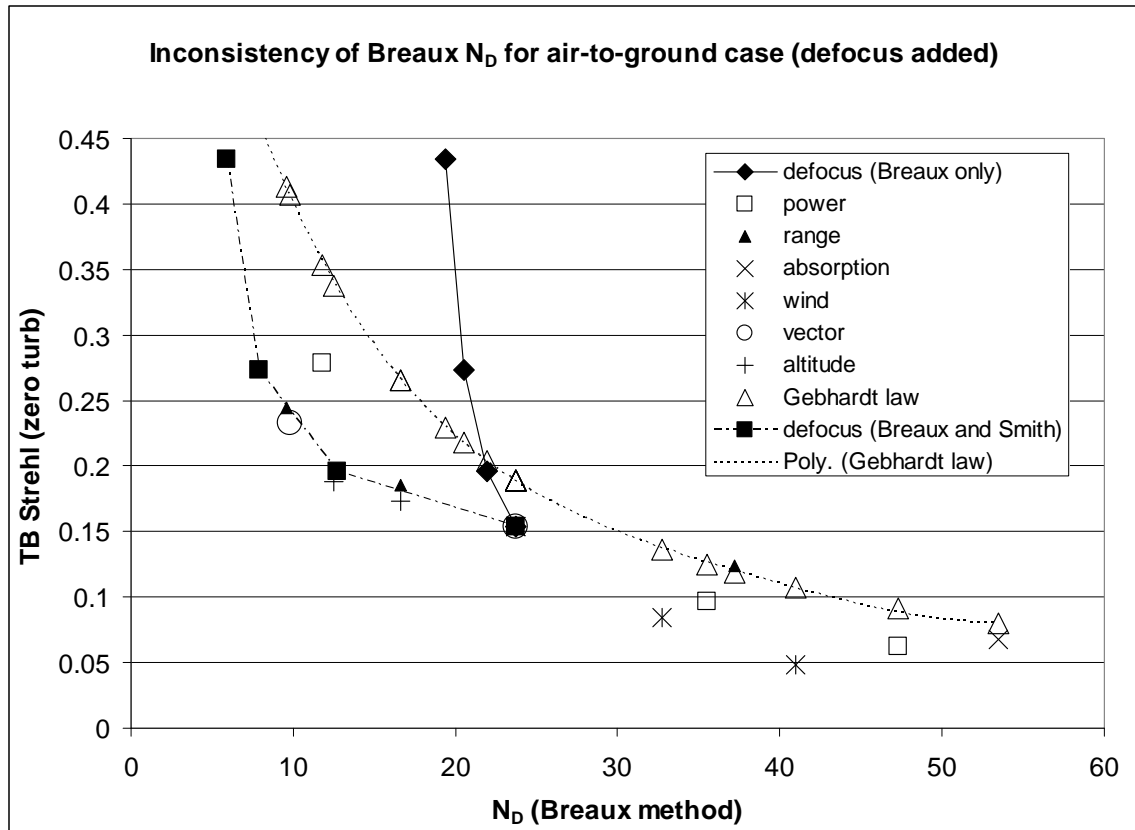


Figure 3.30. Use of Smith correction factor removes gross inconsistency in Breaux N_D with respect to defocus scaling. The dashed “Poly” line is a fit to the Gebhardt law points to distinguish them from the scenario excursions. Pivot point is baseline scenario at 100 kW.

3.15. Conclusion

Computer simulation evidence has been presented that a high energy COIL air-to-ground system can realize significant benefits simply by defocusing the beam during an engagement. This result is consistent with the maximum expected benefit of phase correction when the thermal lens is located near the target plane [Wallace]. Further, the optimal defocus amount is proportional to the thermal blooming distortion number of the focused case.

The functional form of optimal defocus appears to be sensitive to the size of the central obscuration for the uniform beam with the 10% obscuration having a fairly flat

response to Breaux N_D . The obvious benefit of using defocus is that because it is a radial phase parameter, precise knowledge of the wind direction is unnecessary to implement it, unlike the use of coma and astigmatism, as suggested elsewhere [Gebhardt, 1979]. Additionally, most systems could take advantage of this phenomenon without major hardware modification.

Another important aspect of defocus benefit is related to radial beam spreading due to diffraction from aerosol forward scattering. In the boundary layer, significant aerosol densities can occur, which not only contribute to thermal blooming and extinction, but can also cause beam spreading on the same order of magnitude as turbulence [Sadot *et al.* 1994; Sadot *et al.* 1995; Fiorino *et al.* 2005]. This spreading cannot be compensated for by phase changes at the aperture. However, such spreading may have the same effect as intentional defocusing on an HEL under thermal blooming conditions so that the effect of aerosol spreading could be to improve peak irradiance, as long as the spreading does not overshoot the optimal defocus. On the other hand, aerosol spreading can only negatively impact the peak irradiance of lasers that do not operate under thermal blooming conditions.

Similarly, if aero-optic effects at the turret cause a high-bandwidth beam spreading, it may be that the focused, thermally bloomed beam benefits from the spreading, or at least is not adversely impacted, favoring the already preferred larger angle between the propagation and velocity vectors which reduces N_D . Alternatively, if the aero-optic spreading is low bandwidth, then an interaction with thermal blooming similar to that with turbulence could arise, forcing a smaller angle to be selected.

If the defocus effect on thermal blooming ATL-like systems is to be utilized, the capability to capture the effect of defocus in scaling laws is needed for systems analysis. Currently, scaling laws that use the Breaux N_D (Equation 3.1) cannot adequately represent this phenomenon. One path to correcting this deficiency is the use of the Smith correction factor, Equation 3.3.

4. Interaction between Turbulence and Thermal Blooming in ATG Scenarios and Relation to Use of Defocus for Irradiance Improvement

4.1. Introduction

In this chapter, we add the assumption of turbulence to several of the scenarios studied in the previous chapter, and at the end, report on a case study that is closely related to the system being built by the USAF for experimentation. Modeling of turbulence in wave-optics requires averaging since any given turbulent atmosphere is a random draw from distributions which define the turbulence. We found that averaging ten realizations was adequate to dampen noise in estimated mean performance; however, the consequence is that an ACS run for any test point is at least 10x longer than for the same point with no turbulence assumed. Therefore, we used the no-turbulence results to guide our selection of test points to gather data on with-turbulence performance.

4.2. Defocus Versus Turbulence

One of the early hopes for this research was to use main beam defocus to avoid having to model turbulence in the wave optics representations since, as mentioned, the latter can be quite time-consuming from a computer run time standpoint. The goal was to let defocus be a surrogate for turbulence and thus eliminate the need for averaging and free the computers up to run more scenarios. However, it was not to be. In this chapter, we will show that defocus and turbulence often have opposite effects on thermal blooming (TB) in the air-to-ground (ATG) scenarios, eliminating this surrogate approach as useful for analysis and scaling law development in this engagement paradigm.

The reason for their different effects on TB lies in the bandwidths of the three processes considered—defocus, TB, and turbulence. Defocus is an instantaneous process in that the act of defocusing a beam has an immediate effect on peak irradiance. The bandwidths of the other two depend on the strengths of TB and turbulence, respectively. In the ATG COIL cases considered here with the beam focused or almost focused, the bandwidth of the thermal blooming process in our scenarios is at slowest on par with and usually much faster than that of turbulence; that is, the steady state peak irradiance due only to TB is usually reached very quickly with respect to turbulence dynamics. Turbulence generally takes the longest to arrive at steady state, in terms of finding the average peak irradiance for a scenario. Of course, turbulence is never steady state itself but is constantly fluctuating. These fluctuations are responded to by the usually faster TB process and often the result is that their combined effect on average, or steady state, peak irradiance is worse than the impacts of the two processes considered independently (*i.e.*, TB without turbulence, and turbulence without TB).

According to Smith [1977], when the turbulence bandwidth is higher than that of the TB process, TB scaling laws can be applied to the time-averaged turbulence-spread beam—this was the source of our plan to use defocus as a surrogate, and indeed we do find a few cases where this is a plausible explanation for the combined effect of turbulence and TB. However, Smith also suggested that when the bandwidth situation is reversed, a TB scaling law could be applied first, after which the effect of turbulence on the resulting beam could be applied. Again, this appears to explain some of the phenomena we see; however, there are other phenomena this theory cannot explain. For instance, the higher the power, the higher is TB bandwidth, so the magnitude of the TB

interaction with turbulence should decrease as TB worsens (*i.e.*, their effects on peak irradiance should become more independent)—we observe the opposite in the ATG COIL scenarios. Finally, Smith states when the bandwidths are about the same, a combined approach must be used for analysis, such as wave-optics or a combined turbulence-TB scaling law. It is important to note that Smith’s paper dwelt mostly on collimated and/or ground-to-space applications, though scaling laws were developed for focused, atmospheric cases. The point is, however, that Smith appears to have considered primarily whole-beam blooming with respect to turbulence.

The atmospheric fluctuation due to turbulence that affect a given beam can be divided into two categories, intrabeam fluctuations and whole-beam fluctuations, and the TB process responds to them differently. Intrabeam fluctuations cause local focusing of the beam in the optical path which, if the beam is powerful enough in an absorbable wavelength, will cause a local thermal lens that spreads that portion of the beam before reaching the target. This is known as Stimulated Thermal Reimann Scattering (STRS) [Gebhardt, 1990] and can be thought of as an amplification of the small scale turbulence structure. Whole beam fluctuations are caused by turbulence structures in the atmosphere larger than the beam diameter and move the entire hit spot around at the target plane—these are the kinds of fluctuations the target tracking system attempts to remove from the beam (up to the limit of the tracker bandwidth, of course). As suggested above, when this motion is slow compared to the speed of the TB process, the effect is similar to the application of a point spread function to a steady-state TB hit spot under no turbulence—and when fast in comparison, the TB process can be thought of as applying to the time-averaged beam.

Furthermore, the detrimental interaction between turbulence and TB appears to worsen with defocus for many scenarios, as we will demonstrate. The nature of this dependence on defocus appears to be related in part to the fact that, as discussed in the previous chapter, defocusing in the presence of TB and the absence of turbulence improves peak irradiance by producing a narrower hit spot that, when subject to residual motion due to turbulence uncompensated by the tracker, as well as STRS, has a peak irradiance more vulnerable to reduction in the time average than is the broader hit spot of the focused beam under TB but no turbulence conditions.

The bottom line of this finding is that defocus cannot be considered as a surrogate for turbulence for an ATG HEL operating in TB conditions. Rather, defocus becomes a parameter not only for optimization of performance but also for understanding the complicated interaction between turbulence and TB. Since turbulence is well researched and understood in the ATG domain, we will focus on the interaction.

4.3. Interaction Strehl

The Strehl ratio for a treatment is defined in this paper as the peak irradiance before the treatment divided into the peak irradiance after the treatment. Ideally, Strehl ratios for treatments under consideration would be independent, in which case, scaling laws could be developed for each, and the product of all Strehl ratios would be effect of all treatments simultaneously applied to an untreated beam. As noted above, however, for many ATG scenarios, the Strehl ratios for turbulence and TB are not independent. Therefore, we define a Strehl ratio for the interaction of turbulence and TB, hereafter called the interaction Strehl, and denoted $S_{interact}$.

$$\begin{aligned}
S_{turb} S_{TB} S_{interact} &= \frac{I_{peak_{turb+TB}}}{I_{peak_{extinct}}} \\
&= S_{turb+TB}
\end{aligned} \tag{4.1}$$

$$\begin{aligned}
&\therefore \\
S_{interact} &= \frac{I_{peak_{turb+TB}} / I_{peak_{extinct}}}{S_{turb} S_{TB}} \\
&= \frac{I_{peak_{turb+TB}} / I_{peak_{extinct}}}{S_{turb} (I_{peak_{TB}} / I_{peak_{extinct}})} \\
&= \frac{I_{peak_{turb+TB}} / I_{peak_{TB}}}{S_{turb}} \\
&= \frac{S_{turb+TB}}{S_{turb}}
\end{aligned} \tag{4.2}$$

where $S_{turb+TB}$ is the Strehl ratio for turbulence given TB has been applied (that is the ratio of turbulence to no-turbulence peak irradiances under TB conditions). $I_{peak_{extinct}}$ is the diffraction limited peak irradiance with atmospheric extinction applied. The final two lines of Eq. 4.2 are very useful since data on peak irradiance under TB-only conditions were widely collected for Chapter 3 results. Beyond that, one need only know S_{turb} , which is dependent on just a few scenario settings, and to determine the peak irradiance under both turbulence and TB conditions. With $S_{interact}$, an approach to scaling laws that decomposes into TB-only, turbulence-only, and the interaction term can be investigated.

To illustrate the effect of the interaction, we recreate the critical power graphs shown in Chapter 3, only this time we include the effect of turbulence. If turbulence had an independent effect, critical power graphs for a scenario with turbulence and no-turbulence assumptions would have the same critical power point; that is, the graph for the with-turbulence assumption would merely be some constant fraction of the one under no turbulence. Figure 4.1 shows this is not the case for the baseline scenario critical

power graph (for 30% and 10% obscuration settings) at optimal defocus when Hufnagel-Valley 5/7 (HV5/7) turbulence is assumed. Instead, Figure 4.1 shows interaction between turbulence and TB worsens as power increases so that the critical power point, the maximum of the graph, occurs at a lower power setting when turbulence is assumed as described below. Figure 4.1 also shows that the interaction is worse in the 10% obscuration case since the with- and without-turbulence graphs (solid lines) diverge much more sharply as power increases than do the 30% obscuration graphs (dashed lines). Similar results were obtained regarding turbulence in the perpendicular propagation cases as well for the 10% obscuration case. Also, despite the negative impact of turbulence, both in turbulence Strehl as well as interaction Strehl, it is still beneficial for the laser system in the presence of turbulence to defocus. Figure 4.2 shows that there remains an approximate 33% benefit to optimal defocusing at 100 kW with either obscuration size.

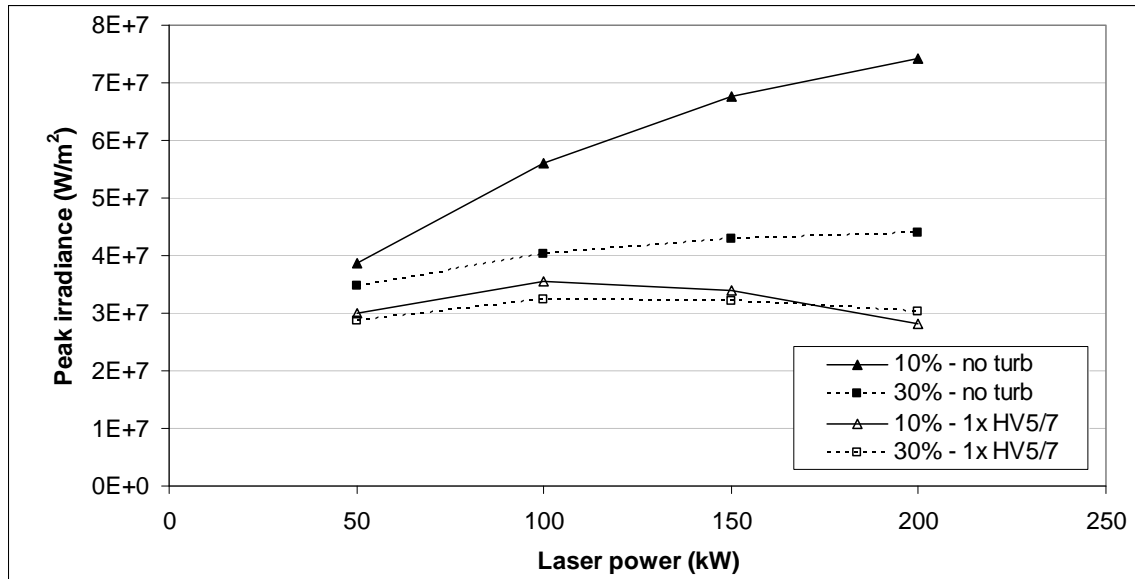


Figure 4.1. Peak irradiance at optimal defocus for baseline scenario by obscuration and turbulence assumption.

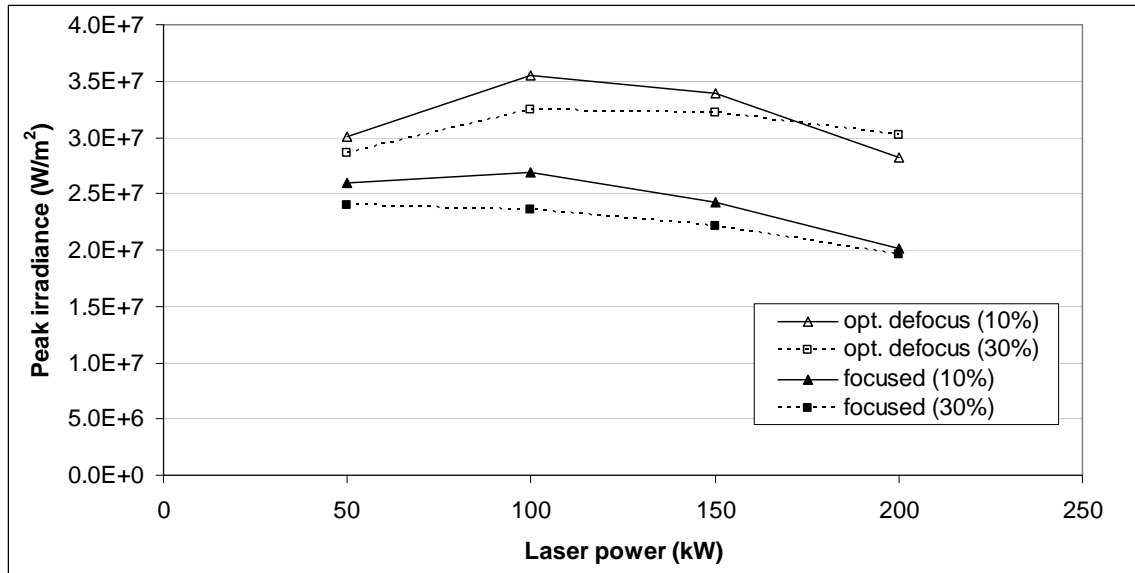


Figure 4.2. Critical power graphs for baseline scenario under HV 5/7 turbulence, by obscuration size illustrate defocus is beneficial in the presence of turbulence.

As can be seen in Figure 4.1, an important effect of turbulence is that it diminishes the advantage of the 10% obscuration over 30% that was seen in Chapter 3 under no turbulence. Another difference diminished by turbulence between the two obscuration assumptions is the advantage of perpendicular propagation over parallel propagation scenarios. Figure 4.3 shows the improvement factor of perpendicular propagation at optimal defocus. Note that the effect was disproportionately large for 30% obscuration with no turbulence assumed. Under turbulence, you can see the effect of this scenario change is similar for both obscuration settings. Even so, as discussed later, it appears that perpendicular propagation is always the better operating point unless some consideration not accounted for here interferes, such as aero-optic effects at the turret.

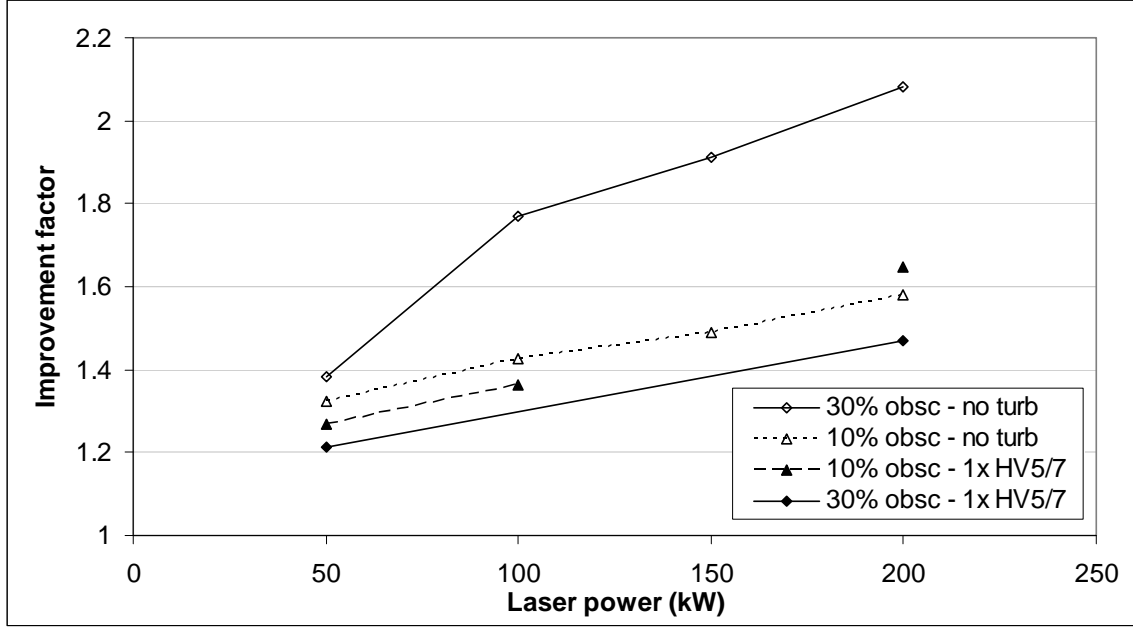


Figure 4.3. Peak irradiance improvement factor for perpendicular propagation over parallel propagation (at optimal defocus) as function of laser power by obscuration and turbulence assumption for otherwise baseline scenario.

4.4. ATG Scenarios Considered

The baseline scenario in this chapter is the same as in Chapter 3, and the variations investigated for turbulence effect are a subset of the variations outlined there, with two major differences: (1) for our case study of a 10% obscuration ATG platform under turbulence, we used a 0.4x Bufton wind instead of 0.5x and 0.25x; and (2) we did not investigate the effect of the summer atmosphere absorption and extinction, though we did show in Chapter 3 that it appears to be strongly aliased with power with respect to the effect of defocus. The Mani atmospheric absorption profile is assumed for all cases in Chapter 4. S_{turb} for these scenarios, needed for calculating $S_{interact}$, is shown in Figure 4.4, and is calculated directly from peak irradiance results for 30 phase screen, turbulence-only runs for 1x and 2x HV5/7. The S_{turb} for the 0.5x HV 5/7 atmosphere is estimated from the relationship between all three turbulence multiples determined from 10 phase

screen runs applied to the values for the 30 phase screen runs. As expected and discussed in more detail below, when TB was not included in the model, there was little difference between the 10 phase screen runs and the 30 phase screen runs under the same strength of turbulence assumption (1x and 2x HV 5/7). As in Chapter 3, both 10% and 30% obscuration sizes will be discussed in each section below, where applicable.

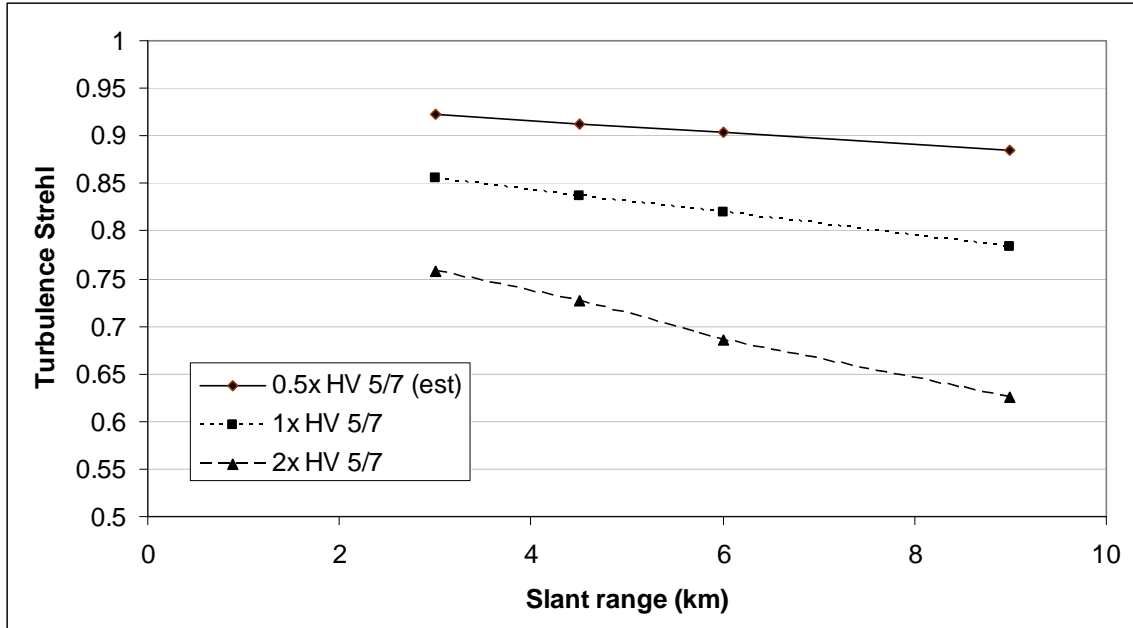


Figure 4.4. S_{turb} as function of target slant range for otherwise baseline scenario by HV 5/7 turbulence multiple. (Note origin of vertical axis is not zero.)

4.5. Phase Screen Selection

While the determination of the adequacy of 30 phase screens was described in Chapter 3, the addition of turbulence to the model required reverification of this result. There are two concerns: (1) Phase screens may be too close together with respect to the assumption of independence between the phase screens inherent in the ACS wave-optics turbulence modeling technique; and (2) turbulence may interact with the phase screen selection resulting in a phase-screen-number dependent $S_{turb/TB}$ which would imply the same dependence in $S_{interact}$.

The first concern would be manifested as a significant downward trend in S_{turb} as the number of phase screens is increased for a given scenario. To test it, we measured S_{turb} at 3, 4.5, 6, and 9 km ranges in an otherwise baseline scenario with ten, 20, and 30 phase screens, using common random numbers for all ranges for a given phase screen setting to reduce variance. The resulting measurements are shown in Table 4.1, and while there is a very slight downward trend in the 3 km range scenario (which is the most stressing case) as phase screen number increases from ten to 30, there was no general downward trend to cause concern. The 4.5 km range case actually has a slight upward trend.

Table 4.1. Values of S_{turb} to check adequacy of phase screen count to model turbulence in ACS at otherwise baseline scenario.

Number of phase screen	Target slant range			
	3 km	4.5 km	6 km	9 km
10	0.857	0.828	0.815	0.765
20	0.856	0.835	0.827	0.798
30	0.854	0.841	0.816	0.780

The second concern would manifest itself as a dependence of $S_{turb/TB}$ upon phase screen number, as increased from the planned operating point of 30. In other words, the concern here is that 30 phase screens is too few, evidence of that being an increase in the number of phase screens causing a significant increase in $S_{turb/TB}$. $S_{turb/TB}$ was determined for the baseline scenario at a more conservative 150 kW to be 0.742 for the 30 phase screen case, and 0.746 for the 40 phase screen case. As a result of the previous finding and this finding of only marginal, and perhaps random, effect on $S_{turb/TB}$ by phase screen number, 30 phase screens was selected as the operating point of choice.

It was particularly important to find this stable operating point because we know that $S_{turb/TB}$ and $S_{interact}$ can be very sensitive to phase screen number, particularly when

that number is too low and especially when N_D is also high. For example, Figure 4.5 shows the value of $S_{interact}$ as a function of power for ten phase screens and 30 phase screens for an otherwise baseline scenario. As illustrated, too few phase screens not only adversely affects the modeling of thermal blooming (as discussed in Chapter 3), it has the additional liability of potentially overestimating the interaction effect between thermal blooming and turbulence. The graph for ten phase screens in Figure 4.5 was presented at the Directed Energy Professional Society Modeling and Simulation Conference, Tampa FL, March 2005 [Long]. This publication corrects that error, as does our 2007 article published in Journal for Directed Energy [Long, Miller, Brigantic, Goda]. However, it is likely that it would have taken longer to discern the prevalence of $S_{interact}$ in this operating regime had our unfortunate error of using ten phase screens (a common setting in the industry at the time) not made the effect so obvious.

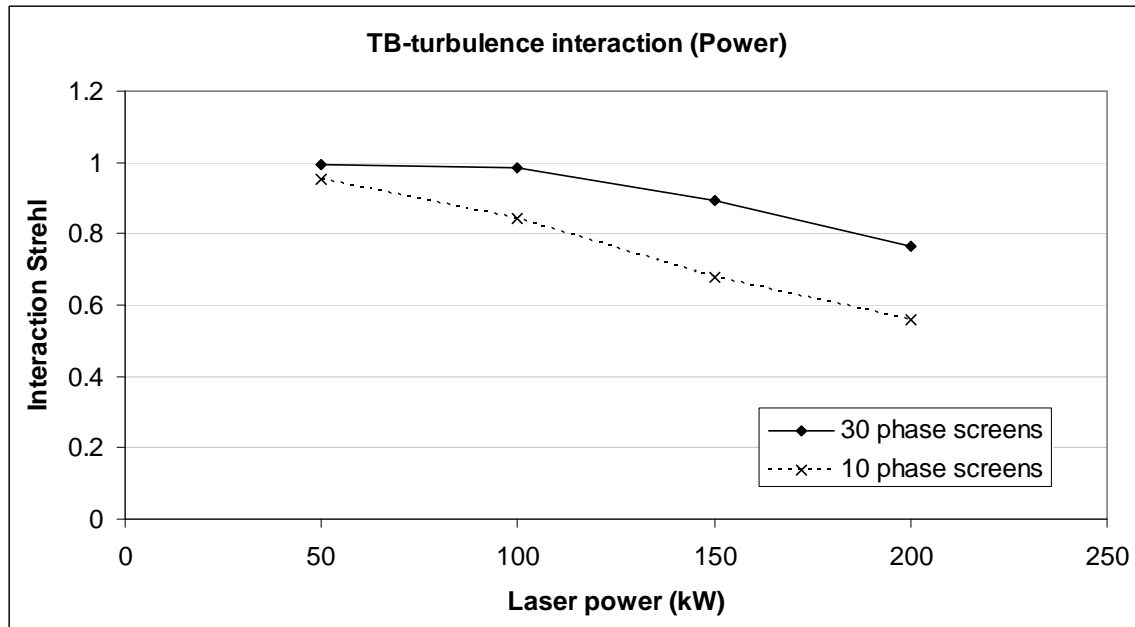


Figure 4.5. $S_{interact}$ at optimal defocus for otherwise baseline scenario as function of power, by phase screen setting in ACS. An insufficient number of phase screens exaggerates the interaction of TB and turbulence.

4.6. Relationship of $S_{interact}$ with Defocus and Power

The interaction between turbulence and TB in these ATG scenarios can occur at all defocus values at which we hope to increase peak irradiance by that means; however, at optimal defocus, $S_{interact}$ is much stronger for the 10% obscuration case than for 30% obscuration. This is due in part to the fact that the optimal defocus for the former is shorter than for the latter, putting the optimal point in a defocus region where $S_{interact}$ is worse for both obscuration sizes. In addition, $S_{interact}$ has a larger impact on the 10% obscuration cases for all defocus values. Figure 4.6 shows $S_{interact}$ for the 10% obscuration case as a function of defocus, by laser power. The circled points on the graph represent the defocus value for optimal peak irradiance with the baseline scenario including 1x HV5/7 turbulence. Note that for all power levels, the optimal defocus is 5% (300 m) of target slant range (6000 m). This is in contrast to the no-turbulence cases shown in Chapter 3, where the optimal defocus distance increased slightly with power for the 10% obscuration case. (See Figure 3.6.) The reason for the difference is that with respect to focal length, the negative slope of $S_{interact}$ offsets the positive slope of S_{TB} when turbulence is present.

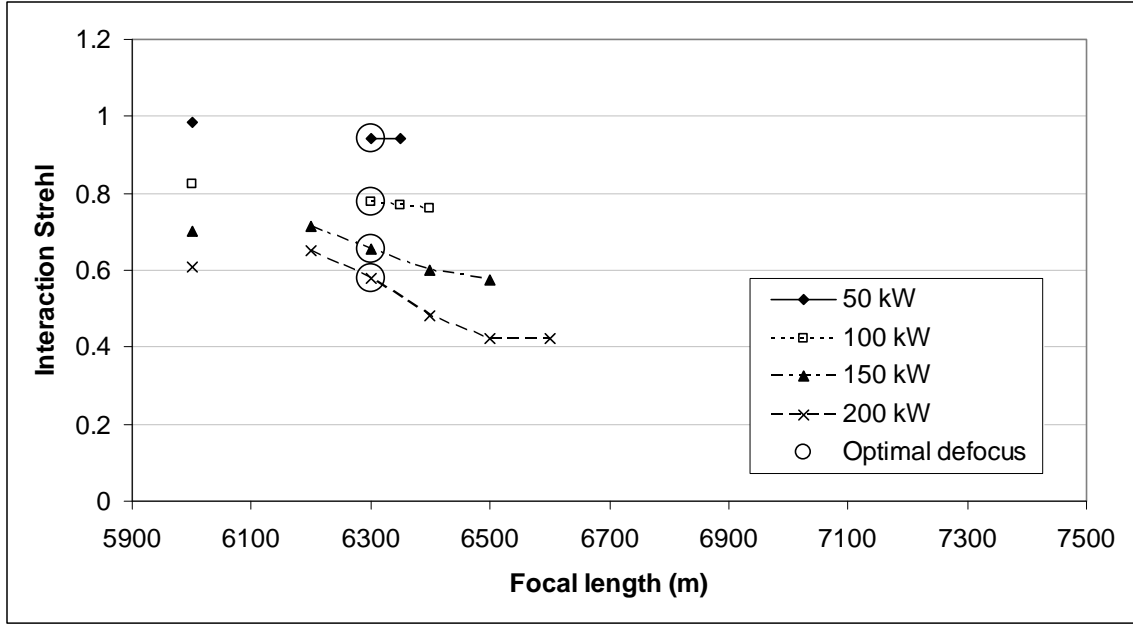


Figure 4.6. $S_{interact}$ for the 10% obscuration case as function of focal length by laser power for otherwise baseline scenario.

The remarkable consistency of the optimal focal range across power settings under turbulence led to selection of 5% defocus as the static defocus multiple for increasing peak irradiance in the case study, discussed later in this chapter. (However, as the reader will see in that section, the optimality of the 5% setting was not explored in the case study, and while significant peak irradiance improvement always occurred over the focused case, 5% defocus is very likely not an optimal setting for many of those experimental points.)

For the 30% obscuration case with 1x HV5/7 turbulence, $S_{interact}$ was not a major contributor to peak irradiance degradation until laser power reached 150 kW, and in no case is $S_{interact}$ worse than a similar scenario with 10% obscuration. This is shown in Figure 4.7. Further, the defocus setting for optimal peak irradiance is the same as for no turbulence and 30% obscuration, the reason being that optimal focal length is much

longer for 30% obscuration which places $S_{interact}$ in a region where it is fairly flat with respect to defocus.

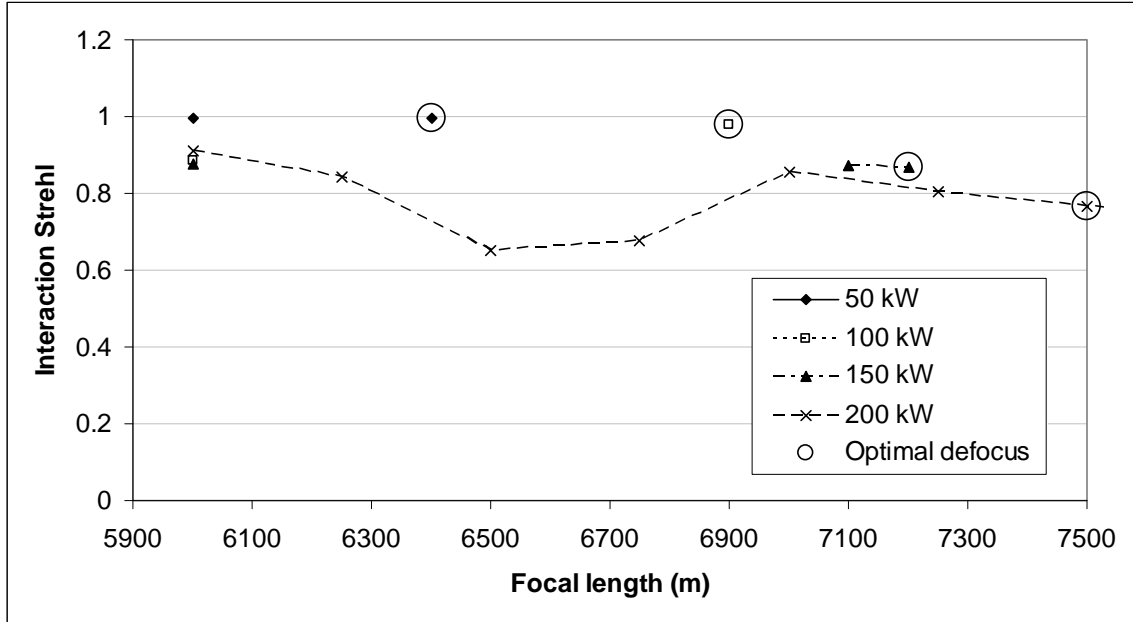


Figure 4.7. $S_{interact}$ for the 30% obscuration case as function of focal length by laser power for otherwise baseline scenario.

It is interesting to note in Figure 4.7 that, as with the 10% obscuration case, the 30% obscuration $S_{interact}$ curve at 200 kW has strong downward slope at about 5% defocus. The resulting negative mode in the $S_{interact}$ curve that occurs between focal lengths 6300 m and 6900 m corresponds to the first mode in peak irradiance in the 200 kW baseline scenario under no turbulence shown in Chapter 3 and in Figure 4.8. Figure 4.8 also shows the peak irradiance response to defocus of the 200 kW baseline scenario with 1x HV 5/7 turbulence, and shows that the first mode is washed out by turbulence.

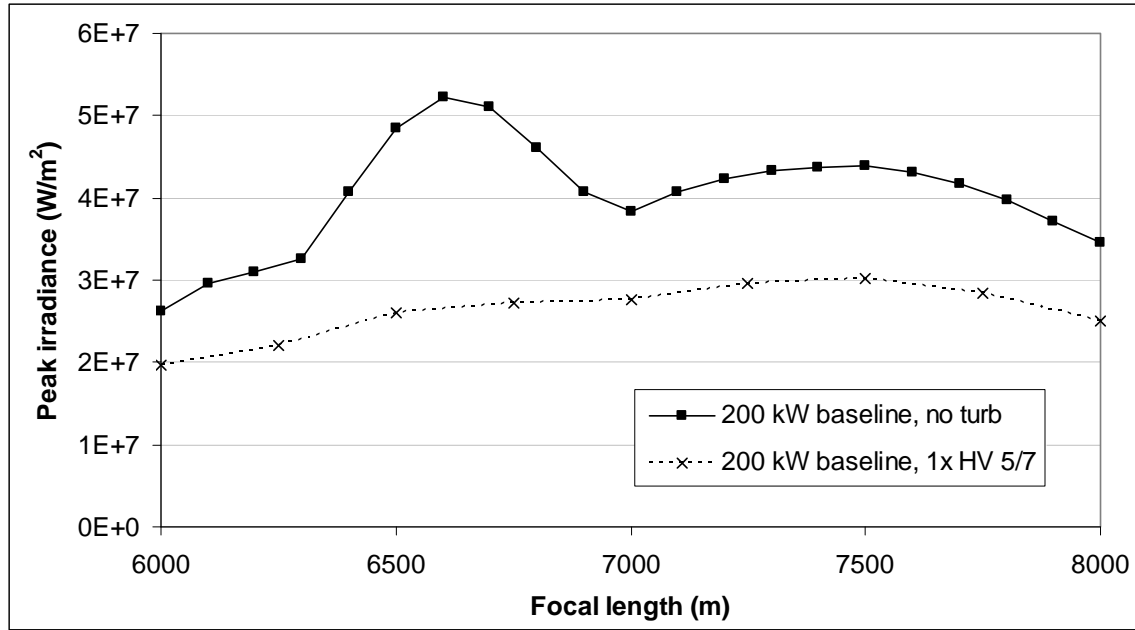


Figure 4.8. Peak irradiance as function of defocus for 200 kW baseline scenario (30% obscuration) under two turbulence assumptions: no turb and 1x HV 5/7.

The single mode that occurs in the same 6300 m to 6900 m focal length region for the 10% obscuration case (Figure 4.9) and 200 kW is washed out even more strongly than the first mode (solid line) in Figure 4.8. Figure 4.9 shows the same scenario as Figure 4.8 except for the 10% obscuration case. Recall that under the no-turbulence assumption, the optimal peak irradiance for 10% obscuration cases generally higher than it is for 30% obscuration. Since power arriving at the target plane is equivalent, this implies that irradiance pattern for the former is sharper and more narrow than the latter, and images of the target plane bear this out. Also, since residual turbulence for the two obscurations is the same, the sharper pattern will be affected more severely by turbulence resulting in worse $S_{interact}$ for the 10% obscuration cases. Similarly for the 10% obscuration case, since the no-turbulence peak irradiance increases and becomes sharper with defocus, $S_{interact}$ worsens as a function of defocus. This is why the optimum peak irradiance under

1x HV 5/7 turbulence occurs at a shorter focal length than under no turbulence in the 10% obscuration cases.

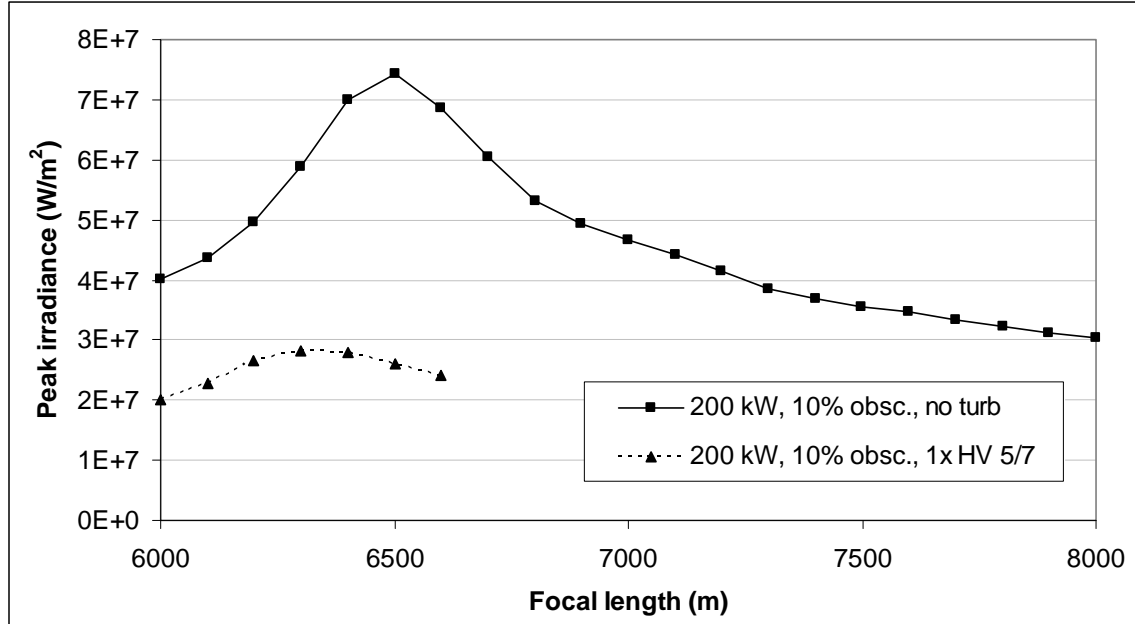


Figure 4.9. Peak irradiance as function of defocus for 10% obscuration and 200 kW for otherwise baseline scenario under two turbulence assumptions: no turb and 1x HV 5/7.

Finally, we present the $S_{interact}$ at optimal, or near-optimal, defocus as a function of laser output power by obscuration setting and turbulence assumption. The case study data allowed the calculation of $S_{interact}$ for 0.5x HV 5/7, but only for 10% obscuration and 50 and 100 kW settings. Figure 4.10 shows that $S_{interact}$ is clearly worse at optimal peak irradiance for the 10% obscuration case, and even the $S_{interact}$ at 0.5x HV 5/7 is not insignificant for the 10% obscuration case at 100 kW. Also, due to strong aliasing between absorption and power discussed in the previous chapter, the low $S_{interact}$ values at higher power settings are relevant even if no system with that power setting is envisioned. The baseline assumption is the 80-percentile winter atmosphere by Mani, whereas an 80-percentile summer atmosphere will roughly double the thermal blooming

distortion strength. Even though no direct calculation of $S_{interact}$ was accomplished for a different atmospheric assumption in this research, there is every reason to suspect the effect of power on $S_{interact}$ is aliased with the effect of absorption, even as the two are aliased with respect to defocus effect on peak irradiance (Figures 3.21 and 3.22). In other words, $S_{interact}$ for 10% obscuration, 50 kW, 80-percentile summer atmosphere case will likely be about 0.8, the approximate value of $S_{interact}$ for 10% obscuration, 100 kW, Mani atmosphere case.

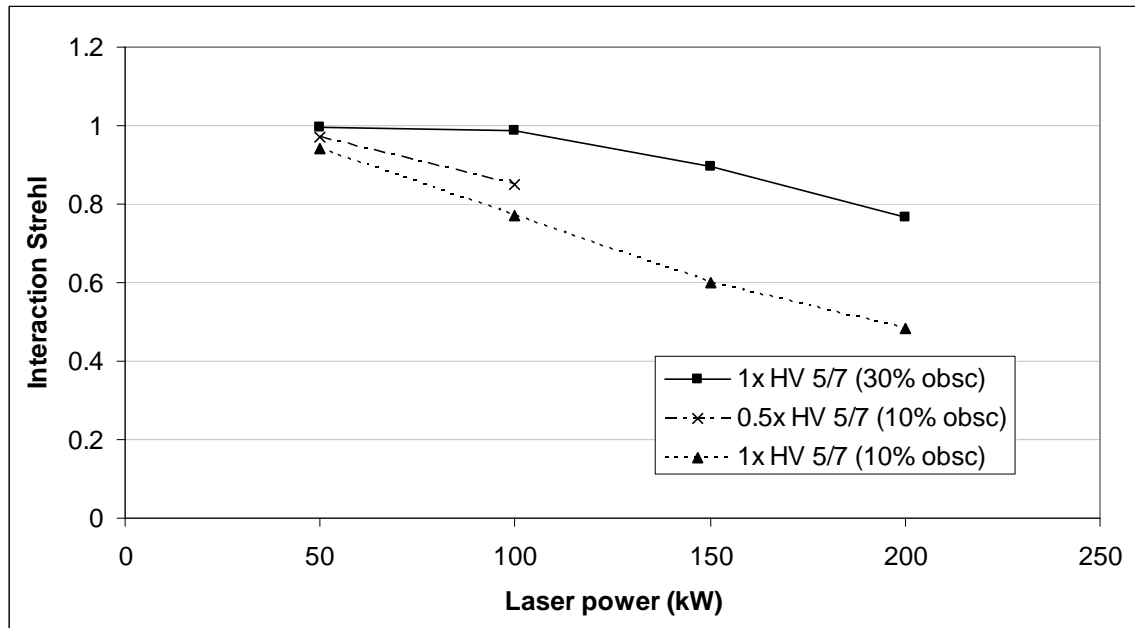


Figure 4.10. $S_{interact}$ at optimal defocus as a function of laser power by obscuration and turbulence assumption for otherwise baseline scenario.

4.7. Velocity Vector Relative to Target

In Chapter 3, there was seen to be a substantial benefit to flying with velocity vector perpendicular to the target vector over the case of flying level towards the target while propagating the laser. Here we investigate the same comparison with turbulence added. As mentioned earlier, we find that the perpendicular propagation remains the better performance point for both obscurations, but there are some interesting differences.

The primary difference between parallel and perpendicular propagation under turbulence is that, due to imperfect tracking, S_{turb} is worse in the perpendicular case even though the atmospheres are the same. We already saw in Chapter 3 that the N_D for the perpendicular propagation is lower due to the higher effective wind velocity through the beam tube. However, that higher wind velocity results in a higher turbulence bandwidth when turbulence is present, which has two effects:

First, the larger-scale, whole-beam tilt turbulence passes through the beam tube at a higher speed in the perpendicular case, but since the bandwidth of the tracker is constant, there is an increase in the residual tilt turbulence causing a reduction in S_{turb} due additional high-bandwidth spot motion at the target. Also, this motion will have a differential impact in the time-averaged irradiance pattern depending on the sharpness of the peak intensity point of the beam spot under a no-turbulence assumption: As discussed above, the sharper the peak under no turbulence, the more vulnerable is the time-averaged peak irradiance to a given beam dynamic due to turbulence.

Second, the smaller-scale turbulence likewise moves through the beam tube at a higher speed, but since the tracker does not compensate for these higher order fluctuations, this does not have an additional effect on S_{turb} ; however, since $S_{interact}$ arises at least in part from STRS, the distortion arising from local focusing and heating due to smaller-scale turbulence, the increase in bandwidth could improve (increase) $S_{interact}$ since there is less time for local focusing to cause thermal lens development, and if so, offset the effect of higher-bandwidth whole-beam turbulence.

Figure 4.11 shows the peak irradiance profile with respect to defocus for both velocity vectors under turbulence plus that for perpendicular propagation under no

turbulence with the 30% obscuration, and Figure 4.9 shows the same for the 10% obscuration, all at 200 kW.

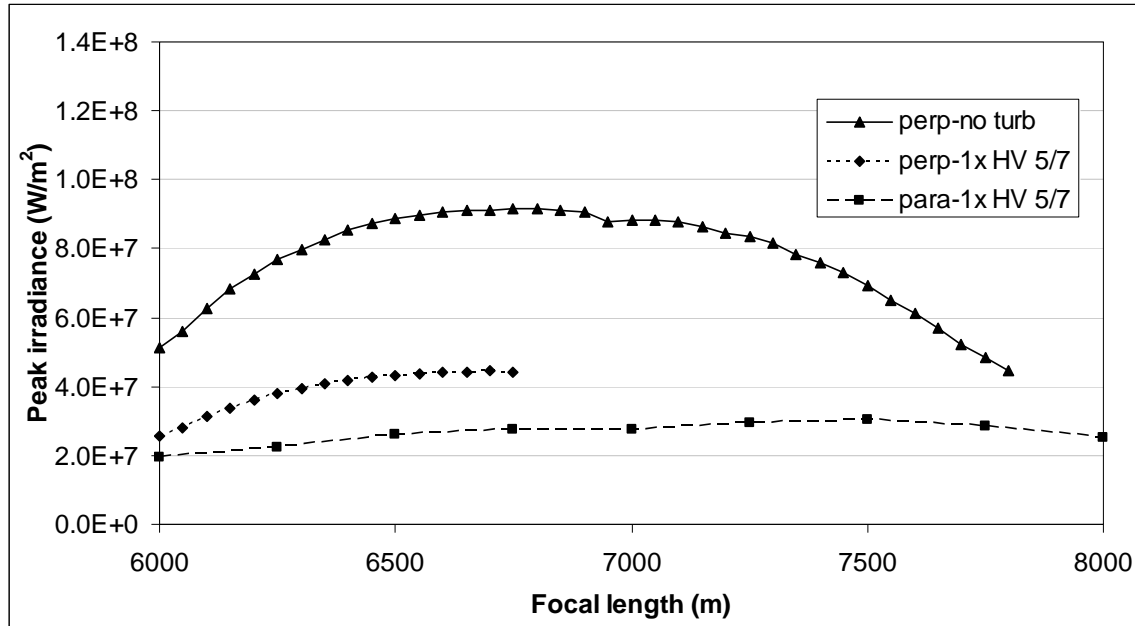


Figure 4.11. Peak irradiance as function of defocus for baseline scenario with 30% obscuration comparing perpendicular propagation performance to parallel case with turbulence and to perpendicular with no turbulence.

All of the points on the graphs in Figures 4.11 and 4.12 represent ACS runs with the exception of the perpendicular propagation lines with turbulence in each. For those, the focused case (focal length = 6000 m) and the focal length set equal to optimal focal length without turbulence for respective obscuration sizes were run in ACS. To estimate the points between the calculated points, a linear relationship between $S_{turb/TB}$ and focal length was assumed based on experience in this operating regime. Then calculating the estimated $S_{interact}$ by Eq 4.2, and applying that result along with known S_{turb} to the no-turbulence peak irradiance values, the estimated peak irradiance profile under turbulence is determined.

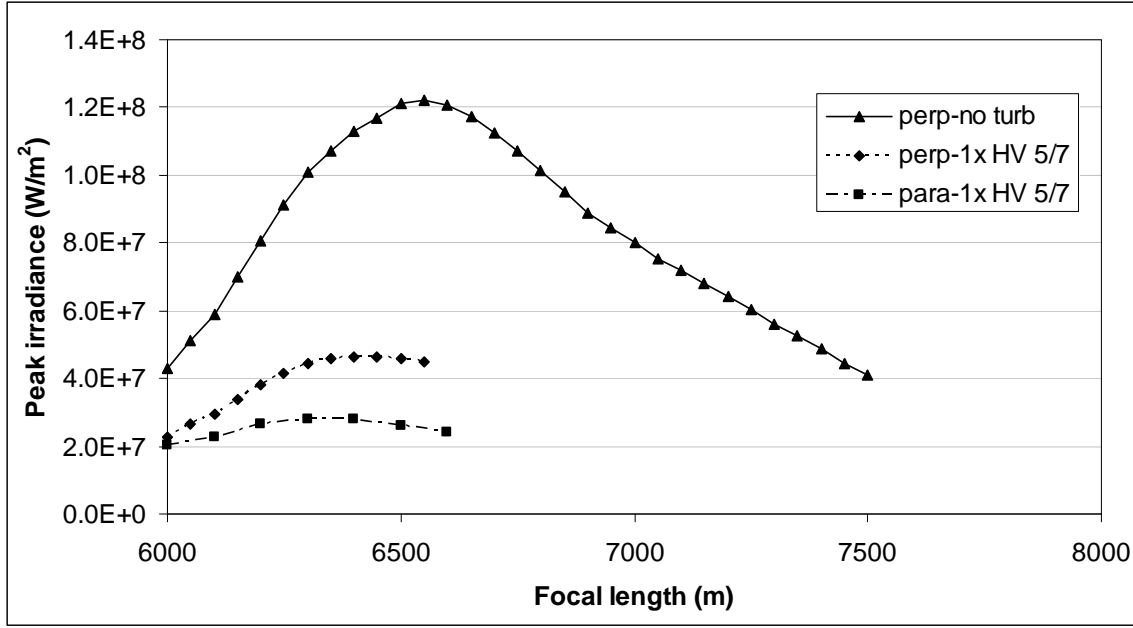


Figure 4.12. Peak irradiance as function of defocus for baseline scenario with 10% obscuration comparing perpendicular propagation performance to parallel case with turbulence and to perpendicular with no turbulence.

As with the parallel propagation cases, the 10% obscuration has an $S_{interact}$ that worsens considerably with defocus, while $S_{interact}$ for the 30% obscuration case is approximately the same at focused operation and at optimal defocus for the no-turbulence case. The result in the latter case is that the optimal operating point is the same regardless of the turbulence assumption. However, in the former case, since $S_{interact}$ worsens with defocus, the optimal focal length under turbulence is shorter than for the no-turbulence case. Figure 4.13 shows the value for $S_{interact}$ at focused and optimally defocused conditions for parallel and perpendicular propagation vectors, for both obscuration assumptions.

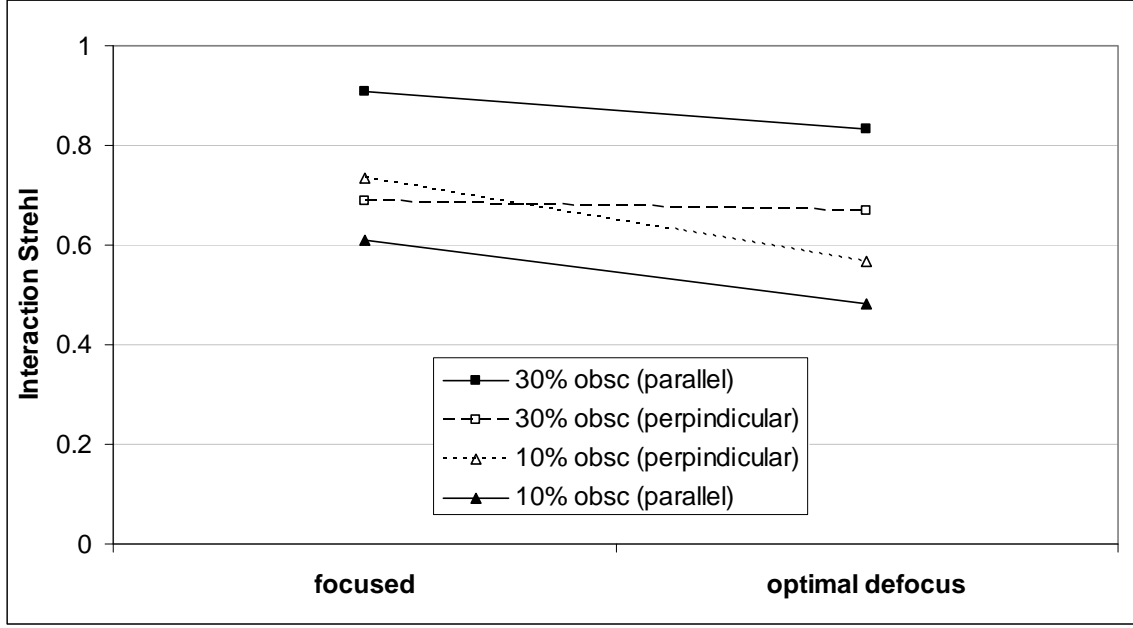


Figure 4.13. $S_{interact}$ at 200 kW as function of focus setting by obscuration size and propagation vector for otherwise baseline scenario.

4.8. Target Range

The impact of target range on ATL performance with respect to turbulence lies both in the interaction Strehl and in the performance difference between the 10% and 30% obscuration sizes. Figure 4.14 shows the baseline scenario (100 kW) interaction Strehl for the 30% obscuration case as a function of range at the optimal focal length for four range values and the same for 10% obscuration for two range values. Note that for the 30% obscuration case, shorter range $S_{interact}$ is actually greater than one, but that it drops below unity and decreases with range. The explanation for this is that at close range, non-turbulence N_D is so high due to tight focusing that time-averaged turbulent motion of the beam reduces N_D , offsetting thermal blooming more than the effect STRS has in contributing to it; however, at longer ranges (and all ranges for 10% obscuration) STRS dominates resulting in $S_{interact} < 1.0$. The $S_{interact}$ function is plotted for two levels of turbulence (1x and 2x HV 5/7), and note that for worse turbulence, the effect whether

positive or negative appears to be amplified. None of these 30% obscuration interaction effects is terrible, especially compared to the 10% obscuration results on the same graph. Note that the vertical axis in Figure 4.14 does not have zero at the origin.

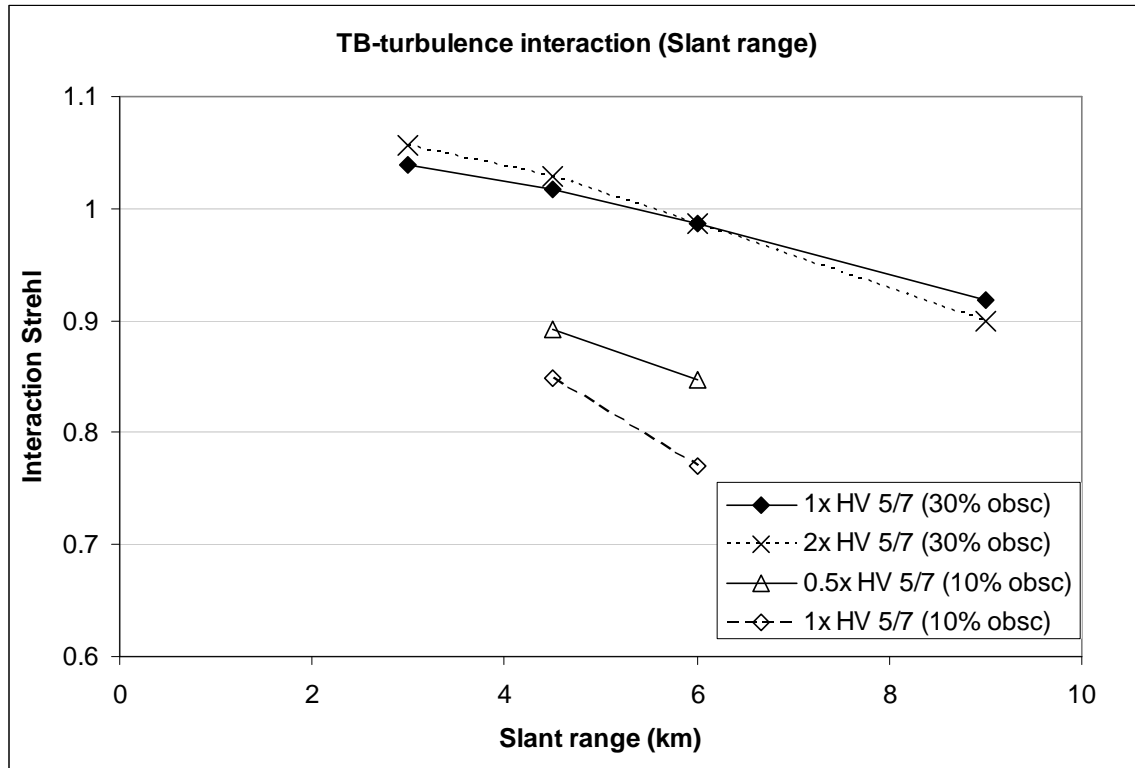


Figure 4.14. $S_{interact}$ for baseline scenario (100 kW) by turbulence multiple and obscuration size as function of slant range.

This differential effect based on obscuration size, already noted earlier, obviously reduces the advantage of the 10% obscuration seen in Chapter 3 as a function of range. Figure 4.15 repeats Figure 3.12 but adds the optimal defocus improvement factors with HV 5/7 turbulence included. The benefit of defocus for 30% obscuration is improved while that for the 10% obscuration is somewhat diminished, which could make a larger obscuration more advantageous in the design trade space.

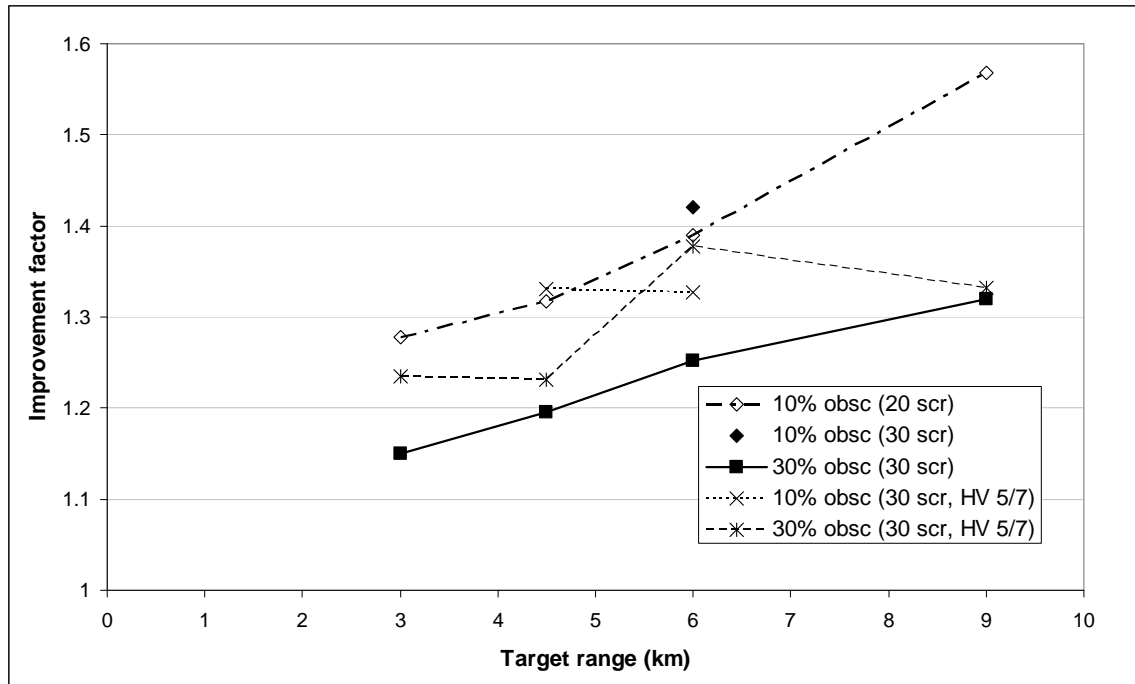


Figure 4.15. Improvement of target peak irradiance at optimal defocus over focused case as function of range to target of otherwise baseline scenario, for no turbulence and HV 5/7 turbulence cases. Note: 10% obsc., no turbulence, dash-dot line is comprised of 20 phase screen results; 10% obsc. & 30 phase screen result at range = 6 km (solid diamond) added as reference to suggest 20 screen line may be biased a bit low.

Figure 4.16 repeats Figure 3.13 from Chapter 3 which had shown a disproportionate advantage of the 10% obscuration which has been diminished due to interaction Strehl to now being merely consistent with the increase in the area of the propagating aperture that results from the smaller obscuration and 0.5 m fixed outer diameter. Again, while the 10% obscuration may well be the best design point, performance of competing obscuration sizes should be evaluated under turbulent rather than no-turbulence conditions.

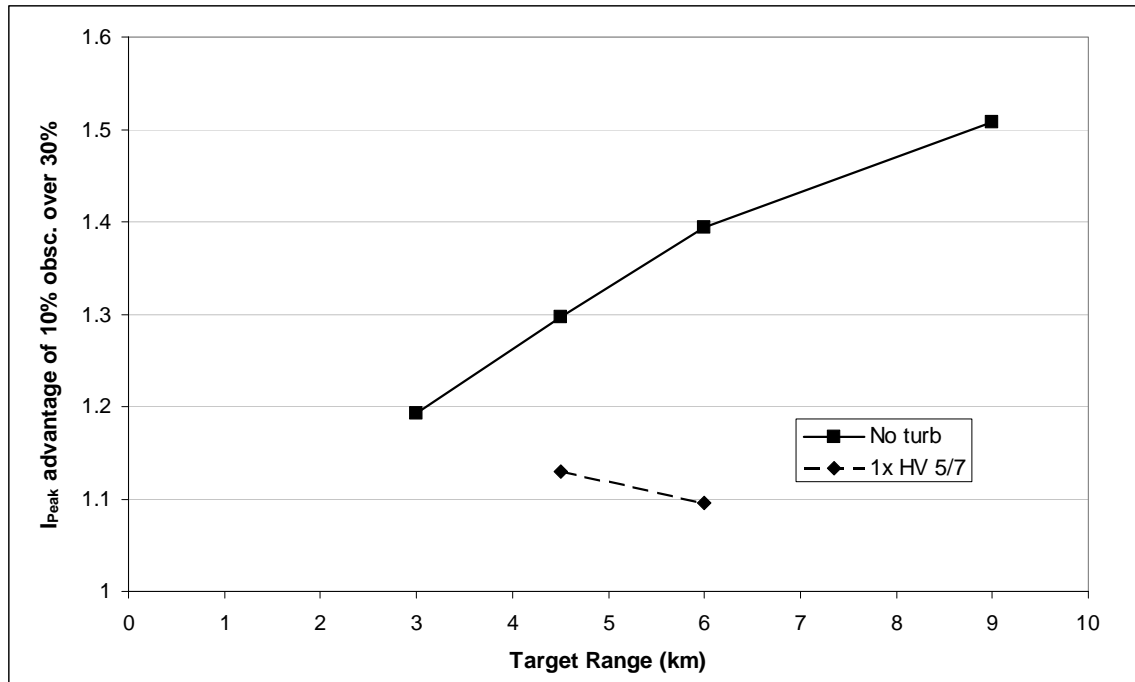


Figure 4.16. Peak irradiance improvement factor of 10% obsc. relative to 30% obscuration by range for otherwise baseline scenario by turbulence assumption.

4.9. Case Study

Using the knowledge gained from this and the previous chapters' work, a case study was undertaken to examine the effect of defocus on an ATL with a 10% obscuration in the presence of turbulence. Given the 10% obscuration, only two focus settings were examined at each operating point: focused and 5% defocus, which was shown to be a relatively stable approximation of the optimal defocus setting for 10% obscuration cases. With the exception of altitude and the variable settings in Table 4.2, the scenario is the same as the baseline scenario with 10% obscuration. Scenario variables were examined at only two settings, which we will denote "high" and "low" for each; the altitude variable is an exception to this since we examine altitudes of 2, 3, and 4 km.

Table. 4.2. “High” and “Low” settings for variables in the case study for otherwise baseline scenario at 10% obscuration.

Scenario variable	Low setting	High setting
Power	50 kW	100 kW
Range	4.5 km	6 km
Turbulence	0.5x HV 5/7	1x HV 5/7
Target azimuth	0 deg (<i>i.e.</i> , parallel)	90 deg (<i>i.e.</i> , perpendicular)
Wind speed at ground	4 m/s	10 m/s

First, we look at the improvement in peak irradiance due to defocus at each altitude as a function of the settings in Table 4.2. Figure 4.17 shows three graphs to illustrate the benefit of 5% defocus. The pivot point where all lines intersect in each graph represents the average result across all experimental points at the respective altitude, whereas each point on the graph represents the average of all experimental points with the given variable setting at that altitude. For example, at 2 km altitude, 5% defocus improves irradiance by about 40%. This is slightly improved upon at 3 km altitude, although, power and ground wind speed are clearly the largest factors affecting defocus improvement (approximately 60% average improvement for 4 m/s wind, 58% for 100 kW). Finally, defocus improvement jumps to 63% average across all experimental points at 4 km altitude, with power and wind providing practically all the variation.

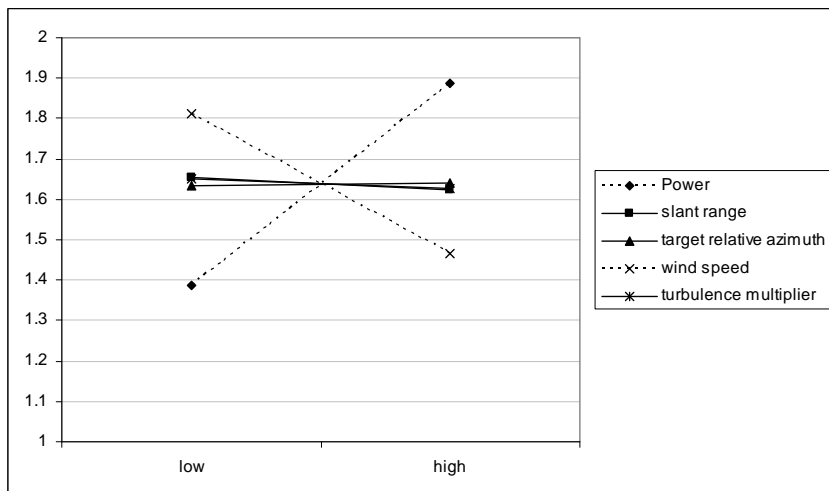
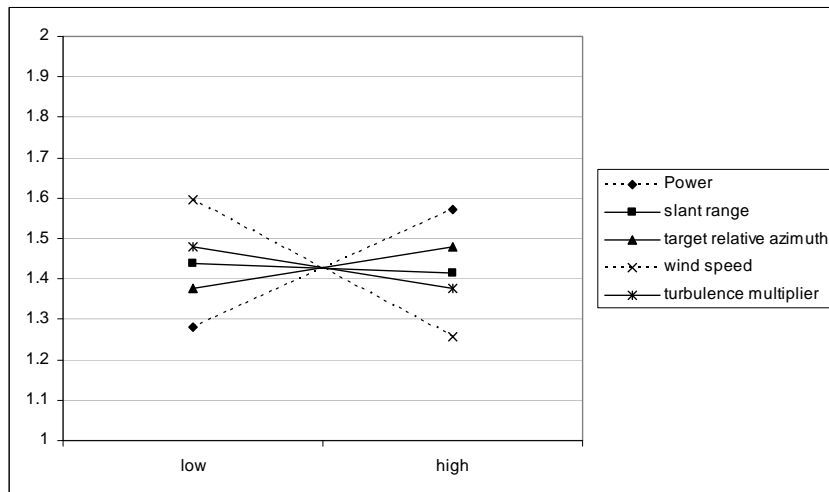
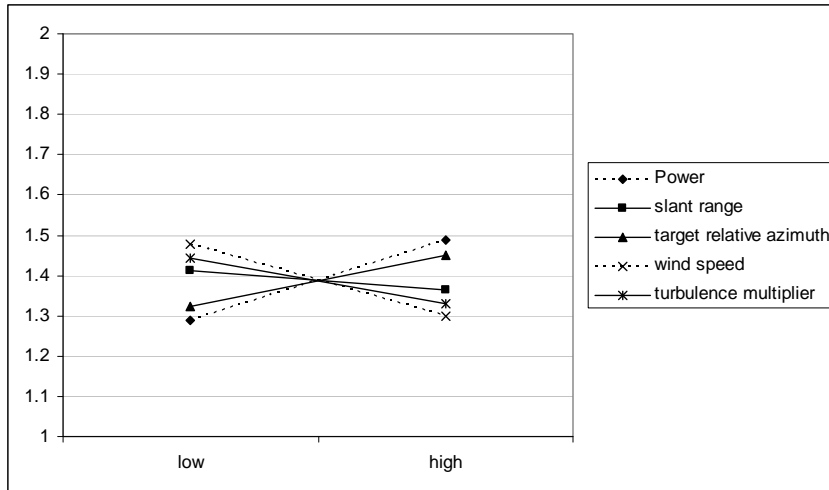


Figure 4.17. Irradiance improvement factor (vertical axis) due to 5% defocus at 2 km, 3km, and 4 km (top to bottom, respectively) by case study variable setting.

The result is evident that defocus can provide substantial performance increase (30-40% average for 50 kW, 50-90% average for 100 kW, depending on altitude). The fact that higher altitude reduces the variation in improvement caused by turbulence multiple, slant range, and target azimuth suggests a scaling law for defocus effect on thermal blooming would be easier to determine for higher altitude platforms. Figure 4.18 illustrates the combined wind and power effects on defocus improvement as a function of platform altitude; again each point is the average of all other points with same power, wind, and altitude variable setting. It also illustrates the aliasing of power and wind with respect to improvement due to defocus: Note the 50 kW-4 m/s defocus improvement graph closely overlays that of the 100 kW-10 m/s graph.

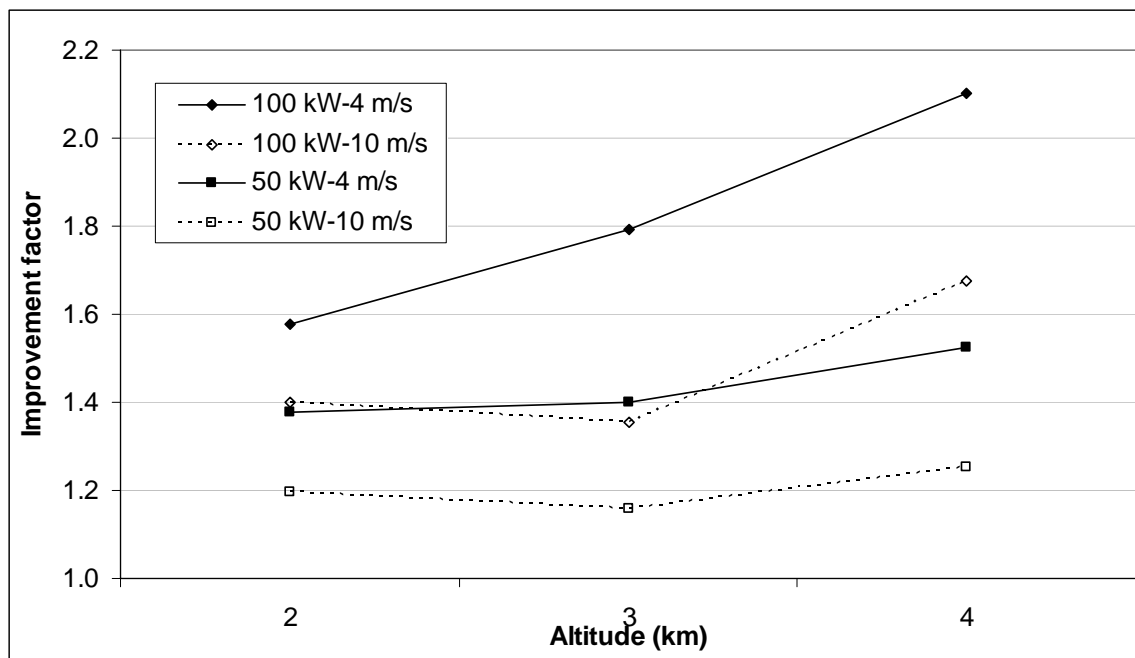


Figure 4.18. Improvement factor of 5% defocus as function of platform altitude by wind and power setting.

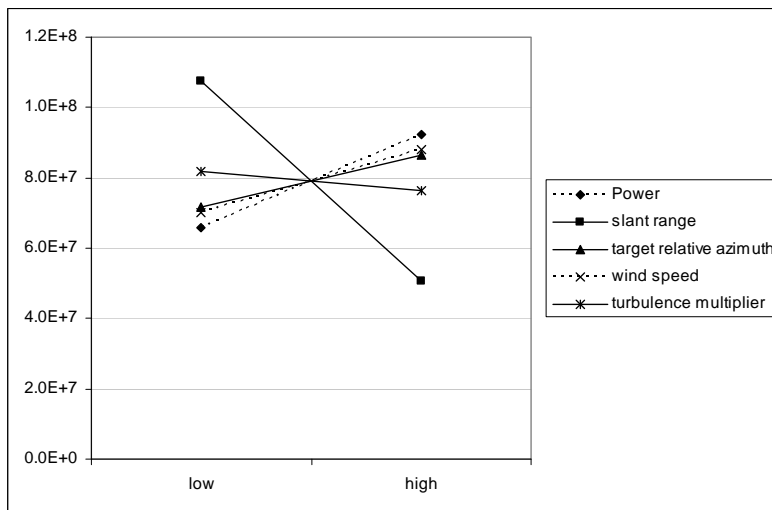
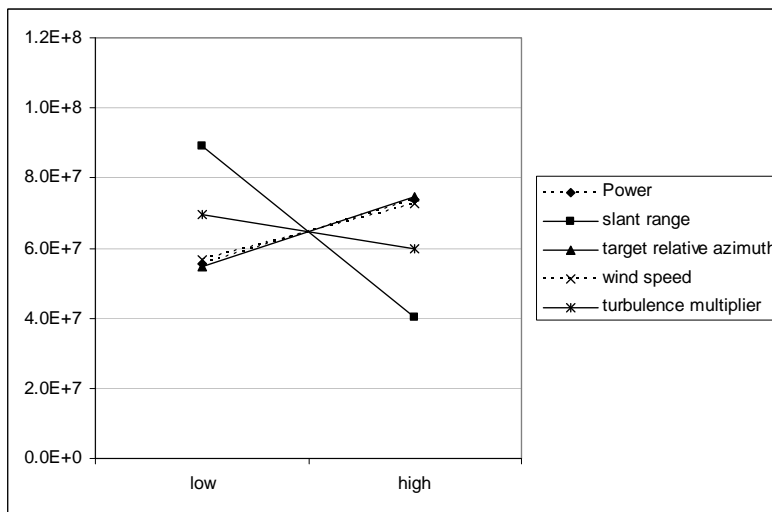
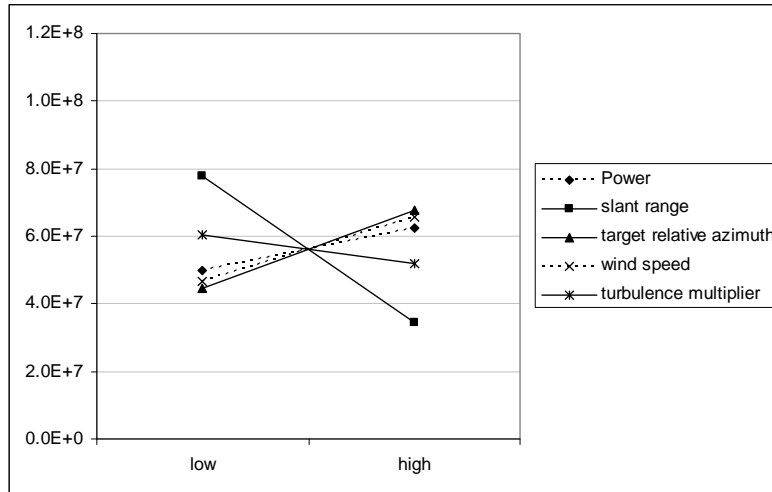


Figure 4.19. Irradiance in W/m^2 (vertical axis) with 5% defocus at 2 km, 3km, and 4 km (top to bottom, respectively) by case study variable setting.

Next we look at the effect of altitude on irradiance performance. Figure 4.19 shows that increased altitude from 2 to 4 km, keeping range constant, improves irradiance by more than a third, averaged across all the experimental points. This improvement at higher altitude is a result of reduced turbulence and absorption in the more vertical beam path, in addition to the increased responsiveness to defocus observed earlier for higher altitude. The figure shows that slant range has a huge effect on irradiance, which is to be expected, and that as altitude increases, the effects of wind and azimuth start to diminish relative to the impact of laser power. So, not only does a higher altitude operating point allow taking greater advantage of designed laser power, it also reduces the impact of the target azimuth during engagement. While the perpendicular azimuth is still better, the target azimuth scenario feature is one an operating crew may have little control over when engaging targets in a time sensitive or highly threatening environment, so reducing the effect of fact-of-life suboptimal engagement azimuths, among the many other benefits of operating at higher altitude, should be weighed against any downsides to operating at higher altitude.

Figures 4.20 and 4.21 show the effects of altitude on irradiance for 50 and 100 kW settings, respectively. These results are broken by slant range and target azimuth. This shows, again, the clear advantage of the perpendicular propagation, particularly at higher N_D values caused by higher absorption at lower altitude and higher power. Also, there is a geometric component to the reduced effectiveness of perpendicular propagation as altitude increases: For a given slant range, the higher the altitude of parallel propagation (defined in Chapter 3 as a target vector having component vectors parallel only to the ATL's velocity and altitude vectors) at a target on the ground, the greater the

angle between the propagation vector and the velocity vector. This results in increased effective wind through the beam tube reducing N_D , partially accomplishing what perpendicular propagation causes at lower altitude.

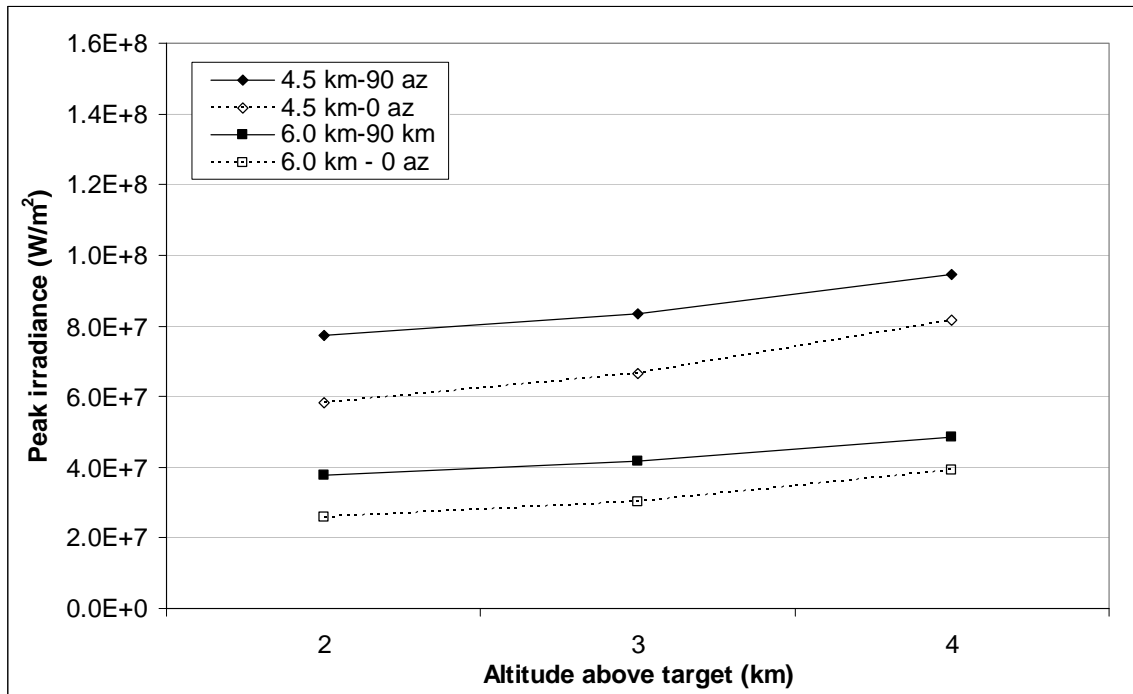


Figure 4.20. Peak irradiance at target for 50 kW output power as a function of platform altitude by target range and target azimuth averaged across all other settings in the case study.

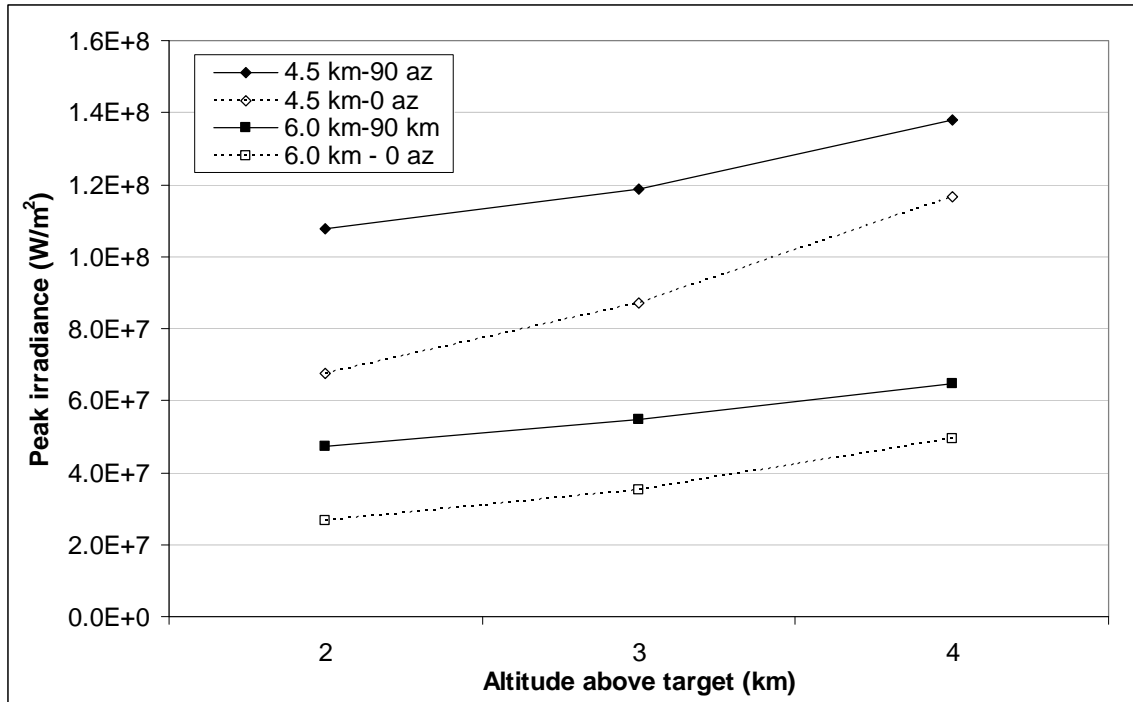


Figure 4.21. Peak irradiance at target for 100 kW output power as a function of platform altitude by target range and target azimuth averaged across all other settings in the case study.

This case study is useful for illustrating improved ATL operating points for the scenario considered, particularly for the assumption of a 10% obscuration. While earlier results presented in this chapter indicate that 5% defocus may be stable near the optimum defocus, such was not shown for every setting in the case study. Optimal irradiance at each design point almost certainly occurs at at least a slightly different defocus setting, but clearly 5% defocus provides extensive benefit across the design points and suggests using defocus to improve irradiance may work with open loop settings based on experiments with the actual system, as well as further study.

4.10. Conclusion

This research started with an important negative finding that defocus cannot be used as surrogate turbulence in the presence of TB for the ATG case as originally hoped. However, this finding led to realization in the ATL analytic community of significant negative turbulence-TB interaction in these scenarios.

The error in the previously common approach of using ten phase screens for ATL-type scenarios actually assisted in detecting the interaction phenomenon. As discussed in Chapter 3, 30 phase screen are required for adequate wave optics modeling of peak irradiance, particularly the latter's response to defocus. Additionally, too few phase screens inappropriately amplifies $S_{interact}$ which, in our effort, boosted $S_{interact}$ detectability when gathering data for and modeling irradiance and defocus under the 10 phase screen assumption. Concerns about 30 phase screens being too numerous and therefore undermining performance of the turbulence wave optics model appear to be unfounded in the ATL cases at turbulence strengths up to 2x HV5/7.

$S_{interact}$ is much worse for 10% obscuration than for 30% obscuration at optimal defocus in the scenarios investigated. This appears to be related to the phenomenon that causes 10% obscuration performance to be significantly better than 30% obscuration in no-turbulence cases at optimal defocus, which is that the former's more peaked irradiance pattern is more vulnerable to being knocked down by the time-averaged motion due to turbulence. The result of this is that 10% obscuration performance at optimal defocus under turbulence is not disproportionally superior as it is under the no turbulence assumption. It would be useful to further investigate this disproportionality at different turbulence settings since there is such high sensitivity in the response between 0x and 1x

HV5/7. This finding suggests that, especially when defocus is considered, not accounting for $S_{interact}$ inappropriately imbalances the obscuration-size trade space towards the 10% obscuration, though of course many other factors will be involved in the obscuration size decision.

Despite the foregoing, a primary finding from this chapter that still strongly favors the 10% obscuration is the near constant defocus length for optimal performance across many scenarios. From Chapter 3, recall that no-turbulence optimal defocus for the 30% obscuration case (the baseline scenario) varied widely based on power, range, and other aliasing factors that affect N_D . In this chapter, a stable $S_{interact}$ is reported with respect to defocus for the 30% obscuration, meaning turbulence and non-turbulence optimal defocus lengths are almost equivalent. No-turbulence optimal defocus for 10% obscuration scenarios were found to be in a much tighter range. When adding 1x HV5/7 to these scenarios, the phenomenon of worsening $S_{interact}$ as a function of defocus counterbalances the small increase in optimal defocus as N_D increases for no-turbulence cases. The result for 10% obscuration cases is that 5% defocus is approximately optimal for the otherwise baseline scenario at all power settings. Since power is aliased with absorption and wind, this is a strongly significant result, at least for HV5/7.

The most important finding out of the case study is the superiority of higher altitude with respect to performance, primarily in terms of improved peak irradiance on target, but also importantly as a means to offset variation in performance that occurs as the horizontal component of the target vector varies between propagation parallel to the velocity vector (shooting straight ahead and down) and perpendicular to the velocity vector (shooting to the side and down). However, target range is of course also highly

influential to peak irradiance performance and must be traded with altitude to address vulnerability. However, if vulnerability is mainly a function of slant range (and not elevation or ground range, for example), the higher altitudes provide the best performance.

5. Summary and Recommendations

5.1 Introduction

The contributions of this research into modeling the case of the air-to-ground thermally bloomed HEL are summarized below. With some detectable overlap as one reads below, these contributions can be grouped into the following categories:

- (1) Consistent benefit of defocus on peak irradiance (I_{peak})
- (2) Importance of central obscuration size
- (3) Interaction of thermal blooming and turbulence
- (4) Wave-optics modeling issues in ATL environment
- (5) COIL ATL operational considerations
- (6) Analysis and advancement of existing scaling laws
- (7) Improved research techniques

Intermingled with discussion of these contributions will be focused suggestions for additional research. A later section will elaborate on general research suggestions.

5.2. Summary of Research Contributions

5.2.1. Improvement with Defocus

In a generalized space of reasonable ATL scenarios, it was found that defocusing the beam provides a simple and effective way to improve peak irradiance at target when thermal blooming potential is significant. This is important since defocusing is typically available in laser systems even in the absence of higher order wavefront correction functionality. The amount of improvement gained by defocusing varies according to the scenario variables, but for typical ATL scenarios, the improvement seems to be at least

20% and as high as 100% or more in some cases. Beyond defocusing alone, adding higher order correction wavefront correction may further improve peak irradiance but this approach can be quite expensive in terms of design and engineering resources, and the incremental gain in the thermal blooming environment (beyond that achievable from defocus) may not justify the expense—although the latter would be an excellent subject of additional research.

5.2.2. Defocus Stability for 10% Obscuration

Additionally, for the 10% obscuration, it was found that a 5% defocus was optimal or near optimal for many ATL scenarios and at least quite beneficial in every scenario of the case study of Chapter 4. On the other hand, for a 30% obscuration, the optimal defocus was less stable and more dependent upon the focused-case thermal blooming distortion number. Further, we found the addition of turbulence to the model affects the 10% obscuration case more than the 30% obscuration case: For the 10% case, turbulence-thermal blooming interaction Strehl is both worse and has a larger negative partial derivative with respect to defocus distance. This difference in impact has to do with the reasons the 10% obscuration case generally has higher irradiance than the 30% case with no turbulence, that is, the 10% case has a higher peak irradiance resulting from a narrower, more focused beam spot. The narrower beam spot is more susceptible to reduction due to turbulence than the less-peaky, wider beam spots of the 30% obscuration case. The lesson here is that turbulence is something of an equalizer of performance between the two obscuration cases (though optimal defocus is still more stable for 10% case), and the warning is that modeling ATL performance with a 10% obscuration

affected by thermal blooming only, and no turbulence (a common temptation due to computer run time cost), will produce overly optimistic results that simply applying turbulence Strehl after the fact will not correct, particularly when trying to capture the defocus effect. The warning is even sterner for modeling 30% obscuration cases with thermal blooming and defocus without turbulence, since higher order effects that appear to offer attractive performance will arise at defocus distances that turn out to be suboptimal when the reality of turbulence is added.

5.2.3. Sensitivity to Obscuration Size

An unexpected difference in performance between the 10% and 30% obscurations and defocus in thermal blooming environment was discovered. While this difference may be mitigated by turbulence, as discussed above, since much thermal blooming modeling is accomplished without the turbulence assumption (which requires multiple runs for averaging), scientists need to be aware that nonlinearities in thermal blooming effect, apparently resulting from different far field patterns, may arise as the obscuration parameter is varied. It will be important to test the design region with turbulence factors applied to ensure optimalities found during system engineering are not undone due to the turbulence-thermal blooming interaction.

5.2.4. Thermal Blooming-Turbulence Interaction

For those same ATL scenarios, when thermal blooming is significant, as mentioned above, we have found that an interaction between turbulence and thermal blooming arises that usually reduces peak irradiance performance. This interaction

worsens with N_D , causing an even tighter limitation on critical power than thermal blooming alone. The effect appears worse for the 10% obscuration critical power, which for the baseline scenario has a critical power of about 250 kW. With turbulence, critical power is reduced to 100 kW. For the 30% obscuration, the analogous critical powers are 200 kW and 125 kW without turbulence and with turbulence, respectively (though the 10% case retains a performance advantage). The common practice of applying turbulence independently will not cause the critical power to shift.

5.2.5. Phase Screen Count

For ATL-like scenarios in which thermal blooming is significant, the common standard of using ten phase screens in wave optics models is inadequate to model thermal blooming both with no turbulence assumed and also with turbulence present. In the no-turbulence case, the effect of ten phase screens being too few is much more noticeable at defocused settings than focused settings, which in addition to the habit of not simultaneously modeling turbulence, explains why this standard has not been problematic. When turbulence is added to the wave optics models however, the fact that ten phase screens is too few is noticeable regardless of focus setting. Too wide spacing of the phase screens for these cases, especially near the target where thermal blooming is strongest and turbulence is strongest, inappropriately magnifies the thermal blooming and turbulence interaction—this is due to long moment arms between the phase screens that allows local focusing to occur in the model that would be offset by thermal blooming in a more finely modeled atmosphere. This in itself is noteworthy since the negative interaction is little reported in literature, suggesting this interactive regime of modeling

has much more to discover in it. At the 2005 Directed Energy Symposium, several researchers approached, glad to hear our presentation [Long *et al.* 2005] because they were seeing similar results and did not have good explanations for them.

5.2.6. Defocus Improvement at Lower ATL Powers

Based on this research, aliasing between power, transverse wind, and absorption could lead to significant thermal blooming even at a planned ATL power of 50 kW. In the baseline scenario, the 50 kW case experienced some thermal blooming such that defocus was helpful, but the results were not as dramatic as they were for higher powers. However, our baseline scenario can be considered somewhat optimistic since we assumed a relatively fast 10 m/s (20 knot) ground wind, and thermal blooming is reduced in proportion to ground wind. Realistically, ground winds can very often be less than half or even a quarter of that velocity, meaning the 100 kW and 200 kW analyses for the baseline scenarios would be applicable to the 50 kW case---and for those higher powers, defocus is much more helpful. The same goes for absorption. The baseline scenario was pessimistic for winter (worse than 80% of winter atmospheres), but the equally pessimistic summer case has about twice the absorption, so the 100 kW analysis would be applicable. Further, these are independent so that together, the thermal blooming effect could be that of a 400 kW laser which is past the critical power point, at least for 2 km altitude. The suggestion here is that defocus should still be quite helpful to a 50 kW ATL and the warning is that thermal blooming could be devastating in some scenarios, unless better operating regimes are found, such as higher altitudes.

5.2.7. Higher Altitude, Transverse Propagation Improve Performance

During this research most concepts of operation discovered had the ATL operating below 3 km altitude. Also, little discussion was found on the subject of the propagation vector relationship to the velocity vector. This research shows that significant performance improvements in the presence of thermal blooming can be gained by having the ATL operate at higher altitudes for a given range, or equivalently that range could be increased at higher altitudes to get similar performance to a lower altitude shorter range engagement. Also, engaging the target with a side (perpendicular) shot significantly improves performance over engagement of the target while flying towards it (parallel shot). The advantage of the perpendicular shot attenuates with altitude so the two approaches could be traded off to find the best engagement geometry that also affords the platform security against ground-to-air threats. However, the higher altitude (between 3 and 4 km) appears to be the best position when the crew is uncertain where the next target will be. Additionally, when the engagement takes advantage of increased altitude or a more perpendicular shot, the benefit of defocus is magnified, making it all the more important to explore this effect experimentally, both pre-design and post-design. One unknown that should be the subject of future research is the aero-optic effect of perpendicular propagation. If turbulence across the face of the exit aperture degrades the beam, there may be an optimal angle off the velocity vector (probably scenario dependent and likely more forgiving at higher altitude) to be discovered that is short of full perpendicular propagation. Another bit of research that would be useful is development of critical power graphs for higher altitude. This could reveal whether higher power lasers in the COIL wavelength could be effectively deployed in the ATL mission.

5.2.8. Improved HELEEOS Scaling Law Model

During this research, a scaling law improvement was discovered for the widely-used SAIC's HELCOMES HEL model, which was the basis for AFIT's HELEEOS scaling law model. The original, uncorrected formulation had suppressed the sensitivity of N_D to output power due to overfitting for other parameters at 50 kW only. We showed that linear scaling of the HELCOMES N_D for output power vastly improved accuracy of the model for other powers ranging from 10 to 200 kW for the air-to-ground scenario. HELEEOS authors quickly incorporated the change.

5.2.9. Scaling Law Consistency Analysis Technique

A technique was crafted and demonstrated in this research that can be used to determine consistency of a scaling law in all of its variables. The purpose of a scaling law is to find accurate relationships between the factors that affect a laser's performance, usually in term of Strehl which is the ratio of peak irradiance performance after application of a factor (or set of factors) to performance prior to application. By representing such relationships, scaling laws intend to reduce dimensionality of the problem by rolling several factors into a single scaling variable. In thermal blooming analysis, N_D is the scaling variable we seek to define for which there is a one-to-one relationship with thermal blooming Strehl. In a good scaling law, the effect of a change in a factor (*e.g.*, defocus or power) on N_D should preserve the relationship between N_D and thermal blooming Strehl as the latter is determined from application of the factor. In other words at every value of N_D , the derivative of Strehl with respect to N_D should be the

same regardless of which factor is changed. When this derivative is discovered to have different values for changes to different factors in the N_D equation, the scaling variable can be said to be inconsistent and that a better relationship between factors should be found for the scaling variable.

5.2.10. Defocus Scaling Law Structure

This research identified an adjustment to the Breaux N_D , a successful focused-case scaling law, by using the Smith focus correction factor to craft an equally successful defocused scaling law and utilized the consistency analysis described above to evaluate the success of the adjustment. If defocus is going to be a common approach for ATG lasers, it will be useful to build scaling laws that represent the amount of improvement as a function of defocus. We showed that Breaux's N_D formulation was unable to account for the effect of defocus due to inherent static assumptions about beam spread due to thermal blooming. This renders the Breaux law only suited for focused case use in the ATG regime. However, application of the Smith correction factor, which he derived for a completely different scaling law, was determined to be effective for the Breaux law. The combined formulation preserves the advantages of Breaux, but adds the flexibility of defocusing. It also suggests minimal modifications would be necessary to existing code that uses the Breaux law as a basis.

5.2.11. Wave Optics Processing Improvements

This research resulted in technique to leverage AFIT's linux blade server to run many ACS scenarios at once, tremendously enabling our research (to include recovery

from the 10 phase screen problem discovered late in research) and vastly accelerated HELEEOS team to build up experimental design tie points. The HELEEOS design team has been able to run thousands of scenarios using this approach, whereas when trying to run using the High Performance Computing Center, runs were very difficult to get started, and when started, frequently terminated before execution completion. We also found that despite early advice, it was more efficient to conduct several runs using a single processor each rather than attempting to use multiple processors to speed up a single run.

5.3. Recommendations and Suggestions for Future Research

5.3.1. Power-in-the-Bucket Scaling Law

This research initially attempted to investigate the development of a scaling law to address power-in-the-bucket (PIB) performance of a laser system rather than peak irradiance which is the common practice. In this effort, there was tremendous success in developing non-linear techniques that fit Gaussian surfaces, bivariate Gaussian surfaces, and distorted versions of the foregoing to beam spots that had been subjected to thermal blooming. The results were particularly successful when fitting to irradiance values larger than $1/e$ times the peak value when fitting to the main lobe of the beam spot. However, since this was a multi-dimensional scaling law we were seeking, for a PIB measure, it was important to preserve power in predicted Gaussian fits. This meant we could not fit the parameters independently, but had to constrain them to the power propagated. The obvious parameter to fit independently is peak irradiance, so we went back to that in hopes of perfecting those scaling laws. The next step would be

development of derivative scaling laws (that depend on accurate peak irradiance prediction) for the purpose of predicting power inside a given radius around a target aimpoint. Initial findings are that only one or two more parameters would be needed to develop an accurate PIB scaling law from an accurate peak irradiance scaling law. The attraction to PIB measures are that the effects are more intuitive and physical than mere peak irradiance at a point, and the performance is less sensitive to range. Also, it may be easier to develop vulnerability models from a PIB perspective than a peak irradiance perspective. Finally, peak irradiance limited approaches may lead to system designs that are optimal in a narrow range of assumptions that may not be robust in real engagements.

5.3.2. Higher Order Approaches

It is important to keep in mind that application of defocus to a thermally bloomed beam in the ATL environment is probably not best thought as a phase correction. Rather, it is a trade between thermal blooming Strehl on the one hand and defocus Strehl on the other. With increased defocus in our ATL scenarios, the value of N_D decreases which results in thermal blooming Strehl increasing faster than defocus Strehl decreases. This causes peak irradiance to rise until the slopes of both Strehl profiles (defocus and thermal blooming) are equal and opposite as a function of defocus. There may be other, higher order shapes to explore for effect, in particular a cylinder. Since it is the beam spreading transverse to the wind vector that contributes most to reduced peak irradiance, application of cylinder (one-dimensional prespreading of the beam) to forestall thermal blooming in substitution for some defocus could result in even higher peak irradiances. There are many challenges with this approach: (1) Investment in capability to apply cylindrical

prespreading would be expensive, so performance above defocus alone would have to be significant to justify; (2) the Smith correction factor is based on defocus. An additional correction factor would be needed to further adjust the Breaux N_D to account for cylindrical prespreading; (3) precise knowledge of wind direction and ability to orient the cylindrical prespreading with it would be needed. Related work was presented at 2005 Directed Energy Symposium in which a fitting method was used to determine a “phase correction” to a thermally bloomed beam to optimize peak irradiance. The amount of cylinder in fits like these could indicate potential for this research.

5.3.3. Investigate Other Wave Optics Codes

Other popular wave optics codes, in particular WaveTrain, should be examined using the lessons learned from ACS. Investigations of optimal numbers and placement of phase screens and sensitivity to deviations from optimal would be very useful for building a body of knowledge that the modeling community could use for setting up runs with confidence of accurate results.

5.4. Conclusion

It is interesting that despite having an early goal to move beyond modeling of peak irradiance by looking at power-in-the-bucket performance in the air-to-ground thermally bloomed HEL, we ended up focusing even more deeply on accurate prediction of peak irradiance and improvement thereof. Stepping back, this was not a terribly surprising turn in the research since peak irradiance will always be a useful and probably necessary parameter in establishing PIB scaling law models, a goal which this research

nevertheless advances. Additionally, it remains an open question as to the best way to develop target vulnerability models (based on I_{peak} or PIB), in part because there is always trade off between the pristine-ness of the vulnerability model and the ability to predict all of the engagement parameters needed to apply that pristine a model. However, all other things being equal, it would be surprising if increased I_{peak} (achieved, *e.g.*, by defocus or increased altitude) would not be a better operating point, and certainly useful to know how to do it.

As suggested in previous chapters, this research was motivated in part by the US Air Force's Advance Tactical Laser (ATL) program. By necessity, such programs are fast-moving with the resulting possibility of missing a performance-improving, or risk-reducing, feature in the systems engineering phase. It is satisfying therefore to identify the benefits of defocus and of other operational enhancements; the warnings of thermal blooming potential and interaction with turbulence; and a pathway to a defocus scaling law for I_{peak} that could benefit even this fairly mature system, as well as future concepts to be considered.

Bibliography

1. AFIT short course notes, 2003: "Introduction to Adaptive Optics," Dept. of Electrical Engineering and Computer Science, July 2003.
2. Al-Habash, M. A., L. C. Andrews, and R. L. Phillips, 2001: "Mathematical model for the irradiance probability density function of a laser beam propagating through turbulent media," *Opt. Eng.*, Vol. 40, No. 8 (August 2001), pp. 1554-1562.
3. Andrews, Larry C. and Ronald L. Phillips, 1998. *Laser Beam Propagation through Random Media*, SPIE Press.
4. Andrews, Larry C., Ronald L. Phillips, and Cynthia Y. Hopen: 2001. *Laser Beam Scintillation with Applications*, SPIE Press.
5. Azar, Maurice, 2003. "Assessing the Treatment of Airborne Tactical High Energy Lasers in Combat Simulations", Masters Thesis, Air Force Institute of Technology.
6. Berger, Paul J., Robert D. Stock, and J. Herrmann, 1994: "Plan for Comparing Propagation Codes Used in Navy ASMD Simulations" (Draft), MIT, Lincoln Laboratory
7. Born, Max and Emil Wolf, 1999: *Principles of Optics*, 7th Ed., Cambridge Press.
8. Bradley, L. C. and Herrmann, J., 1974; "Phase Compensation for Thermal Blooming," *Applied Optics*, Vol. 13(2), pp. 331-334 (Feb 1974).
9. Breaux, Harold J., 1979: "Simplified predictive methodology for nonlinear repetitive pulse and CW high energy laser propagation," SPIE Vol. 195 *Atmospheric Effects on Radiative Transfer*, 1979, pp. 192-202.
10. Breaux, H., W. Evers, R. Sepuche, and C. Whitney, 1979: "Algebraic model for cw thermal-blooming effects," *Applied Optics*, Vol. 18, No. 15 (1 August 1979), pp. 2638-2644.
11. Chambers, D. H.; Karr, T. J.; Morris, J. R; Cramer, P; Vieceili, J. A.; Gautesen, A. K., 1990; "Linear theory of uncompensated thermal blooming in turbulence," *Physical Review A*, Vol. 41, No. 12 (15 Jun 1990), pp. 6982-6991.
12. Edwards, Brian, 2004: "*Thermal blooming mitigation: experimental results*," presentation, Directed Energy Professional Society, Modeling and Simulation Conference, March 2004.

13. Fante, Ronald L., 1980: "Electromagnetic Beam Propagation in Turbulent Media: An Update," *Proceedings of the IEEE*, Vol. 68, No. 11 (November 1980), pp. 1424-1443.
14. Fante, Ronald L., 1983: "Inner-scale effect on the scintillations of light in the turbulent atmosphere," *J. Opt. Soc. Am.*, Vol. 73, No. 3 (March 1983), pp. 277-281.
15. Fiorino, S.; Bartell, R.; Perram, G.; Manning, Z.; Long, S.; Houle, M.; Krizo, M.; Bunch, D.; and Gravely, L.; 2005: "Critical Assessment of Relative Humidity and Aerosol Effects on Lower-Atmospheric High Energy Laser Engagement," presentation, Directed Energy Professional Society, Modeling and Simulation Conference, March 2005.
16. Fried, D. L., 1966: "Optical Resolution Through a Randomly Inhomogeneous Medium for Very Long and Very Short Exposures," *J. Opt. Soc. Am.*, Vol. 56, No. 10 (Oct 1966), pp. 1372-1379.
17. Gebhardt, Frederick G., 1976: "High Power Laser Propagation," *Applied Optics*, Vol. 15, No. 6 (June), pp. 1479-1493.
18. Gebhardt, Frederick G., 1993: "Nonlinear Propagation: Thermal Blooming," chapter 4 in *The Infrared & Electro-Optical Systems Handbook, Vol 2: Atmospheric Propagation of Radiation*. Fred G. Smith, Ed. SPIE, pp. 287-311.
19. Goda, Matthew E., 2004: personal conversation, Sep 2004.
20. Golnik, Gary, 1993. "Directed Energy Systems," chapter 5 in *The Infrared & Electro-Optical Systems Handbook, Vol 8: Emerging Systems and Technologies*. Stanley R. Robinson, Ed. SPIE, pp. 403-480.
21. Goodman, Joseph W, 1996: *Introduction to Fourier Optics*, McGraw Hill.
22. Hogge, Charles B., 1974: "Propagation of High Energy Laser Beams in the Atmosphere," chapter 4 in *High Energy Lasers and Their Applications, Vol 1: Laser Physics*. Stephen Jacobs *et al.* Eds. Addison-Wesley Publishing, pp. 177-246.
23. Isaimaru, Akira, 1981: "Theory of optical propagation in the atmosphere," *Optical Engineering*, Vol 20 (January/February 1981), pp. 63-70.
24. Kanev, F.; Lukin, V.; and Lavrinova, L.; 1998: "Analysis of algorithms for adaptive control of laser beams in a nonlinear medium," *Applied Optics*, Vol. 37, No. 21 (20 July 1998), pp. 4598-4604.

25. Link, Don, 2003a: "Atmospheric Compensation Simulation" users manual. SAIC, 19 Mar 2003.
26. Link, Don, 2003b: "Thermal Blooming in ACS," SAIC technical report, 22 July 2003.
27. Long, Scott N., 2004a: "*Gaussian fits to wave-optics thermal blooming simulation output*," presentation, Directed Energy Professional Society, Modeling and Simulation Conference, March 2004.
28. Long, Scott N., 2004b: Specialty exam write-up for Dr J.O. Miller. Apr 2004.
29. Long, Scott N.; and Miller, J. O.; 2005: "Thermal blooming PIB Scaling Law Development for COIL HEL—Work to Date," presentation, Directed Energy Professional Society, Modeling and Simulation Conference, March 2005.
30. Long, Scott N.; Miller, J. O.; Brigantic, Robert T.; and Goda, Matthew E., 2007: "Using Defocus to Improve Peak Irradiance for Air-to-Ground High Energy Laser Weapons", *Journal of Directed Energy*, Vol. 2, No. 3 (Spring 2007), pp. 189-209.
31. Lukin, Vladimir P. and Boris V. Fortes, 1998: "Estimation of turbulent degradation and required spatial resolution of adaptive systems," SPIE Vol. 3494, pp. 191-202.
32. Lutomirski, R. F., and H. T. Yura, 1971: "Propagation of a Finite Optical Beam in an Inhomogeneous Medium," *Applied Optics*, Vol. 10, No. 7 (July 1971), pp. 1652-1658.
33. Magee, Eric P.; and Ngwele, Amy M.; 2005: "ATMTools: A Toolbox for Atmospheric Modeling Propagation Modeling, User's Guide, Version 2.2" ATK Mission Research Corporation document, 15 April 2005.
34. MatLab user documentation, 2004. Version 7.0. The MathWorks, Inc.
35. Mani, S.; 2004: "Atmospheric Transmission Models," unpublished paper, 2004.
36. Pearson, J. E., 1978: "Thermal blooming compensation with adaptive optics," *Optics Letters*, Vol. 2, No. 1 (January 1978), pp. 7-9.
37. Perram, Glenn, 2003: personal conversation, Nov 2003.
38. Roggemann, Micheal and Byron Welsh, 1996: *Imaging Through Turbulence*, CRC Press.

39. Sadot, D.; Melamed, A.; Dinur, N.; and Kopeika, N. S.: 1994; "Effects of aerosol forward scatter on the long- and short-exposure atmospheric coherence diameter," *Waves in Random Media*, Vol. 4 (1994), pp. 487-498.
40. Sadot, D.; Shamriz, S.; Sasson, I.; Dror, I.; Kopeika, N. S.; 1995: "Prediction of overall atmospheric modulation transfer function with standard weather parameters: comparison with measurements with two imaging systems," *Optical Engineering*, Vol. 34, No. 11 (November 1995), pp. 3239-3248.
41. Schoen, N. C.; and Novoseller, D. E.; 1983: "Multiple aperture laser systems for thermal blooming environments," *Applied Optics*, Vol. 22, No. 21 (1 November 1983), pp. 3366-3370.
42. Siegman, A.E., 1990. "New developments in laser resonators", SPIE Vol. 1224 *Optical Resonators*.
43. Smith, David C, 1977: "High-Power Laser Propagation: Thermal Blooming," *Proceedings of the IEEE*, Vol. 65, No. 12, Dec 1977.
44. Tyson, Robert K. and Peter B. Ulrich, 1993. "Adaptive Optics," chapter 2 in *The Infrared & Electro-Optical Systems Handbook, Vol 8: Emerging Systems and Technologies*. Stanley R. Robinson, Ed. SPIE, pp. 165-237.
45. Valley, George C., 1979: "Long- and short-term Strehl ratios for turbulence with finite inner and outer scales," *Applied Optics*, Vol. 18, No. 7 (1 April 1979), pp. 984-987.
46. Verdeyen, Joseph T, 1995. *Laser Electronics*, Prentice Hall.
47. Vernon, Russ, 2003: "First Order Equations and Scaling Laws for Evaluating High Energy Laser Performance," SAIC presentation to AFIT Center for Directed Energy, 29 May 2003
48. Vernon, R. and St. John, R; 2003: "HELCOMES User's Guide", Science Applications International Corporation document, 25 Aug 2003.
49. Wallace, J., and Pasciak, J.: 1977; "Theoretical aspects of thermal blooming compensation," *Journal of the Optical Society of America*, Vol. 67(11), pp. 1569-1575 (November 1977).
50. Williams, Marion, 2004: "AFOTEC Directed Energy Long Range Plan," presentation, Directed Energy Professional Society, Test and Evaluation Conference, August 2004.
51. Yura, H. T., 1971: "Atmospheric Turbulence Induced Laser Beam Spread," *Applied Optics*, Vol. 10, No. 12 (December 1971), pp. 2771-2773.

REPORT DOCUMENTATION PAGE				Form Approved OMB No. 074-0188	
<p>The public reporting burden for this collection of information is estimated to average 1 hour per response, including the time for reviewing instructions, searching existing data sources, gathering and maintaining the data needed, and completing and reviewing the collection of information. Send comments regarding this burden estimate or any other aspect of the collection of information, including suggestions for reducing this burden to Department of Defense, Washington Headquarters Services, Directorate for Information Operations and Reports (0704-0188), 1215 Jefferson Davis Highway, Suite 1204, Arlington, VA 22202-4302. Respondents should be aware that notwithstanding any other provision of law, no person shall be subject to a penalty for failing to comply with a collection of information if it does not display a currently valid OMB control number.</p> <p>PLEASE DO NOT RETURN YOUR FORM TO THE ABOVE ADDRESS.</p>					
1. REPORT DATE (DD-MM-YYYY) 29-04-2008		2. REPORT TYPE PhD Dissertation		3. DATES COVERED (From – To) Sep 2002 – Jun 2008	
4. TITLE AND SUBTITLE CHARACTERIZING EFFECTS AND BENEFITS OF BEAM DEFOCUS ON HIGH ENERGY LASER PERFORMANCE UNDER THERMAL BLOOMING AND TURBULENCE CONDITIONS FOR AIR-TO-GROUND ENGAGEMENTS				5a. CONTRACT NUMBER	
				5b. GRANT NUMBER	
				5c. PROGRAM ELEMENT NUMBER	
6. AUTHOR(S) Long, Scott N., Lt Col, USAF				5d. PROJECT NUMBER	
				5e. TASK NUMBER	
				5f. WORK UNIT NUMBER	
7. PERFORMING ORGANIZATION NAMES(S) AND ADDRESS(S) Air Force Institute of Technology Graduate School of Engineering and Management (AFIT/EN) 2950 Hobson Street, Building 642 WPAFB OH 45433-7765				8. PERFORMING ORGANIZATION REPORT NUMBER AFIT / DS / ENS / 08-05	
9. SPONSORING/MONITORING AGENCY NAME(S) AND ADDRESS(ES) High Energy Laser Joint Technology Office, Mr. Mark Niece, Director 901 University Av Albuquerque NM 87106 Mark.niece@jto.hpc.mil				10. SPONSOR/MONITOR'S ACRONYM(S) HEL JTO	
				11. SPONSOR/MONITOR'S REPORT NUMBER(S)	
12. DISTRIBUTION/AVAILABILITY STATEMENT APPROVED FOR PUBLIC RELEASE; DISTRIBUTION UNLIMITED.					
13. SUPPLEMENTARY NOTES					
14. ABSTRACT <p>This dissertation makes contributions towards knowledge of optimizing of laser weapon performance when operating in the air-to-ground (ATG) regime in thermal blooming conditions. Wave optics modeling techniques were used to represent laser weapon performance in a high fidelity sense to allow progress to be made toward improving lower-fidelity scaling laws that can be used in systems level analysis which has need for better representations of thermal blooming. Chemical-oxygen iodine laser (COIL) based weapon systems that operate near the ground will experience thermal blooming due to atmospheric absorption if output power is sufficiently high. The thermal lens in the ATG case is predominantly in the far-field of the optical system which puts the problem outside the envelope for most classical phase correction techniques. Focusing the laser beyond the target (defocus) in the air-to-ground regime is shown to improve irradiance at the target and can be thought of as reducing the thermal blooming distortion number, ND, rather than phase correction. Improvement is shown in a baseline scenario presented and all variations from it explored herein. The Breaux ND is examined for potential use in a defocus scaling law, and a correction factor due to Smith (1977), developed for a different context, is proposed to address deficiencies. Optimal defocus settings and expected improvement are presented as a function of Breaux ND. Also, the generally negative interaction between turbulence and thermal blooming is investigated and shown to further limit performance potential of ATG laser weapons. This negative interaction can impact the weapon design trade space and operational methods for minimizing the interaction and thermal blooming are explored in a case study.</p>					
15. SUBJECT TERMS High energy lasers, engagement modeling, scaling laws, advanced tactical laser, thermal blooming, turbulence interaction, chemical oxygen iodine laser, thermal blooming distortion number					
16. SECURITY CLASSIFICATION OF:			17. LIMITATION OF ABSTRACT	18. NUMBER OF PAGES	19a. NAME OF RESPONSIBLE PERSON
a. REPORT	b. ABSTRACT	c. THIS PAGE			19b. TELEPHONE NUMBER (Include area code)
U	U	U	UU	167	J.O. Miller, PhD, DAF (ENS) (937) 255-6565, ext 4326; e-mail: john.miller@afit.edu